INSTITUTE FOR DIRECT ENERGY CONVERSION

TOWNE SCHOOL

UNIVERSITY OF PENNSYLVANIA

PHILADELPHIA, PENNSYLVANIA

MANFRED ALTMAN, DIRECTOR

STATUS REPORT

INDEC-SR-7

NATIONAL AERONAUTICS AND SPACE ADMINISTRATION

GRANT NSG - 316

April 1, 1966

TABLE OF CONTENTS

LIST OF ILLUSTRATIONS

1. INTRODUCTION AND SUMMARY

1. Introduction and Summary

This progress report reflects the research activities within the Institute. Since the report covers many disciplines, and is lengthy, short abstracts have been included in this section of the report to facilitate the obtainment of an overall picture.

In addition to the performance of research, the Institute continues to play a significant part in academic life. To date eight students have obtained doctorate degrees under the auspices of the Institute. It is expected that the yearly production of doctorates will be a minimum of five.

A two year sequence of graduate courses in Energy Conversion has been developed, and advanced course offerings in various areas of specialization are being planned.

The demand for our graduates continues to be satisfactory, with the majority working in the Energetics area.

With respect to our research activities, special note should be taken of the fact that several programs are truly multi-disciplinary, and it is in this category that we expect to be able to make significant contributions.

Abstracts of Research Projects

Activities of the Plasma Engineering Branch

1. Characteristics of Plasma Probes in Dense Plasmas

Past work in this area has neglected the effects of recombination. An analytical investigation of the sheath region has been made and range of validity into separating the entire region into a collision dominated one, and a free field zone has been made. Closed form solutions for several important cases have been found. Present work is concerned with an experimental study which utilizes probes which are biased with kilocycle frequencies. The results of this work to date will be presented at the 1966 International MHD Meeting.

2. Plasma Diagnostics

This work is concerned with the development of a new technique for making local property measurements in a plasma. This technique is an improvement over probe measurements and interferometric measurements in that it makes possible the determination of true local values of plasma parameters. The method consists of determination of the transverse rate of decay of a wave as a function of helix pitch, frequency and wave mode. A mathematical model has been developed which relates measurements of insertion loss, phase shifts and Doppler shift to the local values of electron number density, electron-neutral molecule collision frequency, and electron drift velocity. From these measurements, it is possible to deduce the percentage of ionization, electron temperature, and conductivity. Experiments are in progress, and the results to date have been submitted for publication.

3. Measurement of Plasma Transport Properties

The objective of this work was the measurement of the non-equilibrium ionization which is produced by an externally applied electric field in a sodium-potassium seeded argon plasma. This work has been completed. The major result was the demonstration that the plasma is remarkably uniform except for a very small region in the neighborhood of the confining wall. It was also shown that not only are increased electron temperatures obtained, but the temperature of the bulk plasma itself increases significantly over its equilibrium value. The results of this work are being prepared for publication. This work is now being extended to the determination of electron thermal conductivity and radiation.

4. Characteristics of Thermionic Plasma Diodes with Gas Mixtures

This project has the objective of developing a quantitative mechanical model for "seeded" diodes for the purpose of evaluating the Penning effect. At the conclusion of the analytical work an attempt will be made to obtain experimental verification. This project is just getting under way.

5. Electron Emission Studies

The Thomas-Fermi-Dirac theory has been used to evaluate the microscopic charge distribution and the total energy of metal plasma interface. Results of this work show that quantum mechanical corrections are a significant part of the total energy and may not be neglected. A quantum-chemical microscopic model of electron emission for metals in gaseous environments has been developed. Electron emission S curves have been calculated for cesium-tungsten and cesium-fluorine-

molybdenum. Good agreement for experimental data has been obtained. Future work is directed at obtaining an understanding of the process whereby the efficiency of the cesium thermionic converter is increased by the halogen additives.

6. Transport Properties of Partially Ionized Gases

The primary purpose of work is to obtain a simplification of the well-known Chapman-Enskog method of the solution of the Boltzman equation. The results of this work have shown that existing methods of predicting the behavior of mixtures are not reliable and can sometimes over-estimate the electrical conductivity as much as 70%. Results of this work have been published in the Proceedings of the Sixth MHD Symposium, April 1965. Future research is concerned with extending the analytical technique to thermal conductivities.

7. Plasma Centrifuge

The work is concerned with an evaluation of obtainable velocities in a plasma spinning in the annular space between two concentric cylinders under the influence of a longitudinal magnetic field and a radial electric field. Results to date have been the analytical determination of the velocity distribution in finite cylinders and viscous incompressible fluids. To date, only mercury has been studied. Current work is concerned with the determination of possible secondary flow phenomena due to field non-uniformities. Possible applications, which will be studied in the future, include the possible use of uranium hexifluoride, the possible use of rapidly spinning heavy metals as ship stabilizers, gyroscopes and bearings. It is planned to present the preliminary results by the end of 1966.

Activities of the Electrochemical Engineering Branch

1. Atomic Scale Electrode Processes

Field-ion emission microscope studies - the objectives of this work are to develope techniques for the use of the field-ion microscope to allow the determination of the electrochemical adsorption of oxygen onto platinum. The successful development of this technique will make it possible to obtain a visualization of the motion of atoms and ionic species on metal electrodes and across the junctions between electrodes and electrolyte. This work is now in progress and the results are expected by September of 1966.

2. Natural Convection Mass Transport in Electrolytic Systems

A technique has been developed which allows the measurement of convective transport within the pores of fuel cells. The method is based on the variation of concentration overpotential with time following the interruption of a constant current or the application of constant current. The experimental technique consists of positioning a Luggin-Haber probe electrode along the working electrode which makes it possible to obtain the variation of the local boundary layer thickness as a function of current density and position. The use of a capillary probe makes the testing within the miniscus possible. The system which was chosen for the initial program was the anodic solution of silver in silver-nitrate solutions. Work is in progress.

3. Fuel-Cell Porous-Electrode Models

The purpose of this investigation is to develope an analytical model of the local heat effects within a single pore of an electrode. An

experimental technique has been developed which uses a scaled-up two dimension pore which allows the determination of local heat effects. This method will eventually be extended to a study of oxygen consuming cathodes and to hydrogen and oxygen nickel electrodes.

4. Transport Parameters in Fuel Cell Electrolytes

A new technique has been developed which makes it possible to determine rapidly the solubility and diffusivity constants for hydrogen, oxygen and hydrocarbons. The essential feature involves a virtual capillary tube of non-conducting material which is filled with electrolyte. The upper surface of the electrolyte is in contact with the gas phase. The bottom end of the tube is in contact with an electrolyte reservoir. A mesh electrode attached to the bottom is potentiostatically controlled so as to cause immediate oxidation (or reduction) of the dissolved gas. A measurement of the current required to cause complete conversion of the dissolved gases or hydrocarbons provides the numerical value of the gradient at the bottom of the tube. From this measurement, the diffusion coefficients can be determined by analytical techniques which have been developed.

5. Battery Materials

This study is concerned with a determination of the electrode behavior of silver oxide. A method has been perfected for obtaining large single crystals of Ag_2O by the use of large current densities for carbon anodes in silver nitrate-potassium nitrate electrolytes. The properties of these silver oxide crystals will be determined experimentally such as the conductivity as a function of temperature.

This work is now in progress.

Activities of the Materials Engineering Branch

1. High Temperature Thermal Diffusivity Measurements.

A transient technique has been developed which makes it possible to determine thermal diffusivities of solids in the temperature range of up to 2000°C. The method offers several advantages over those used in the past.

a. It depends only on the measurement of temperatures as a function of time, thus obviating the need for determination of a heat flux.

b. It makes it possible to study solids up to their melting points.

c. It provides data over large temperature ranges very quickly. The apparatus has been built and tested and shown to be reliable. Results of this work are being prepared for publication.

Future work is concerned with extension of the experimental technique to study liquids and mixtures.

2. Thermoelectric Properties of Graphite Compounds

The objective of this work is to determine the feasibility of synthesizing a new class of thermoelectric compounds which would have superior thermoelectric properties. It is believed that the introduction of metallic impurities into a graphite crystal will result in a broadening of the band gap and will, at the same time, decrease phonon conduction without effecting electronic conduction. At the present time, theoretical studies are in progress which will result in the prediction of obtainable band gaps and the prediction of achievable electron transport by the

hopping mechanism. It is planned to use the results of this theoretical work in the fabrication of such new materials and to determine their thermoelectric properties experimentally.

3. Development of Efficient Tunnel Cathodes

The purpose of this investigation is to develope efficient cold cathodes for electric devices, and, eventually to the development of tunnel emission devices and the study of hot electron transport phenomena. The by-products of this work are expected to be a better understanding of the electron scattering mechanisms in thin films with applicability to thin film solar cells and similar devices.

This work is now in progress.

General Studies

1. Mathematical Simulation of Solar-Thermal Energy Conversion Systems.

Analytical methods have been developed in cooperation with the Aerospace Corporation which allow the prediction of behavior of systems depending on solar energy. These methods are based on the development of "cone optics" which make it possible to calculate the flux density of any optical image which is formed by single reflection.

2. Interdisciplinary Studies of Charged Interfaces

The objectives of this work are to study the parallelisms which exist between the techniques used in plasma physics, surface physics, surface chemistry and electrochemistry. As an example, the quantum mechanical techniques which were developed for the study of thermionic

emission will be applied to problems of the adsorption of organic species on electrodes. Other applications will include such diverse areas as the metal in plasma, metal in electrolyte, semiconductor in electrolyte, metal in gas, etc.

3. Optimization of Large Systems with Non-Linear Heat Transfer Phenomena

The purpose of this research was to develope a procedure which makes it possible to optimize a large system whose equilibrium temperatures depend on conduction, convection and radiation. This work which was also supported by NASW-960 has been completed. Computer programs have been developed which require approximately one-eighth of the running time which was required by previously existing methods. Publication is now in preparation.

2. MATERIALS ENGINEERING

Branch Chief: Dr. Solomon Pollack

Senior Members: Dr. Manfred Altman, Dr. Louis Girifalco,

Dr. Ram Sharma

2.1 Thermal Diffusivity Studies

Faculty Advisor: Dr. M. Altman
Senior Research Assistant: Dr. Ram Sharma
Graduate Students: K. Sreenivasan, H. Keramaty, H. Chang

A. Solid Thermal Diffusivities

This work has resulted in several significant achievements.

1. Mr. H. Chang obtained his doctorate with the acceptance of his thesis with the title of "Thermal Diffusivity Measurements of High Temperature Thermal Energy Storage Materials."

2. Specific accomplishments were as follows:

   a. A novel measurement technique was perfected which has been described in detail in previous reports.

   b. A major contribution was made in extending measurements up to the melting point of the specimen. Previous techniques did not allow this — due to softening and deformation — and much speculation concerned itself with the variation of thermal diffusivities close to the melting point. Table 1 presents the data for CaF_2. Measurements of LiF have also been extended to the melting point. The significant result was that no significant change in the neighborhood of the melting point occurred. It is planned to publish a paper on the above in the near future.

Table 1 Thermal Diffusivities for CaF_2

Temp. °C	cm^2/sec
70	0.0124
150	0.0104
195	0.0097
242	0.0086
330	0.0081
475	0.0076
550	0.0069
630	0.0068
760	0.0067
850	0.0067
970	0.0069

B. Liquid Thermal Diffusivities

The experimental technique which is being developed has been presented in previous reports. Briefly, the method consists of raising the surface temperature of a solid cylindrical specimen which contains the liquid to be measured in the form of a thin annulus, at a uniform rate. Temperature is monitored on the surface and the center of a composite cylinder. Note that it is not necessary to measure the temperature of the liquid!

An analytical solution has been obtain, and is as follows:

$$\Delta T = \frac{b^2 \lambda}{\alpha_1} \left\{ \frac{1}{4} \left(\frac{c}{a}\right)^2 + \frac{1}{4} \left(1 - \frac{\alpha_1}{\alpha_2}\right) \left[\left(\frac{a}{b}\right)^2 - 1\right] + \right.$$

$$+ \frac{1}{2} \left(1 - \frac{\alpha_1}{\alpha_2} \frac{k_2}{k_1}\right) \left(\ln \frac{c}{a}\right) \left[\left(\frac{a}{b}\right)^2 - 1\right] -$$

$$\left. - \frac{1}{2} \left(\ln \frac{a}{b}\right) \left(\frac{a}{b}\right)^2 \left(\frac{k_1}{k_2} - \frac{\alpha_1}{\alpha_2}\right) \right\}$$

Here:

ΔT - temperature difference between surface and axis after the transient terms become negligible.

α - Thermal diffusivity

Subscripts 1, 2, 3 refer to the outer solid, the liquid, and the inner solid respectively.

λ - rate of rise of surface temperature

K - thermal conductivity

a and b are the outer and inner radii of the annulus respectively.

In order to check the sensitivity of this method, two calculations were made to determine whether ΔT would be great enough for reasonable heating rates and geometrics. The results are:

	a	b	c	λ	ΔT
LiF in BV	1.00 in.	1.125 in.	2.00 in.	200°F/hr.	5.3°F.
LiF in W	1.00 in.	1.125 in.	2.00 in.	200°F/hr.	2.1°F.

Experiments are in progress now to establish design parameters from which the final test apparatus will be built.

It is expected that the contact, or interfacial, resistance between solid and liquid may present a problem. It is planned to use solids which are wet by the liquid, and also to check on the effects of varying surface areas in order to take account of this possibility.

C. Mixture Diffusivities

Samples of mixtures of LiF and CaF_2 are being prepared. Since the diffusivities of these materials are known, the immediate program calls for a comparison of predicted and experimental results.

2.2 Tunnel Emission Cold Cathodes

Faculty Advisor: Dr. S. R. Pollack

Graduate Student: S. Basavaiah

Since the time of the previous report, a considerable amount of progress has been made in this project. The vacuum system is now permanently installed with all the necessary power and water connections. All pumps and gauges are in proper working order and the vacuum system is in operation. The thin film deposition system has been installed. This enables several different materials to be evaporated through masks onto a substrate whose temperature can be controlled from $77^{\circ}K$ to $600^{\circ}K$. Preliminary thin film depositions are presently being carried out using a 2KVA power supply capable of delivering 400 Amps. Mask registration of ± 0.003" has been achieved, however it is anticipated that ±0.001" will be possible with further alignment. Final evaporation masks are being designed using the 0.003" tolerance and it is anticipated that in 6 weeks samples will be made for testing.

A Westinghouse Quartz Crystal Microbalance, hp Electronic Counter, Tetronic 565 Dualbeam Oscilloscope, Kethley 610 B Electrometer have been installed. Preliminary tests on the Quartz Crystal Microbalance were made. This method of monitoring the thin film deposition is extremely important in determining the device performance as a function of base film thickness, and rate of evaporation.

The delivery of the electron beam gun evaporating system was delayed by the vendor. However it has arrived, and is being installed into the system. The testing of the electron beam gun is in progress.

Vacuum feed-throughs have been designed and built for making in situ measurements. A test jig for making contact to the sample in the vacuum chamber is presently under consideration.

3. PLASMA ENGINEERING

Branch Chief: Dr. George L. Schrenk

Senior Members: Dr. Hsuan Yeh, Dr. Maurice A. Brull

Dr. Leon W. Zelby, Dr. Chad F. Gottschlich, Dr. George L. Schrenk

Postdoctoral Research Associates: Dr. Michael Kaplit,

Dr. Samuel Schweitzer

3.1 Characteristics of Plasma Probes in Dense Plasmas

Dr. Hsuan Yeh, Mr. A. Whitman

Plasma (electrostatic) probes have been in use for a long time as a means for experimentally determining the electron temperature, ion temperature, and charged particle number densities. The use of these devices, however, has been limited to lower pressure ranges due to the lack of a suitable theory for high pressure plasmas — such as for one atmosphere plasmas. The purpose of this research is to extend the theory of plasma probes to high-pressure, non-equilibrium plasmas in externally imposed electrical fields — such as existing in MDH power generators.

A new formulation of probe theory in a collision dominated plasma has been made; this formulation includes the effects of recombination of electrons and ions. It has been found that the inclusion of recombination effects is indeed an important consideration; such effects have almost always been neglected by previous workers. This research is also investigating the sheath region to determine the range of validity for separating the entire plasma region into a collision-dominated region and a free-fall zone. With some simplifications, closed form solutions have been obtained for several important cases.

Research continues on the problem of a spherical probe — both in uniform discharges and in spherical discharges. Comparisons are presently being made between this theory and some experimental current-voltage data from Emmons at Harvard; preliminary indications are that this theory does appear to check out with experiment.

3.2 Slow Waves as a Plasma Diagnostic Tool

Dr. Leon W. Zelby, Mr. W. O. Mehuron, Mr. R. J. Kalagher

Accurate knowledge of the character of such plasma parameters as electron density, electron-neutral molecule collision frequency, and electron drift velocity, is important in all devices using a plasma either as an active medium—e.g., MHD—or as a charge neutralizing agent—e.g., thermionic diodes. Presently existing techniques like Langmuir probes, as well as interferometric methods, provide only average values of the measured plasma parameters. In inhomogeneous plasmas such values may deviate substantially from the local values of the parameters.

In order to improve the accuracy of determination of values of the parameters mentioned, a new diagnostic technique is being developed. This method is based on the interaction of slow electromagnetic waves with a plasma column along the axis of the column, instead of in a direction transverse to it as in other techniques. Since the depth of penetration of the wave from the slow wave circuit into the column is a function of guide wavelength, local plasma parameters can be determined as a function of coordinates transverse to the direction of propagation.

Present research concerns itself with the determination of the radial distribution of plasma parameters. Two approaches are under investigation: one approach describes the plasma as an inactive dielectric with an effective dielectric coefficient; the other describes the plasma as an active medium by including an energy exchange mechanism between the electromagnetic waves and electrons. In the

former, the electron density and collision frequency distributions are determined; in the latter, the electron drift velocity and the density distribution are determined. The theoretical aspects of these two approaches are described in detail in the following pages. The experimental results will be given in a subsequent report.

3.2.1 Electron Density and Collision Frequency in a Radially Inhomogeneous Plasma Column

Dr. Leon W. Zelby, Mr. R. J. Kalagher

We shall derive the dispersion relation and the attenuation relation for a cylindrical plasma column surrounded by a sheath helix. In particular, we shall be concerned with a plasma which has a varying electron density and collision frequency. These parameters are assumed to be inhomogeneous in the radial direction only and the plasma drift velocity is zero.

The equation of motion for an electron in a plasma is given by

$$m \frac{d\bar{v}}{dt} = - e\bar{E} - m\bar{v}\,\nu \tag{1}$$

where

m = mass of electrons

e = magnitude of electron charge

$\bar{E}$ = electric field

ν = collision frequency

The term $e\bar{E}$ is the force on the electron due to the electric field while the term $m\bar{v}\,\nu$ is the momentum loss per second, assuming that the entire momentum of the electron is transferred by an inelastic collision, where ν is the frequency that the collisions occur. In the steady state, letting $\bar{E} = \bar{E}e^{j\omega t}$ and $\bar{v} = \bar{v}\,e^{j\omega t}$, equation (1) becomes

$$\bar{v} = \frac{- eE}{m(\nu + j\omega)} \tag{2}$$

The convection current density $\bar{J}$ then is given by

$$\bar{J} = -Ne\bar{v} = \frac{Ne^2\bar{E}}{m(\nu+j\omega)}$$

where N is the electron density. Substituting this value for J in Maxwell's curl equation for $\bar{H}$ we obtain

$$\nabla \times \bar{H} = j\omega\epsilon_0\bar{E} + \frac{Ne^2\bar{E}}{m(\nu+j\omega)}$$

$$= j\omega\epsilon_0\left[1 - \frac{Ne^2}{\epsilon_0 m(\nu^2+\omega^2)} - j\frac{Ne^2}{\omega\epsilon_0 m(\nu^2+\omega^2)}\right]\bar{E}$$

$$= j\omega\epsilon_r\epsilon_0\bar{E} \qquad (3)$$

Thus the plasma can be thought of as a dielectric with a relative dielectric constant given by the bracketed expression in equation (3).

Throughout the remainder of this paper we shall assume that $\nu << \omega$ and discard terms of $\frac{\nu 2}{\omega 2}$. Making this approximation and defining the plasma frequency, $\omega_p^2 = \frac{Ne^2}{m\epsilon_0}$, the relative dielectric constant becomes

$$\epsilon_r = 1 - \frac{\omega_p^2}{\omega^2} - j\frac{\nu\omega_p^2}{\omega\omega^2}$$

For a radial inhomogeneous plasma

$$\epsilon_r(r) = 1 - \frac{\omega_p(r)^2}{\omega^2} - j\frac{\nu(r)\,\omega_p(r)^2}{\omega^3} \qquad (4)$$

where

$$\omega_p(r)^2 = \frac{N(r)e^2}{m\epsilon_0}$$

The Field Equations

In this section we shall derive the field equations for a cylindrical plasma column. The plasma is represented by the inhomogeneous dielectric constant given in equation (4). (The subscript on ϵ will be dropped to avoid confusion.) In this case, Maxwell's equations are

$$\nabla \times \bar{E} = -j\omega u \bar{H} \tag{5a}$$

$$\nabla \times \bar{H} = j\omega \epsilon_o \epsilon(r) \bar{E} \tag{5b}$$

$$\epsilon_o \nabla \cdot \epsilon(r) \bar{E} = 0 \tag{5c}$$

$$\nabla \cdot \bar{B} = 0 \tag{5d}$$

Since we will have a combination of TE and TM modes we must solve equations (5) for both E_z and H_z. All of the other components can then be derived from these two. Assuming that all field components vary as $e^{j\omega t - \gamma z}$, where $\gamma = \alpha + j\beta$, and that there is no variation in the θ direction we obtain the following equations for E_z and H_z (see Appendix I)

$$\frac{d^2E_z}{dr^2} + \left[\frac{1}{r} + \frac{\gamma^2 \frac{d\epsilon(r)}{dr}}{\epsilon(r)\left(k_o^2\epsilon(r) + \gamma^2\right)}\right]\frac{dE_z}{dr} + \left(k_o^2\epsilon(r) + \gamma^2\right)E_z = 0 \tag{6}$$

$$\frac{d^2H_z}{dr^2} + \left[\frac{1}{r} - \frac{k_o^2 \frac{d\epsilon(r)}{dr}}{k_o^2\epsilon(r) + \gamma^2}\right]\frac{dH_z}{dr} + \left(k_o^2\epsilon(r) + \gamma^2\right)H_z = 0 \tag{7}$$

where $k_o^2 = \omega^2 u \epsilon_o$.

These equations can be simplified somewhat if we speculate the occurrence of slow waves on the helix. In this case $\frac{k_o^2}{|\beta^2|} \approx \sin^2 \Psi$ where Ψ is the pitch angle of the helix. Thus if Ψ is small we can neglect terms of $\frac{k_o^2}{|\beta^2|}$ and let $k_o^2 \epsilon(r) + \gamma^2 \simeq \gamma^2$. Using this approximation equations (6) and (7) become

$$\frac{d^2 E_z}{dr^2} + \left[\frac{1}{r} + \frac{1}{\epsilon(r)} \frac{d\epsilon(r)}{dr}\right] \frac{dE_z}{dr} + \gamma^2 E_z = 0 \tag{8}$$

$$\frac{d^2 H_z}{dr} + \frac{1}{r} \frac{dH_z}{dr} + \gamma^2 H_z = 0 \tag{9}$$

Before discussing the solutions of these equations we will turn to the derivation of the dispersion equation.

Boundary Conditions and Dispersion Relation

The system under consideration is a circular plasma column of radius a surrounded by a sheath helix. The boundary conditions at r = a are

$$E_z^i + E_\theta^i \cot \Psi = 0 \tag{10a}$$

$$E_z^e + E_\theta^e \cot \Psi = 0 \tag{10b}$$

$$H_z^i + H_\theta^i \cot \Psi = H_z^e + H_\theta^e \cot \Psi \tag{10c}$$

$$E_z^i \cot \Psi - E_\theta^i = E_z^e \cot \Psi - E_\theta^e \tag{10d}$$

where the superscripts i and e refer to r < a and r > a

respectively. We also have the boundary conditions that the fields must be finite at $r = 0$ and $r = \infty$. The fields for $r > a$ are given by

$$E_z^e = C K_o(\tau r) \tag{11a}$$

$$E_\theta^e = D \frac{j\omega u}{\tau} K_1(\tau r) \tag{11b}$$

$$H_z^e = C K_o(\tau r) \tag{11c}$$

$$H_\theta^e = - C \frac{j\omega \epsilon_o}{\tau} K_1(\tau r) \tag{11d}$$

where $e^{j\omega t - \gamma z}$ is understood, K_o and K_1 are modified Bessel functions of the second kind, C and D are arbitrary constants, and $\tau^2 = -(\gamma^2 + k_o^2)$.

For $r < a$ the fields are determined from equations (8) and (9). Equation (9) is recognized as Bessel's equation with solution $I_o(\gamma r)$ (for $\gamma = j\beta$). We will represent the solution to equation (8) as $AE_z(r)$ until it is solved in the next section. The fields for $r < a$ become

$$E_z^i = A E_z(r) \tag{12a}$$

$$E_\theta^i = B \frac{j\omega u}{\tau} I_1(\gamma r) \tag{12b}$$

$$H_z^i = B I_o(\tau r) \tag{12c}$$

$$H_\theta^i = - A \frac{j\omega \epsilon}{\tau^2} \frac{dE_z(r)}{dr} \tag{12d}$$

where I_o and I_1 are modified Bessel functions of the first kind and A and B are arbitrary constants.

Substituting equations (11) and (12) in equation (10) we obtain four equations in four unknowns, A, B, C, and D. In order that these equations possess a non-trivial solution it is necessary that the determinant of the coefficients of A, B, C, and D vanish. After evaluating the determinant and going through a lot of algebra we obtain the following dispersion equation:

$$\beta^2 K_o(\beta a) E_z(a) - k_o^2 \cot^2 \Psi K_1(\beta a) I_1(\beta a) \left[\beta K_1(\beta a) E_z(a) + K_o(\beta a) E'_z(a)\right] = 0 \qquad (13)$$

In deriving equation (13) use was made of the slow wave approximation ($-\tau^2 \approx \gamma^2$) and it was assumed that $\alpha << \beta$ so that the arguments of the Bessell functions depend on β only. Preliminary measurements indicate that this is a reasonable assumption, and if it is not made equation (13) will become hopelessly transcendental. Furthermore, the presence of a finite collision frequency suggests that E_z and E'_z will be complex, i.e., $E_z = E_{zr} + jE_{zi}$ and $E'_z = E'_{zr} + jE_{zi}$. The real part of the dispersion relation becomes

$$\beta^2 K_1(\beta a) E_{zr}(a) - k_o^2 \cot^2 \Psi K_1(\beta a) I_1(\beta a) \left[\beta K_1(\beta a) E_{zr}(a) + K_o(\beta a) E'_{zr}(a)\right] = 0 \qquad (14)$$

The imaginary part of the dispersion relation is the same with E_{zr} and E'_{zr} replaced by E_{zi} and E'_{zi}.

Solution of Field Equations and Final Dispersion Relation

It is now necessary to solve equation (8) for E_z to obtain curves of β vs. k_o and α vs. k_o from equation (14). To solve equation (8) some form for $N(r)$ and $\gamma(r)$ must be assumed. It has been shown theoretically[1] that a cylindrical plasma column should have an electron density which behaves as $N(r) = N_o(1 - \frac{r^2}{a^2})$ where N_o is the electron density at $r = 0$, and $r = a$ is the radius. Although no similar investigation has been made for collision frequency, it seems that a similar expression should hold since the collisions will be roughly proportional to the number of electrons present. Thus we shall assume $\nu(r) = \nu_o(1 - \frac{r^2}{a^2})$.

Using this assumption $\epsilon(r)$ becomes

$$\epsilon(r) = 1 - \frac{\omega_{po}^2}{\omega^2}\left(1 - \frac{r^2}{a^2}\right) - j\,\frac{\omega_{po}^2 \nu_o}{\omega^3}\left(1 - \frac{r^2}{a^2}\right)^2 \qquad (15)$$

With (15) substituted in (8) a rather complicated equation is obtained which cannot be solved in terms of known functions. We can, however, approximate the solution by the first few terms of the series solution. This also has the further advantage of keeping equation (14) algebraic so that it can be solved. The details of the series solution are given in Appendix II. The first three terms evaluated at $r = a$ are:

$$E_{zr}(a) = 1 + \frac{\beta^2 a^2}{4} + \frac{\beta^4 a^4}{64} - \frac{\beta^2 a^2}{16}\,\frac{\omega_{po}^2}{\omega^2 - \omega_{po}^2} - \frac{\alpha\beta a^2}{8}\,Q \qquad (16a)$$

$$E_{zi}(a) = -\frac{\alpha\beta a^2}{2} - \frac{\alpha\beta^3 a^4}{16} + \frac{\alpha\beta a^2}{8}\,\frac{\omega_{po}^2}{\omega^2 - \omega_{po}^2} - \frac{\beta^2 a^2}{16}\,Q \qquad (16b)$$

$$E'_{zr}(a) = \frac{\beta^2 a^2}{2} + \frac{\beta^4 a^4}{16} - \frac{\beta^2 a^2}{4}\,\frac{\omega_{po}^2}{\omega^2 - \omega_{po}^2} - \frac{\alpha\beta a^2}{2}\,Q \qquad (16c)$$

1. Allis, Buchsbaum and Bers, Waves in Anisotropic Plasmas MIT Press, p. 213.

$$E'_{zi}(a) = -\alpha\beta a^2 - \frac{\alpha\beta^3 a^4}{4} + \frac{\alpha\beta a^2}{2} \frac{\omega_{po}^2}{\omega^2 - \omega_{po}^2} \frac{\beta^2 a^2 Q}{4} \tag{16d}$$

where

$$Q = \frac{\nu_o}{\omega} \left[2 \frac{\omega_{po}^2}{\omega^2 - \omega_{po}^2} + \left(\frac{\omega_{po}^2}{\omega^2 - \omega_{po}^2} \right)^2 \right]$$

Again, it is assumed that $\alpha << \beta$ and terms of α^2 are neglected with respect to β^2. Equations (16) can now be substituted into equation (14) giving a real and an imaginary dispersion equation. This will give two, rather complicated, simultaneous equations in the unknowns, β, α, and k. The equations are of the form

$$f_1(\beta, \alpha, k) = 0 \tag{17a}$$

$$f_2(\beta, \alpha, k) = 0 \tag{17b}$$

These equations are solved in the following manner. A value of βa is assumed. Equation (17b) is then solved for αa giving $\alpha a = f_3(k)$. This value of αa is then substituted into equation (17a). Various values of ka are assumed until the function f_1 is zero. The value of ka for which f_1 is zero is substituted back into f_3 to give αa. For the assumed value of βa, these are the correct corresponding values of ka and αa. Another βa is chosen and the process is repeated.

In this way, given the values of ω_{po} and ν_o we can plot βa vs. ka and αa vs. ka. At the present time the calculations

outlined above are being carried out on a digital computer. After some preliminary curves are obtained, measurements will be made to obtain the experimental dispersion and attenuation curves. Then more theoretical curves will be run on the computer for various values of the parameters ω_{po} and ν_o. The curves which match the experimental ones will indicate the correct values of the above parameters.

APPENDIX I Derivation of Equation for E_z and H_z for a Radial Inhomogeneous Dielectric Constant

In this appendix we derive the equations for H_z and E_z assuming that the relative dielectric constant is a function of the radius only. A standard circular cylindrical coordinate system (r, θ, z) is used and all field quantities are assumed to vary as $e^{j\omega t - \gamma z}$ i.e. $\overline{E} = \overline{E}(r, \theta)e^{j\omega t - \gamma z}$ etc. Maxwell's source free equations are

$$\nabla \times \overline{E} = -j\omega u \overline{H} \tag{I-1}$$

$$\nabla \times \overline{H} = j\omega \epsilon_o \epsilon(r)\overline{E} \tag{I-2}$$

$$\epsilon_o \nabla \cdot \epsilon(r)\overline{E} = 0 \tag{I-3}$$

$$u \nabla \cdot \overline{H} = 0 \tag{I-4}$$

If equations (I-1) and (I-2) are written in component form and rearranged, the r and θ components can be written in terms of the z components as follows.

$$E_r = -\frac{1}{\gamma^2 + k_o^2 \epsilon(r)} \left[\gamma \frac{\partial E_z}{\partial r} + \frac{j\omega u}{r} \frac{\partial H_z}{\partial \theta}\right] \tag{I-5}$$

$$E_\theta = \frac{1}{\gamma^2 + k_o^2 \epsilon(r)} \left[-\frac{\gamma}{r} \frac{\partial E_z}{\partial \theta} + j\omega u \frac{\partial H_z}{\partial r}\right] \tag{I-6}$$

$$H_r = \frac{1}{\gamma^2 + k_o^2 \epsilon(r)} \left[\frac{j\omega \epsilon_o \epsilon(r)}{r} \frac{\partial E_z}{\partial \theta} - \gamma \frac{\partial H_z}{\partial r} \right] \tag{I-7}$$

$$H = -\frac{1}{\gamma^2 + k_o^2 \epsilon(r)} \left[j\omega \epsilon_o \epsilon(r) \frac{\partial E_z}{\partial r} + \frac{\gamma}{r} \frac{\partial H}{\partial \theta} \right] \tag{I-8}$$

where $k_o^2 = \omega^2 \mu \epsilon_o$.

It is thus seen that all the components (and thus the total fields) can be derived from the z components alone.

To obtain the equation for H_z we take the curl of equation (I-2)

$$\nabla \times \nabla \times \bar{H} = j\omega \epsilon_o \nabla \times \epsilon(r) \bar{E}$$

$$= j\omega \epsilon_o \left[\nabla \epsilon(r) \times E + \epsilon(r) \nabla \times E \right] \tag{I-9}$$

Letting $\hat{a}_r$, $\hat{a}_\theta$, and $\hat{a}_z$ be unit vectors along the r, θ, and z directions, we can evaluate the first term in the brackets.

$$\nabla \epsilon(r) = \frac{\partial \epsilon(r)}{\partial r} \hat{a}_r$$

$$\nabla \epsilon(r) \times \bar{E} = E_\theta \frac{\partial \epsilon(r)}{\partial r} \hat{a}_z \tag{I-10}$$

The second term in the brackets is given by equation (I-1). Substituting for the terms in the brackets and using the vector identity

$$\nabla \times \nabla \times \bar{H} = \nabla \nabla \cdot \bar{H} - \nabla^2 \bar{H}$$

and noting that $\nabla \cdot H = 0$ from (I-4), we obtain

$$-\nabla^2 \bar{H} = j\omega\epsilon_0 E_\theta \frac{\partial \epsilon(r)}{\partial r} \hat{a}_z + k_0^2 \epsilon(r) \bar{H} \qquad \text{(I-11)}$$

We now assume that we have no θ dependence. This corresponds to the $n = 0$ mode on the helix. The z dependence is contained in the factor $e^{-\gamma z}$. Under these conditions

$$\nabla^2 = \frac{d^2}{dr^2} + \frac{1}{r} + \frac{d}{dr} + \gamma^2$$

Taking the z component of equation (I-11), substituting the above expression for ∇^2 and the value of E_θ from equation (I-6) we have

$$\frac{\partial^2 H_z}{\partial r^2} + \left[\frac{1}{r} - \frac{k_0^2 \frac{d\epsilon(r)}{dr}}{k_0^2 \epsilon(r) + \gamma^2}\right] \frac{dH_z}{dr} + (k_0^2 \epsilon(r) + \gamma^2) H_z = 0 \qquad \text{(I-12)}$$

The equation for E_z is derived in an analogous manner. Taking the curl of (I-1) and using (I-2) and the double curl vector identity we obtain

$$\nabla \nabla \cdot \bar{E} - \nabla^2 \bar{E} = k_0^2 \epsilon(r) \bar{E} \qquad \text{(I-13)}$$

From equation (I-3)

$$\epsilon_o \nabla \cdot \epsilon(r)\,\overline{E} = \epsilon_o (\overline{E} \cdot \nabla \epsilon(r) + \epsilon(r) \nabla \cdot E) = 0$$

Solving for $\nabla \cdot E$ we obtain

$$\nabla \cdot \overline{E} = - \frac{1}{\epsilon(r)} E_r \frac{\partial \epsilon(r)}{\partial r}$$

then

$$\nabla \nabla \cdot \overline{E} = - \frac{1}{\epsilon(r)} \frac{\partial \epsilon(r)}{\partial r} \frac{\partial E_r}{\partial z} \hat{a}_z$$

but

$$\frac{\partial E_r}{\partial z} = -\gamma E_r$$

and E_r is obtained from equation (I-5). When all these substitutions are made in (I-13) and the z component is taken, we obtain the following equation for E_z

$$\frac{d^2 E_z}{dr^2} + \left[\frac{1}{r} + \frac{\gamma^2 \frac{d\epsilon(r)}{dr}}{\epsilon(r)\left(k_o^2 \epsilon(r) + \gamma^2\right)} \right] \frac{dE_z}{dr} + \left(k_o^2 \epsilon(r) + \gamma^2\right) E_z = 0 \qquad \text{(I-14)}$$

The solutions of (I-12) and (I-14) give all the components of the electromagnetic field through equations (I-5) through (I-8).

APPENDIX II Series Solution of the Differential Equation for E_z

In this appendix we obtain a series solution to the equation

$$\frac{d^2E_z}{dr^2} + \left[\frac{1}{r} + \frac{1}{\epsilon(r)}\frac{d\epsilon(r)}{dr}\right]\frac{dE_z}{dr} + \gamma^2 E_z = 0 \qquad \text{(II-1)}$$

where

$$\epsilon(r) = 1 - \frac{\omega_{po}^2}{\omega^2}\left(1 - \frac{r^2}{a^2}\right) - j\frac{\omega_{po}^2 \nu_e}{\omega^3}\left(1 - \frac{r^2}{a^2}\right)^2 \qquad \text{(II-2)}$$

It will prove convenient to work with the normalized variable $y = \frac{r}{a}$. Equation (ii-1) then becomes

$$\frac{d^2E_z}{dy^2} + \left[\frac{1}{y} + \frac{1}{\epsilon(y)}\frac{d\epsilon(y)}{dy}\right]\frac{dE_z}{dy} + \gamma^2 a^2 E_z(y) \qquad \text{(II-3)}$$

Substituting the expression for ϵ (y) in (II-3) and clearing of fractions we obtain the equation

$$(Dy^5 + By^3 + Ay)\,E''_z + (5Dy^4 + 3By^2 + A)\,E'_z$$

$$+ \gamma^2 a^2 (Dy^5 + By^3 + Ay)\,E_z = 0 \qquad \text{(II-4)}$$

where

$$A = 1 - \frac{\omega_{p0}^2}{\omega^2} - j\,\frac{\omega_{p0}^2 \nu_0}{\omega^3}$$

$$B = \frac{\omega_{p0}^2}{\omega^2} + j\,\frac{\omega_{p0}^2 \nu_0}{\omega^3}$$

$$D = -j\,\frac{\omega_{p0}^2 \nu_0}{\omega^3}$$

and the prime denotes differentiation with respect to y.

Consider expanding the solution in a series of the form

$$E_z = y^s \sum_{n=0}^{\infty} a_n y^n \qquad \text{(II-5)}$$

where s is a constant to be determined and a_n are coefficients to be determined. The multiplicative term y^s is necessary since the equation has a regular singular point at $y = 0$.

Equation (II-5) is differentiated twice and substituted into equation (II-4). In order that (II-4) be identically zero it is necessary that the coefficients of each power of y be separately equal to zero. The constant term in the series is

$$A s^2 = 0 \qquad \text{(II-6)}$$

Since $A \neq 0$ we obtain two values of s from equation (II-6) (the indicial equation) i.e. $s_1 = 0$, $s_2 = 0$. Each value of s corresponds to a separate linearly independent solution of the equation. The equality

of the two roots of the indicial equation indicate that one solution will contain a multiplicative factor of log y. Since E_z must be finite at $r = 0$, we will only keep the analytic solution.

Setting the remaining coefficients of each power of y to zero we obtain a recursion relation for the coefficients a_n. The first coefficient a_o is arbitrary and will be set equal to one. a_1 is zero and all odd terms in the series are therefore zero. The recursion relation for the even terms is found to be

$$-A n^2 a_n = \left[B(n-2)^2 + 2B(n-2) + \gamma^2 a^2 A\right] a_{n-2} \qquad \text{(II-7)}$$

$$+ \left[D(n-4)^2 + 4D(n-4) + \gamma^2 a^2 B\right] a_{n-4} + \gamma^2 a^2 a_{n-6}$$

By allowing n to take different integer values we obtain all the a's in terms of a_o. The first three terms of the series solution are

$$E_z^{(y)} = 1 - \frac{\gamma^2 a^2 y^2}{4} + \frac{B\gamma^2 a^2 y^4}{16A} + \frac{\gamma^4 a^4}{16} y^4 \qquad \text{(II-8)}$$

The ratio $\frac{B}{A}$ can be written in terms of its real and imaginary parts

$$\frac{B}{A} = \frac{\frac{\omega_{po}^2}{\omega^2}\left(1 - \frac{\omega_{po}^2}{\omega^2}\right)}{\left(1 - \frac{\omega_{po}^2}{\omega^2}\right)^2 + \left(\frac{\omega_{po}^2}{\omega^2}\frac{\nu_o}{\omega^2}\right)^2} + j\,\frac{2\left(1 - \frac{\omega_{po}^2}{\omega^2}\right)\frac{\nu_o}{\omega} + \frac{\omega_{po}^4}{\omega^5}}{\left(1 - \frac{\omega_{po}^2}{\omega^2}\right)^2 + \left(\frac{\omega_{po}^2}{\omega^2}\frac{\nu_o}{\omega}\right)^2} \qquad \text{(II-9)}$$

Again neglecting terms of $\frac{\nu^2}{\omega^2}$ equation (II-9) becomes

$$-\frac{B}{A} = \frac{\omega_{p_o}^2}{\omega^2 - \omega_{p_o}^2} + j\frac{\nu_o}{\omega}\left[\frac{2\omega_{p_o}^2}{\omega^2 - \omega_{p_o}^2} + \left(\frac{\omega_{p_o}^2}{\omega^2 - \omega_{p_o}^2}\right)^2\right]$$

$$= P + jQ$$

Finally we obtain the desired approximation for E_z

$$E_z(y) = 1 - \frac{(\gamma a)^2 y^2}{4} + \frac{(\gamma a)^4 y^4}{64} + \frac{(\gamma a)^2 P y^4}{16} + j\frac{(\gamma a)^2 Q y^4}{16} \quad \text{(II-10)}$$

Note that this solution is approximately a Bessel function as would be expected from the form of the equation.

For radial variations where $\epsilon(r)$ has a value other than 1 at $r = a$ (i.e. $1 - \delta\frac{r^2}{a^2}$, where δ is a constant between zero and 1) it is only necessary to replace P and Q by $P\delta$ and $Q\delta$ respectively.

3.2.2 Electromagnetic Wave Interaction in an Inhomogeneous Drifting Plasma

Dr. Leon W. Zelby, Mr. W. O. Mehuron

The published literature on electromagnetic wave interaction and propagation in plasma[1-10] and the related work on electron beams[11-15] and beam-plasma interaction[15-20] has generally been restricted to studies of homogeneous plasma. In the plasma studies this restriction is in addition to the usual assumption of a collisionless, zero electron temperature, single velocity plasma. The predictions from these simple theories based on a homogeneous plasma have been in good agreement with laboratory measurements although some discrepancies[21] have been found that have been attributed to the inhomogeneous nature of the plasma. Even though the agreement between theory and measurement has been good, the discrepancies and the fact that in many cases inhomogeneities in plasma parameters are known to exist,[22,23] it seems desirable to consider the problem of electromagnetic wave interaction in an inhomogeneous plasma.

Very little work has been carried out for the case of interaction or propagation in a bounded inhomogeneous plasma because of the mathematical difficulties that arise in this type of problem. Samaddar,[24] Briggs and Paik,[21] and Stepanov[25] have considered the problem of wave propagation on inhomogeneous plasma columns using a dielectric representation for the plasma. This type of representation, or model, has yielded interesting results in the area of resonance absorption and its effects on wave propagation, but it is not a useful representation for the study of the effects of interaction within an

inhomogeneous drifting plasma.

It is well known[17,18] that electromagnetic wave interaction in a drifting plasma primarily involves the electron density, or plasma frequency and electron drift velocity when the dynamical equations governing the interaction have been linearized by suitable small-signal approximation. The problem of electromagnetic wave interaction in an inhomogeneous drifting plasma will involve providing these plasma parameters with a spatial variation. In this paper a theoretical model will be developed for the case of an inhomogeneous drifting plasma column where the inhomogeneity of the plasma will be represented by radial variations in the electron density and electron drift velocity. The solutions obtained from the model have been used to obtain dispersion relations for the column in free-space, the plasma column bounded by a thin dielectric tube and for the case of a bounded plasma column surrounded by a helix. The dispersion relations have been evaluated on a digital computer to obtain the real and imaginary components of the electromagnetic wave propagation constant as a function of frequency, plasma parameters, and type of inhomogeneity. The inhomogeneous plasma-helix system is of particular interest because it allows the study of the interaction between the slow surface waves of the helix and the inhomogeneous drifting plasma. This system is also of interest because of its relation to traveling-wave tube work,[13] plasma amplifiers,[18] and plasma diagnostic techniques.[26]

Formulation of the Problem.

In the following development of a model for electromagnetic wave interaction in a bounded, inhomogeneous drifting plasma, the

circular cylindrical coordinate system shown in Figure 1 will be used. A harmonic time variation of the form $\exp(i\omega t)$ and longitudinal variation of the form $\exp(-i\beta z)$ will be used for all field quantities through the analysis. It will be assumed that ω is a real variable and β a complex variable although comparable results would be obtained if one treated ω as complex and β as a real variable.[27]

The inhomogeneous drifting plasma will be described by a volume electron density $\rho(\vec{r},t)$, an average electron velocity $\vec{u}(r,t)$ and an associated current density $\vec{J}(\vec{r},t)$. Starting with this general description of the plasma, the dynamical equations that govern the electromagnetic wave interaction will be considered. The current density is related to the charge density by

$$\vec{J}(\vec{r},t) = \rho(\vec{r},t)\,\vec{u}(\vec{r},t) \tag{1}$$

This equation is obviously nonlinear in ρ and $\vec{u}$ and must be linearized by means of a small signal approximation that will be considered later in this section. The current density and electron volume charge density are also related by the equation of continuity which can be expressed as

$$\nabla\cdot\vec{J}(\vec{r},t) = -\frac{\partial\rho(r,t)}{\partial t} \tag{2}$$

The equation of motion for the electrons within the plasma is given in general by the following expression[28]

$$\frac{d\,m\vec{u}(r,t)}{dt} = -e\left(\vec{E}+\vec{u}\times\vec{B}\right) - \nabla p - m\nu\vec{u} \tag{3}$$

where $\vec{E}$ = total electric field,

$\vec{B}$ = total magnetic field,

p = thermal pressure at the point

ν = electron collision frequency (electron-electron collisions),

m = electron mass,

e = electron charge.

In this paper the effects of pressure gradients and collisions will be neglected and the equation of motion becomes

$$\frac{d}{dt} m\vec{u}(\vec{r},t) = -e\left(\vec{E} + \vec{u} \times \vec{B}\right) \tag{4}$$

or

$$\frac{\partial \vec{u}}{\partial t} + \vec{u} \cdot \nabla \vec{u} = -\frac{e}{m}\left(\vec{E} + \vec{u} \times \vec{B}\right) \tag{5}$$

The equation of motion for the electrons is also a nonlinear equation in velocity and will have to be linearized by means of a small signal approximation and amplified through other assumptions before a solution can be obtained.

The final set of equations that govern the electromagnetic wave interaction are Maxwell's equations given by

$$\nabla \times \vec{E} = -\mu_0 \frac{\partial \vec{H}}{\partial t} = -j\omega\mu_0 \vec{H} \tag{6}$$

$$\nabla \times \vec{H} = \vec{J} + \epsilon_0 \frac{\partial \vec{E}}{\partial t} = \vec{J} + j\omega\epsilon_0 \vec{E} \tag{7}$$

where μ_0 = permeability of free-space,

ϵ_0 = dielectric constant of free-space,

$\frac{\partial}{\partial t} = j\omega$

A set of five equations has been presented that must be linearized into a set of small-signal equations and solved simultaneously. To linearize the equations, the usual small-signal approximation will be introduced into the system of equations. Let

$$\left\{ \begin{array}{l} \vec{u}(\vec{r},t) = \vec{u}_0(\vec{r}) + \vec{u}_1(\vec{r},t) \\ \rho(\vec{r},t) = -\rho_0(\vec{r}) + \rho_1(\vec{r},t) \\ \vec{J}(\vec{r},t) = -\vec{J}_0(\vec{r}) + \vec{J}_1(\vec{r},t) \end{array} \right. \qquad (8)$$

where the zero subscript implies a d-c, or time average term, and the one subscript and a-c term assumed to be much smaller than the d-c term.

The negative signs in the above expressions is a convenient convention that has been used by Beck[13] and others and has been found to be useful when relating these equations to the field equations. Substitutions of the expressions in (8) into Eqn. (1) yields

$$\vec{J} = -\vec{J}_0 + \vec{J}_1 = (-\rho_0 + \rho_1)(\vec{u}_0 + \vec{u}_1) \qquad (9)$$

or

$$\vec{J}_1 = -\rho_0\vec{u}_0 - \rho_0\vec{u}_1 + \rho_1\vec{u}_0 + \rho_1\vec{u}_1 + \vec{J}_0 \qquad (10)$$

Noting that $\vec{J}_0 = \rho_0 \vec{u}_0$ and neglecting the product of the small a-c terms yields a small-signal approximation for the a-c current density

$$\vec{J}_1 = -\rho_0 \vec{u}_1 + \rho_1 \vec{u}_0 \tag{11}$$

Substitution of the expressions in (8) into the equation of continuity (2) yields

$$\nabla \cdot (\vec{J}_0 + \vec{J}_1) = -\frac{\partial}{\partial t}(\rho_0 + \rho_1) = -j\omega\rho_1 \tag{12}$$

Separating the a-c and d-c components of this equation yields

$$\begin{cases} \nabla \cdot \vec{J}_0 = 0 \\ \\ \nabla \cdot \vec{J}_1 = -j\omega\rho_1 \end{cases} \tag{13}$$

To linearize the equation of motion the expression for the particle velocity given in (8) is substituted into the equation of motion. Expansion of the terms and separating the a-c and d-c components yields

$$\begin{cases} j\omega\vec{u}_1 + \vec{u}_0 \cdot \nabla\vec{u}_1 + \vec{u}_1 \cdot \nabla\vec{u}_0 = -\frac{e}{m}\left(\vec{E}_1 + \vec{u}_0 \times \vec{B}_1 + \vec{u}_1 \times \vec{B}_0\right) \\ \\ \vec{u}_0 \cdot \nabla\vec{u}_0 = -\frac{e}{m}\left(\vec{E}_0 + \vec{u}_0 \times \vec{B}_0\right) \end{cases} \tag{14}$$

Note that the small term $\vec{u}_1 \cdot \nabla \vec{u}_1$ has been neglected in the above expression. It should also be noted that the small-signal approximation has linearized the a-c component equation but the d-c component equation remains nonlinear in velocity. Fortunately in this problem the a-c component equation is of interest and can be reduced to a more usable form after some additional simplifying assumptions are introduced.

The linearized equations can be simplified if the flow of the plasma is confined to the longitudinal, or $+z$, direction and the velocity $\vec{u}$ and current density $\vec{J}$ have only z components. This assumption is equivalent to assuming the presence of an infinite d-c magnetic field in the $+z$ direction. It will also be assumed that only radial variations are allowed in the plasma parameters or that the inhomogeneity exists in the radial direction. This assumption means $\rho(\vec{r},t) \rightarrow \rho(r,t)$; $\vec{u}(\vec{r},t) \rightarrow \vec{u}(r,t)$, etc. From Eqns. (11) and (13), the z -component of the current density is given by

$$J_{1z} = -\rho_0 u_{1z} + \rho_1 u_{0z} = -\rho_0 u_{1z} + \left(\frac{\beta J_{1z}}{\omega}\right) u_{0z} \tag{15}$$

or

$$J_{1z}\left(1 - \frac{\beta u_{0z}}{\omega}\right) = -\rho_0 u_{1z} \tag{16}$$

$$J_{1z} = \frac{-\omega \rho_0 u_{1z}}{\omega - \beta u_{0z}} \tag{17}$$

For one-dimensional flow, the equation of motion simplifies to the following form

$$j\omega u_{1z} - j\beta u_{0z} u_{1z} = -\frac{e E_{1z}}{m} \tag{18}$$

$$u_{1z} = \frac{j\frac{e}{m} E_{1z}}{(\omega - \beta u_{0z})} \tag{19}$$

Substitution of (19) into (17) yields

$$J_{1z} = \frac{j\omega \frac{e}{m} \rho_0 E_{1z}}{(\omega - \beta u_{0z})^2} \tag{20}$$

From (6) and (7) the wave equation for E_{1z} can be written as

$$(\nabla^2 + k^2) E_{1z} = -\frac{j\beta\rho_1}{\epsilon_0} + j\omega\mu_0 J_{1z} \tag{21}$$

$$\text{where} \quad k^2 = \omega^2/c^2$$

And from Eqn. (13)

$$(\nabla^2 + k^2) E_{1z} = J_{1z} \left(j\omega\mu_0 - \frac{j\beta^2}{\epsilon_0\omega}\right) \tag{22}$$

In circular cylindrical coordinates the left-hand side of Eqn. (22) can be expressed as

$$(\nabla^2 + k^2) E_{1z} = \frac{1}{r} \frac{\partial}{\partial r} \left(r \frac{\partial E_{1z}}{\partial r}\right) + \frac{1}{r^2} \frac{\partial^2 E_{1z}}{\partial \theta^2} + \frac{\partial^2 E_{1z}}{\partial z^2} + k^2 E_{1z} \tag{23}$$

For an azimuthal variation of the form $\exp(jn\theta)$ Eqn. (22) can now be written as

$$\frac{1}{r} \frac{d}{dr} \left(\frac{r\, dE_{1z}}{dr}\right) - \left(\beta^2 - k^2 + \frac{n^2}{r^2}\right) E_{1z} = \left(j\omega\mu_0 - \frac{j\beta^2}{\omega\epsilon_0}\right) J_{1z}$$

$$\frac{1}{r}\frac{d}{dr}\left(\frac{r\,dE_{1z}}{dr}\right)-\left(\beta^2-k^2+\frac{n^2}{r^2}\right)E_{1z}=\frac{e\rho_0(k^2-\beta^2)E_{1z}}{m\epsilon_0(\omega-\beta u_{0z})^2} \tag{24}$$

If an electron plasma frequency $\omega_p(r)$is defined as

$$\omega_p^2(r)=\frac{e\rho_0(r)}{m\epsilon_0} \tag{25}$$

the equation for E_{1z} is given by

$$\frac{1}{r}\frac{d}{dr}\left(\frac{r\,dE_{1z}}{dr}\right)-\left(\beta^2-k^2\right)\left[1-\frac{\omega_p^2(r)}{(\omega-\beta u_0(r))^2}\right]E_{1z}-\frac{n^2}{r^2}E_{1z}=0 \tag{26}$$

Although the TM-type wave represented by a solution to Eqn. (26) adequately describes the interaction within the drifting plasma the plasma-helix system that will be considered in a later section contains boundary conditions such that a TE-type wave must also be present for them to be satisfied. Maxwell's equations (6) and (7) yield the following wave equation for H_{1z}.

$$(\nabla^2+k^2)H_{1z}=-(\nabla\times\vec{J})_z=0 \tag{27}$$

In circular cylindrical coordinates the equation becomes

$$\frac{1}{r}\frac{d}{dr}\left(\frac{r\,dH_{1z}}{dr}\right)+\left(k^2-\beta^2-\frac{n^2}{r^2}\right)H_{1z}=0 \tag{28}$$

Therefore, the problem of electromagnetic wave interaction in an inhomogeneous drifting plasma column can be reduced to finding the solution of the following set of equations in the plasma region and surrounding dielectric, or free-space, and applying the appropriate boundary conditions.

$$\frac{1}{r}\frac{d}{dr}\left(\frac{r\,dE_{1z}}{dr}\right)-(\beta^2-k^2)\left[1-\frac{\omega_p^2(r)}{(\omega-\beta u_0(r))^2}\right]E_{1z}-\frac{n^2}{r^2}E_{1z}=0$$

$$\frac{1}{r}\frac{d}{dr}\left(\frac{r\,dH_{1z}}{dr}\right)-\left(\beta^2-k^2+\frac{n^2}{r^2}\right)H_{1z}=0 \qquad (29)$$

The inhomogeneity of the plasma is represented in the above equations by radial variations in the plasma frequency and the electron drift velocity. It should also be noted that all the remaining components of the electromagnetic field in the circular cylindrical system can be obtained from the components of the electric and magnetic field in the direction of propagation. Expressions for the remaining four components are given in Appendix A.

Methods of Solution.

In this section solutions will be obtained for the longitudinal components of the electromagnetic field variables Eiz and Hiz.

A. Plasma Region Solutions.

The general equations for these quantities in the plasma region are shown in Eqn. (29) and it is obvious that the solution for H_{1z} can be immediately written as

$$H_{1z} = A\, I_n(pr) \tag{30}$$

where $p = (\beta^2 - k^2)^{1/2}$, I_n is a modified Bessel function of the first kind of order n, and A is an arbitrary constant.

The $\exp j(\omega t - \beta z)$ variation has not been included since it has been assumed for all field quantities. It also should be noted that the other component of the general solution for H_{1z} has not been included since it becomes infinite on the plasma axis. Since the interaction within the plasma involves slow waves where $k^2 << \beta^2$

$$H_{1z} = A\, I_n(\beta r) \tag{31}$$

If $n = 0$ the solution for H_{1z} is azimuthally symmetric and will be finite on the axis of the plasma and increases in magnitude as one moves to the surface of the plasma.

Obtaining a solution for E_{1z} is not quite as simple a matter since the coefficients of the equation involve the plasma parameters $\omega_p^2(r)$ and $u_o(r)$. Before obtaining a solution for the inhomogeneous case, it is worthwhile to consider the homogeneous case where $\omega_p^2(r)$ and $u_o(r)$ become constants. If $\omega_p^2(r) = \bar{\omega}_p^2$ and $u_o(r) = \bar{u}_o$, the solution for E_{1z} is simply

$$E_{1z} = B I_n (q_0 r) \tag{32}$$

where $$q_0 = \left[(\beta^2 - k^2)\left(1 - \frac{\bar{\omega}_p^2}{(\omega - \beta\bar{u}_o)^2}\right)\right]^{1/2}$$

I_n = modified Bessel function of the first kind of order n,

β = arbitrary constant

Since the slow wave modes are of interest the solution becomes

$$E_{1z} = B I_n\left[\beta\left(1 - \frac{\bar{\omega}_p^2}{(\omega - \beta\bar{u}_o)^2}\right)^{1/2} r\right] \tag{33}$$

The solutions for E_{1z} and H_{1z} in the homogeneous case are simply the slow space charge waves, or disturbances, that have been considered by Beck[13] and others[4] and are due to the drift velocity of the plasma. Each of the longitudinal field components will have a maximum at the plasma boundary and decrease away from the boundary when $n = 0$.

In the inhomogeneous case it will be somewhat easier to obtain a solution if the aximuthally symmetric ($\eta = 0$) mode is considered and $\omega_p^2(r)$ and $u_o(r)$ are assumed to be well behaved functions that can be represented by power series in the radius. For this case solutions for E_{1z} can be obtained in terms of conventional series by Frobenius' method,[29] in terms of confluent hypergeometric functions,[30] or by means of the asymptotic methods of Langer[31] that would be valid for large values of β. Solutions obtained in terms of the confluent hypergeometric functions and Langer's methods are interesting but can not readily be used to evaluate the dispersion relations that will be of interest to us in a later section. To obtain a series solution to E_{1z}, the convenient method used by Stepanov[25] will be used rather than the conventional Frobenius approach. To apply this method let us seek a solution to Eqn. (2) in the form of a series of functions

$$E_{1z} = E_o + E_1 + E_2 + \ldots . \tag{34}$$

where E_o, E_1, E_2, ... are determined from solutions of the following set of equations.

$$\begin{cases} \frac{1}{r}\frac{d}{dr}\left(r\frac{dE_o}{dr}\right) = 0 \\ \frac{1}{r}\frac{d}{dr}\left(r\frac{dE_1}{dr}\right) + f(r)E_o = 0 \\ \frac{1}{r}\frac{d}{dr}\left(r\frac{dE_2}{dr}\right) + f(r)E_1 = 0 \end{cases}$$

where $$f(r) = -\beta^2\left[1 - \frac{\omega_p^2(r)}{(\omega - \beta u_o(r))^2}\right] \tag{35}$$

Solutions obtained by solving the equations in (35) in an iterative fashion yielding

$$E_0 = B$$

$$E_1 = -B\int_0^r \frac{dr'}{r'}\int_0^{r'} f(r'')\, r''\, dr''$$

$$E_2 = B\int_0^r \frac{dr'}{r'}\int_0^{r'} f(r'')\, r''\, dr'' \int_0^{r''} \frac{dr'''}{r'''}\int_0^{r'''} f(r'''')\, r''''\, dr'''' \qquad (36)$$

then

$$E_{1z} = B\left[\, 1 - \int_0^r \frac{dr'}{r'}\int_0^{r'} f(r'')\, r''\, dr'' + \ldots.\right] \qquad (37)$$

This solution for E_{1z} can now be evaluated for any given plasma inhomogeneity expressed as a combination of plasma parameters $\omega_p^2(r)$ and $\bar{u}_0(r)$. It is of interest to consider the solution obtained by this method for the homogeneous case where constant. Evaluation of Eqn. (37) yields

$$E_{1z} = B\left[\, 1 - \frac{fr^2}{4} + \frac{f^2 r^4}{64} - \ldots.\right] \qquad (38)$$

This series solution is simply the series representation of the modified Bessel function I_0 and

$$E_{1z} = B\, I_0\left\{ \beta\left[\, 1 - \frac{\bar{\omega}_p^{\,2}}{(\omega - \beta\bar{u}_0)^2}\right]^{1/2} r \right\} \qquad (39)$$

The series solutions represented by Eqn. (37) has been applied to several types of plasma inhomogeneity and the results are shown in Table 1. The first three terms of the solutions are given since it will be shown in a later section that these are sufficient to obtain a reasonably accurate dispersion relation. The types of plasma inhomogeneity that are included are those that one would expect in a bounded, cylindrical plasma.[23,32] These variations include linear and quadratic variations in the electron density, or plasma frequency. Recent measurements by Kerzar and Weissglas[32] of the electron drift velocity in a bounded, cylindrical plasma column have not shown a significant radial variation, hence, only a linear variation in electron drift velocity was considered. Some curves showing variations in plasma frequency, or electron density, and electron drift velocity are shown in Figure 2.

B. Free-Space Region.

In the free-space region surrounding the bounded, cylindrical plasma column, the equations for E_{1z} and H_{1z} can be written as

$$\begin{cases} \frac{1}{r}\frac{d}{dr}\left(r\frac{dE_{1z}}{dr}\right) - (\beta^2 - k^2)E_{1z} - \frac{n^2}{r^2}E_{1z} = 0 \\ \frac{1}{r}\frac{d}{dr}\left(r\frac{dH_{1z}}{dr}\right) - (\beta^2 - k^2)H_{1z} - \frac{n^2}{r^2}H_{1z} = 0 \end{cases} \tag{40}$$

The solutions of these equations are simply the modified Bessel functions of the second kind of order.

$$\begin{cases} E_{1z} = C\,K_n(pr) \\ H_{1z} = D\,K_n(pr) \end{cases} \tag{41}$$

where $p = (\beta^2 - k^2)^{1/2}$

C,D = arbitrary constants

For the azimuthally symmetric ($n = 0$) and slow wave conditions ($k^2 << \beta^2$)

$$\begin{cases} E_{1z} = C\,K_0(\beta r) \\ H_{1z} = D\,K_0(\beta r) \end{cases} \tag{42}$$

Again, the exp $i(\omega t - \beta z)$ variation and a second component of the general solution for E_{1z} and H_{1z} that becomes infinite as $r \to \infty$ have not been included in these expressions.

C. Dielectric Region Solutions.

To obtain a solution for E_{1z} and H_{1z} in the dielectric tube region one can take a linear combination of the plasma region and free-space region solutions appropriately modified by the dielectric constant of the tube. For the homogeneous plasma case the solutions are given by

$$\begin{cases} E_{1z} = A_d\, I_o(n_d \beta r) + B_d\, K_o(n_d \beta r) \\ H_{1z} = C_d\, I_o(n_d \beta r) + D_d\, K_o(n_d \beta r) \end{cases} \tag{43}$$

where n_d = dielectric refractive index = $\epsilon_d^{1/2}$,

A_d, B_d, C_d, D_d are arbitrary constants.

Corresponding solutions can be written for the inhomogeneous plasma cases using the solutions for E_{1z} given in Table 1.

Dispersion Relations.

In this section dispersion relations for the plasma column in free-space, the plasma column bounded by a thin dielectric tube, and for the case of a bounded plasma column surrounded by a helix will be obtained. The dispersion relations will be obtained by utilizing the equations that represent the boundary conditions of the three configurations. The general dispersion relations will also be evaluated for the case of the homogeneous plasma.

For the plasma column in free space, the tangential component of the electric field must be continuous at the boundary of the plasma column at r = a. This boundary condition can be represented by the following set of equations

$$\begin{cases} E_{1z}^{i}(a) - E_{1z}^{e}(a) = 0 \\ H_{1\theta}^{i}(a) - H_{1\theta}^{e}(a) = 0 \end{cases} \tag{44}$$

where the i and e superscripts refer to the plasma region and free-space region respectively. Rearranging these equations yields

$$\frac{E_{1z}^{i}(a)}{H_{1\theta}^{i}(a)} = \frac{E_{1z}^{e}(a)}{H_{1\theta}^{e}(a)} \tag{45}$$

Thus the boundary condition can be considered as an impedance match at the surface of the plasma column. The transverse impedance defined by Eqn. (45) is the absolute value of the transverse impedance used by Stratton.[33] Substituting the solutions obtained in the previous

section and using the relations presented in Appendix A yields the following dispersion relation for the azimuthally symmetric slow plasma wave

$$\frac{\frac{d}{dr} E_{1z}^{i}(a)}{\beta E_{1z}^{i}(a)} = - \frac{K_1(\beta a)}{K_0(\beta a)} \tag{46}$$

This equation can be considered the general dispersion relation for the plasma column in free-space. For the case of the homogeneous plasma, Equation (46) becomes

$$\frac{q_1 a I_1(q_1 a)}{\beta a I_0(q_1 a)} = - \frac{K_1(\beta a)}{K_0(\beta a)} \tag{47}$$

where

$$q_1 = \beta \left[1 - \frac{\bar{\omega}_p^2 a^2 / c^2}{(ka - \beta a \bar{u}_0/c)^2} \right]^{1/2}$$

From Eqn. (47) ka may be determined as a function of βa (βa is assumed to be real in this instance) to yield dispersion curves for the bounded, homogeneous drifting plasma column. The results of this evaluation are shown in Figure 3 as a function of the homogeneous plasma parameters. The curves clearly indicate the familiar[2,4,9] resonance effect that occurs at the plasma frequency for $\bar{u}_0/c = 0$. For representative non-zero values of $\bar{u}_0/c$ the dispersion curves have two branches depending on the sign of $\bar{u}_0$. The resonance is

shifted above or below $\omega = \bar{\omega}_p$, by an amount proportional to $\beta a \bar{u}_o / c$. It is also of interest to note that there is a region on the negative branch where the group velocity and phase velocity are of opposite sign.

It should be noted that only one quadrant of the dispersion diagram was shown in Figures 3 and 4. An entire dispersion is shown in Figure 5 for a case where $\bar{u}_o$ is a reasonably large value. The interesting point is the crossing of the $+\beta a$ axis by the branch labeled B1. This effect will be of interest when the plasma-helix system is considered later in this section.

The same evaluation was carried out using the series solution for E_{1z}^i and the results are shown in Figure 4 for the case of $\bar{u}_o = 0$. These results show that series solutions for E_{1z}^i can be used to obtain relatively accurate dispersion curves. These results will be of importance in the next section where the dispersion curves for the bounded, inhomogeneous drifting plasma will be obtained.

The dispersion relation for the plasma column bounded by a thin dielectric tube is of interest so that the effect of the tube can be determined. Since the effect of the tube can be expected to be the same regardless of whether the plasma is homogeneous or inhomogeneous, the dispersion relation for the case of the homogeneous plasma will be obtained. For this system the tangential component of the electric field must be continuous at the plasma-dielectric ($r = a$) and dielectric-free-space ($r = b$) boundaries and the boundary condition equations can be written as

$$\begin{cases} E_{1z}^i(a) = E_z^d(a) \\ H_{1\theta}^i(a) = H_{1\theta}^d(a) \end{cases} \tag{47}$$

where the d superscript refers to the dielectric region

and

$$\begin{cases} E_{1z}^{d}(b) = E_{1z}^{e}(b) \\ H_{1\theta}^{d}(b) = H_{1\theta}^{e}(b) \end{cases} \tag{48}$$

Again, this type of boundary condition can be interpreted as an impedance match at the two surfaces. Substitution of the solution obtained for the homogeneous plasma and use of the relations in Appendix A leads to the following dispersion relation for the homogeneous plasma-dielectric tube system

$$\eta_p \frac{I_1(\eta_p \beta a)}{I_0(\eta_p \beta a)} = -\eta_d^3 \frac{\Gamma_2}{\Gamma_1}$$

where

$$\eta_p = \left[1 - \frac{\bar{\omega}_p^2 a^2/c^2}{(ka - \beta a \bar{u}_0/c)^2} \right]^{1/2}$$

$$\eta_d = \epsilon_d^{1/2} \tag{49}$$

$$\begin{aligned} \Gamma_2 = & -I_1(\eta_d \beta a) K_0(\eta_d \beta b) K_1(\beta b) \\ & - I_0(\eta_d \beta b) K_1(\eta_d \beta a) K_1(\beta b) \\ & - I_1(\eta_d \beta b) K_1(\eta_d \beta a) K_0(\beta b) \\ & + \eta_d^3 I_1(\eta_d \beta a) K_0(\beta b) K_1(\eta_d \beta b) \end{aligned}$$

$$\begin{aligned} \Gamma_1 = & I_0(\eta_d \beta a) K_0(\eta_d \beta b) K_1(\beta b) \\ & - I_0(\eta_d \beta b) K_0(\eta_d \beta a) K_1(\beta b) \\ & - \eta_d^3 I_0(\eta_d \beta a) K_1(\eta_d \beta b) K_0(\beta b) \\ & + \eta_d^3 I_1(\eta_d \beta b) K_0(\eta_d \beta a) K_0(\beta b) \end{aligned}$$

This complex expression has been evaluated as a function of the ratio of dielectric tube thickness (t) to plasma column radius (a) and the results are shown in Figure 6. The curves shown are for a homogeneous plasma with $\omega_p a/c = 1.0$ and $\bar{u}_o = 0$. The results show that the effect of a thin ($t/a < .2$) dielectric tube can be neglected since only a small deviation occurs when the effect of the dielectric tube is considered. Based on these results, the effect of the dielectric tube will not be considered in the following section where the inhomogeneities of the plasma are considered.

To obtain the dispersion relation for the case of a bounded plasma column surrounded by a sheath helix a model for the helix will be required. The sheath helix will be used as a model for the helix in order to keep the problem in a tractable form. This well-known model[34,35,36] of the helix is a circular cylindrical surface assumed to be perfectly conducting in the ϕ -direction (see Figure 1). Because of the skewed boundary conditions it is necessary that both TE and TM-type modes be present. The applicable boundary conditions at the plasma-helix surface (r = a) are that

a) the tangential component of the electric field be continuous through the surface,

b) the tangential component of the electric field in the helix direction must be zero,

c) the tangential component of the magnetic field intensity must be continuous through the surface.

The boundary conditions listed above can be translated into mathematical equations and expressed as

$$\begin{cases} E_{1z}^{i} + E_{1\theta}^{i} \cot\phi = 0 \\ E_{1z}^{e} + E_{1\theta}^{e} \cot\phi = 0 \\ E_{1z}^{i} \cot\phi - E_{1\theta}^{i} = E_{1z}^{e} \cot\phi - E_{1\theta}^{e} \\ H_{1z}^{i} + H_{1\theta}^{i} \cot\phi = H_{1z}^{e} + H_{1\theta}^{e} \cot\phi \end{cases} \tag{50}$$

where i and e refer to inside the plasma and external to the plasma and ϕ is the helix pitch angle.

Substitution of the solutions for H_{1z}^{i}, H_{1z}^{e}, and E_{1z}^{e} that have been obtained for the homogeneous plasma and use of the relations in Appendix A and many lines of manipulation leads one to the following form of the dispersion relation for the plasma-helix system

$$-\frac{\frac{d}{dr}E_{1z,n}^{i(a)}}{p\,E_{1z,n}^{i(a)}} = -\frac{(p^2a^2 + n\beta a\cot\phi)^2\left[I_n(pa)K_n'(pa) - I_n'(pa)K_n(pa)\right]}{(p^2a^2k^2a^2\cot^2\phi)\,I_n'(pa)\,K_n'(pa)} - \frac{K_n'(pa)}{K_n(pa)} \tag{51}$$

where $p = (\beta^2 - k^2)^{1/2}$

For the slow phase velocity, azimuthally symmetric condition Eqn. (51) simplified to the following form

$$\frac{\frac{d}{dr}E_{1z}^{i}(a)}{\beta\,E_{1z}^{i}(a)} = \frac{\beta^2a^2}{k^2a^2\cot^2\phi}\left[\frac{I_0(\beta a)}{I_1(\beta a)} + \frac{K_0(\beta a)}{K_1(\beta a)}\right] - \frac{K_1(\beta a)}{K_0(\beta a)} \tag{52}$$

The expression can be considered as the general dispersion relation for the plasma-helix system. For small helix pitch angles $\Phi \rightarrow 0$ amd $\cot \Phi \rightarrow \infty$ and the plasma-helix dispersion relation becomes that of the plasma column in free-space (Eqn. 46). Substitution of the homogeneous plasma solution yields

$$\frac{q_1 a I_1(q_1 a)}{\beta a I_0(q_1 a)} = \frac{\beta^2 a^2}{k^2 a^2 \cot^2 \phi}\left[\frac{I_0(\beta a)}{I_1(\beta a)} + \frac{K_0(\beta a)}{K_1(\beta a)}\right] - \frac{K_1(\beta a)}{K_0(\beta a)} \tag{53}$$

For large arguments ($\beta a \geq \sim 4.0$) the ratios of the modified Bessel functions tend toward constants and the dispersion relation simplifies to

$$\frac{q_1 a I_1(q_1 a)}{\beta a I_0(q_1 a)} = \frac{2\beta^2 a^2}{k^2 a^2 \cot^2 \phi} - 1 \tag{54}$$

This dispersion relation has been evaluated as a function of the plasma parameters and helix pitch angle and the results are shown in Figures 7-9. The set of parameters selected for the case shown in Figure 7 resulted in the helix dispersion curve intersecting the higher phase velocity plasma wave and an uncoupled system resulted. The resulting branches of the dispersion curve representing evanescent modes of propagation. In the second case the helix curve did not intersect either of the plasma curves and again an uncoupled system resulted. The third case was arranged so that the helix curve intersected the lower phase velocity plasma curve and the result was a coupled system with growing, or amplifying waves present. These results are quite related to the earlier in traveling wave tubes and wave kinematics.[27,37]

Numerical Evaluation of Dispersion Relations.

In the previous section of this paper, the general form of the dispersion relation for three configurations was considered. Some numerical results and curves were presented for the relatively well-known case of a homogeneous drifting plasma column. We will now consider the case of an inhomogeneous drifting plasma and use the approximate series solutions and the general forms of the dispersion relations to obtain numerical results.

The first case that will be considered is that of the inhomogeneous drifting plasma column in free space. The general form of its dispersion relation is Equation (46). If one takes the inhomogeneous drifting plasma column solutions for E_{1z} shown in Table I and substitutes them into the general dispersion relation, a series of polynomial equations in βa (or ka) will be obtained. The coefficients of the polynomials are functions of frequency, the plasma parameters, and type of inhomogeneity.

For the inhomogeneities considered in cases 1-5, the polynomial forms of the dispersion relations are cubic when a two-term series solution is used. Higher order series solutions and the case where the electron drift velocity has a linear variation result in higher order polynomial equations that can be solved on a digital computer using a program of the type described in Appendix B. The results obtained using the two-term series solution are shown in Figure 10. The dispersion curves show that the inhomogeneity in the electron density tends to reduce the resonance frequency in all cases. The most severe reduction is for the case of a linear variation that goes to zero at the edge of the plasma column. Non-zero wall values and higher order variations in electron density do not reduce the resonant frequency by as large an amount.

References

1. H. Suhl and L. R Walker, Bell System Technical Journal, 33, 939 (1954).

2. L. D. Smullin and P Chorny, Proceedings of the Institute of Radio Engineers, 46, 360 (1958).

3. Ya. B. Fainberg and M. E. Gorbatenko, Zhurnal Tekh. Fiz., 29, 549 (1959). Translation in Soviet Physics - Technical Physics, 9, 487 (1959).

4. A. W. Trivelpiece and R. W. Gould, Journal of Applied Physics, 30, 1784 (1959).

5. B. M. Bulgakov, V. P. Shestopalov, L. A. Shiskin, and I. P. Yakimenko, Zhurnal Tekh. Fiz., 30, 840 (1960). Translation in Soviet Physics - Technical Physics, 5, 791 (1961).

6. S. F. Paik, Journal of Applied Physics, 33, 2468 (1961).

7. W. P Allis, S. J. Buchsbaum, and A Bers, Waves in Anisotropic Plasmas, M.I.T. Press, Cambridge, Mass. (1963).

8. T. H. Stix, The Theory of Plasma Waves, McGraw-Hill Book Co., New York, New York (1963).

9. V. L Granastein, S. P. Schlesinger, and A. Vigants, I.E.E.E., Transactions on Antennas and Propagation, 9, 489 (1963).

10. J. Frey, Université de Paris, Faculté des Sciences - Centre dé Orsay, Laboratoire de Physique des Plasma, Orsay, France; Rapport LP, 53; (2/1965).

11. W. C. Hahn, General Electric Review, 42, 258 (1939).

12. S. Ramo, Physical Review, 56, 276 (1939).

13. A. H W. Beck, Space Charge Waves and Slow Electromagnetic Waves, Pergamon Press, New York - London (1958).

14. N. Marcuvitz, Polytechnic Institute of Brooklyn, Proceedings of the Symposium on Electronic Waveguides, pp. 63-87 (1959).

15. C. C. Johnson, Field and Wave Electrodynamics, McGraw-Hill Book Co., New York (1965).

16. D. Bohm and E. P. Gross, Physical Review, 75, 1851 (1949); 75, 1864 (1949); 79, 992 (1950).

17. E. V. Bogdanov, V. J. Kislov, and Z. S. Tchernov, Proceedings of the Symposium on Millimeter Waves, Polytechnic Institute of Brooklyn (1959).

18. F. H. Clauser, Plasma Dynamics, Addison - Wesley Publishing Co. Reading, Massachusetts (1960). (Chapter 4 by R. W. Gould).

19. R. J. Briggs, Electron - Stream Interactions with Plasmas, M.I.T. Press, Cambridge, Massachusetts (1964).

20. F. W. Crawford, International Journal of Electronics, XIX, 217 (1965).

21. R. J. Briggs and S. F. Paik, "Resonance Absorption of Guided Waves on Inhomogeneous Plasma Columns," to be published in Journal of Applied Physics.

22. F. W. Crawford, Physical Review, 5, 244 (1963) and Journal of Applied Physics, 35, 1365 (1964).

23. S. C. Brown, Basic Data of Plasma Physics, The Technology Press of M.I.T. and John Wiley & Sons, Inc., New York (1959).

24. S. N. Samaddar, Canadian Journal of Physics, 41, 113 (1963).

25. K. N. Stepanov, Zhurnal Tekh. Fiz. 35, 1002 (1965).

26. C. A. Renton and L. W. Zelby, Applied Physics Letters, 6, 167 (1965).

27. P. A. Sturrock, Physical Review, 112, 1488 (1958).

28. L. Spitzer, Physics of Fully Ionized Gases, Interscience Publishers, Inc; New York (1962).

29. E. L. Ince, Ordinary Differential Equations, Dover Publications, New York (1955).

30. W. Magnus, F. Oberhattinger, and F. G. Tricomi, Higher Transcendential Functions, Volume II, A. Erdélyi, Ed., McGraw-Hill Book Company, Inc., New York (1953).

31. R. Langer, Physical Review, 51, 1669 (1937).

32. B. Kerzar and P. Weissglas, Electronics Letters, 1, 43 (1965).

33. J. A. Stratton, Electromagnetic Theory, McGraw-Hill Book Co., New York (1941).

34. S. Sensiper, Electromagnetic Wave Propagation on Helical Conductors, M.I.T. Research Laboratory Electronics Tech. Rpt. 194 (1951).

35. D. A. Watkins, Topics in Electromagnetic Theory, J. Wiley & Sons, Inc., New York (1958).

36. R. E. Collin, Field Theory of Guided Waves, McGraw-Hill Book Co., New York (1960).

37. R. N. Sudan, The Physics of Fluids, 8, 1900 (1965).

CASE NO.	PLASMA FREQUENCY	ELECTRON DRIFT VELOCITY	SERIES SOLUTION for E_{1z}
1	$\omega_p^2(r) = \bar{\omega}_p^2$	$u_o(r) = \bar{u}_o$	$E_{1z} = B\left[1 - \frac{f r^2}{4} + \frac{f^2 r^4}{64} - \cdots\right]$ where $f = -\beta^2\left[1 - \frac{\bar{\omega}_p^2}{(\omega - \beta\bar{u}_o)^2}\right] = -\beta^2\left[1 - \frac{\bar{\omega}_p^2 a^2/c^2}{(ka - \beta a\bar{u}_o/c)^2}\right]$
2	$\omega_p^2(r) = \bar{\omega}_p^2(1 - r^2/a^2)$	"	$E_{1z} = B\left[1 - r^2\left(\frac{f}{4}+\frac{g}{16}\right) + r^4\left(\frac{f^2}{64}+\frac{fg}{576}+\frac{fg}{144}+\frac{g^2}{1024}\right) - \cdots\right]$ where $g = -(f+\beta^2)$
3	$\omega_p^2(r) = \bar{\omega}_p^2(1 - \eta r^2/a^2)$ $0 \le \eta \le 1$	"	$E_{1z} = B\left[1 - r^2\left(\frac{f}{4}+\frac{\eta g}{16}\right) + r^4\left(\frac{f^2}{64}+\frac{fg\eta}{576}+\frac{fg\eta}{144}+\frac{g^2\eta^2}{1024}\right) - \cdots\right]$ $0 \le \eta \le 1$
4	$\omega_p^2(r) = \bar{\omega}_p^2(1 - r/a)$	"	$E_{1z} = B\left[1 - \frac{f r^2}{4} + \frac{g r^3}{9a} - \cdots\right]$
5	$\omega_p^2(r) = \bar{\omega}_p^2(1 - \eta r/a)$	"	$E_{1z} = B\left[1 - \frac{f r^2}{4} + \frac{g\eta r^3}{9a} - \cdots\right]$ $0 \le \eta \le 1$
6	$\omega_p^2(r) = \bar{\omega}_p^2$	$u_o(r) = \bar{u}_o(1 - r/a)$	$E_{1z} = B\left[1 - \frac{f r^2}{4} + \frac{2\beta^3\omega^2\bar{u}_o r^3}{9(\omega - \beta\bar{u}_o)^3 a} - \cdots\right]$

Table 1 Summary of Solutions for E_{1z}.

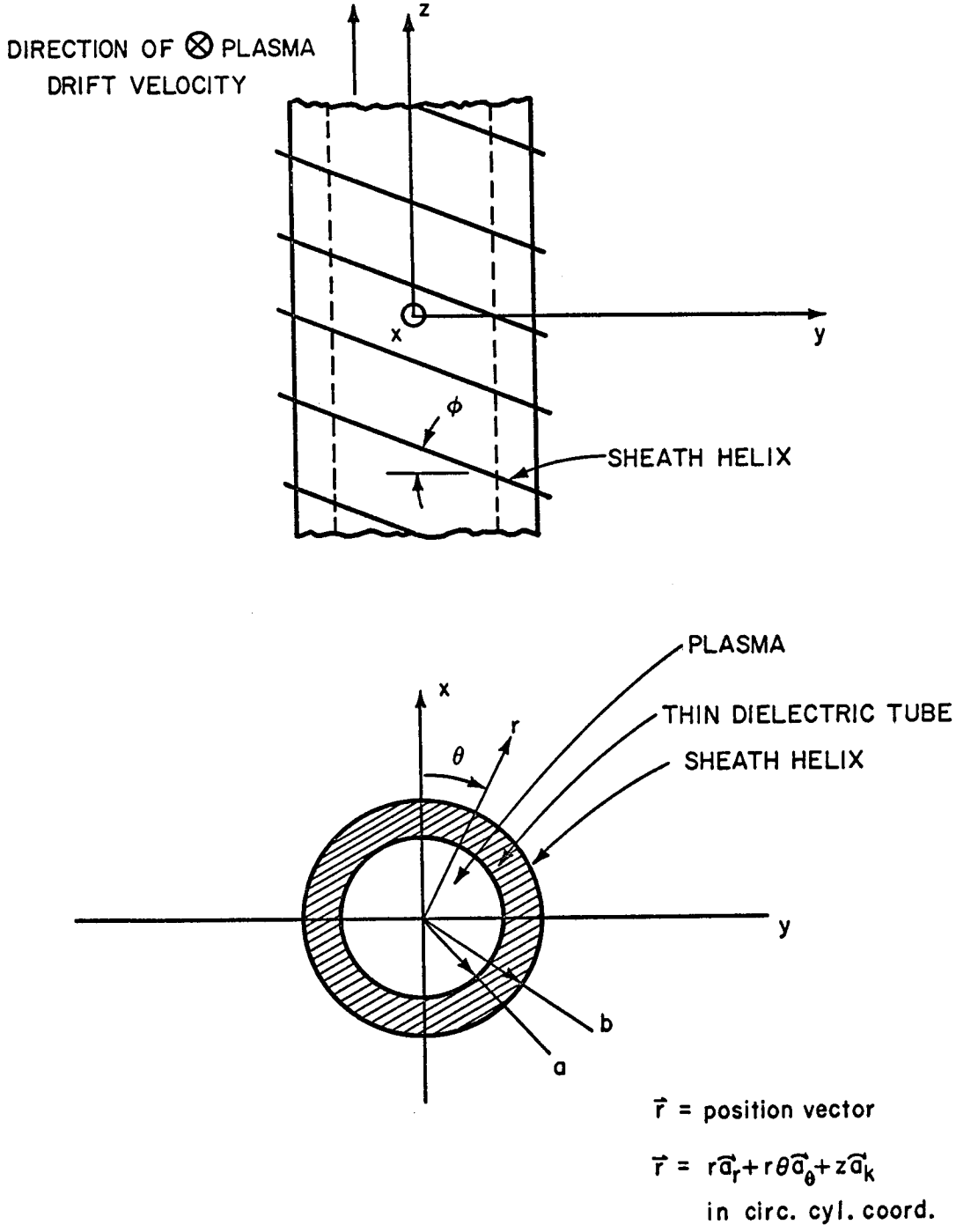

Figure 1. Circular Cylindrical Coordinate System.

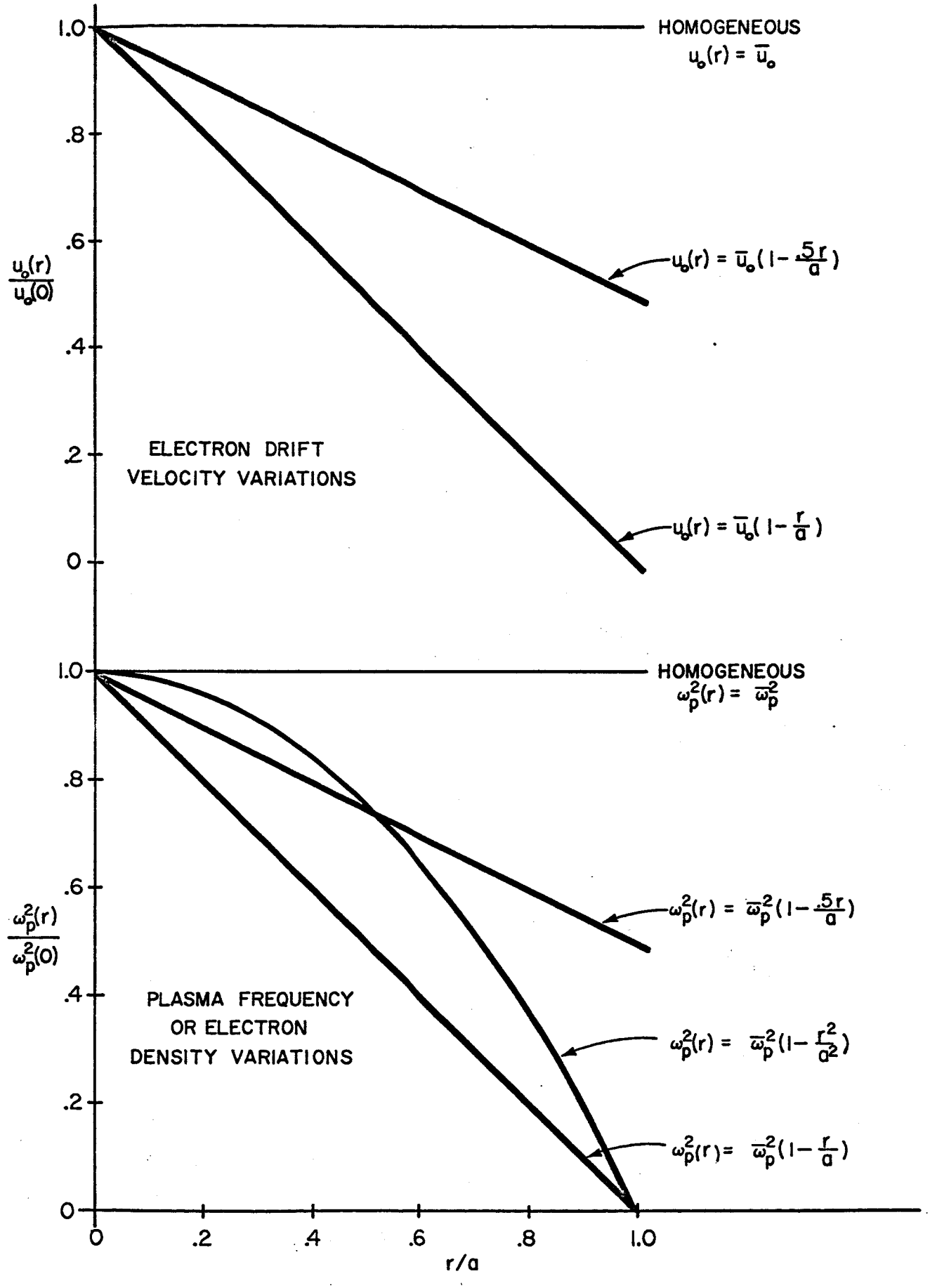

Figure 2. Typical Plasma Inhomogeneities.

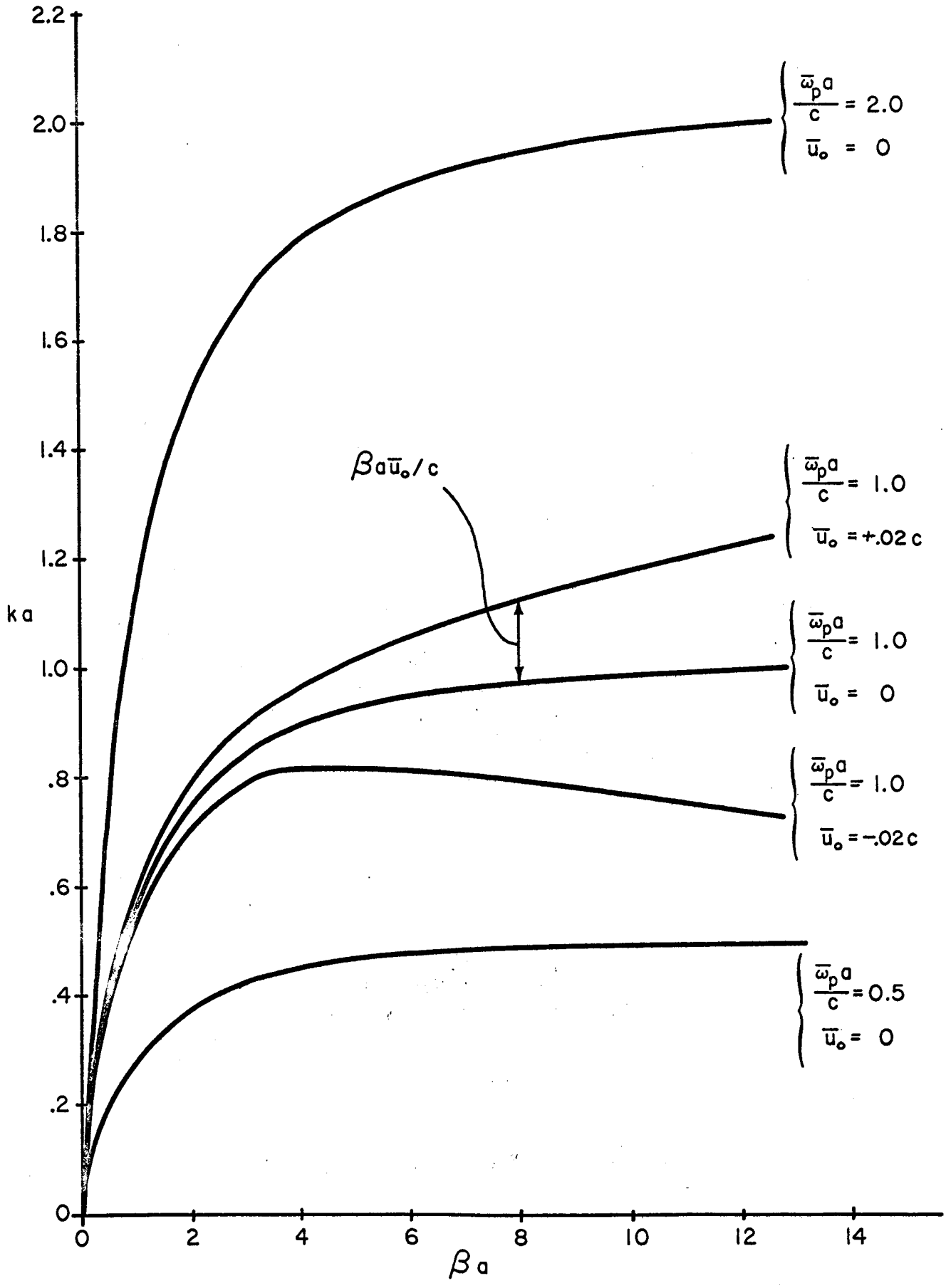

Figure 3. Homogeneous Drifting Plasma Dispersion Curves.

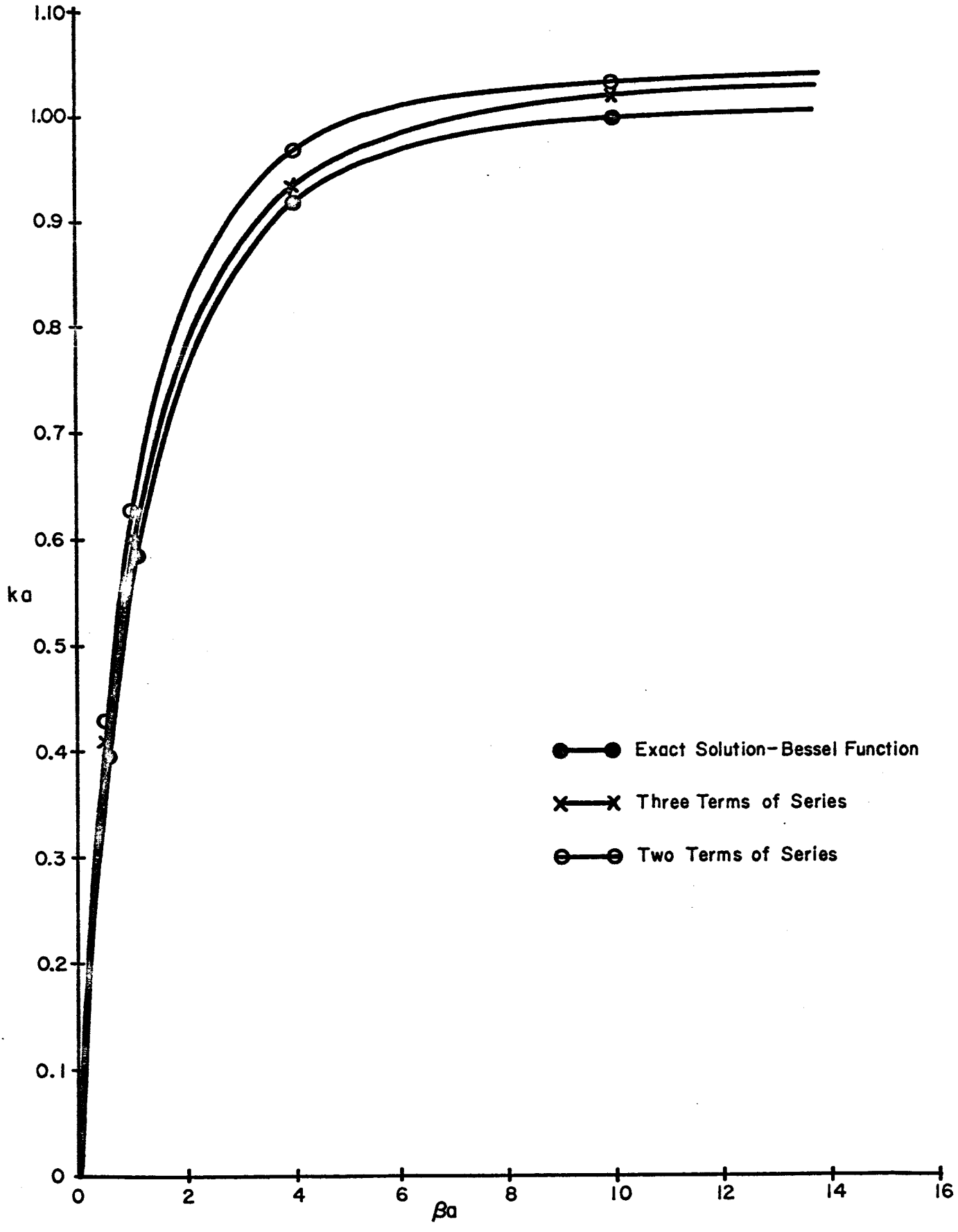

Figure 4. Comparison of Dispersion Curves Obtained with Series Solutions.

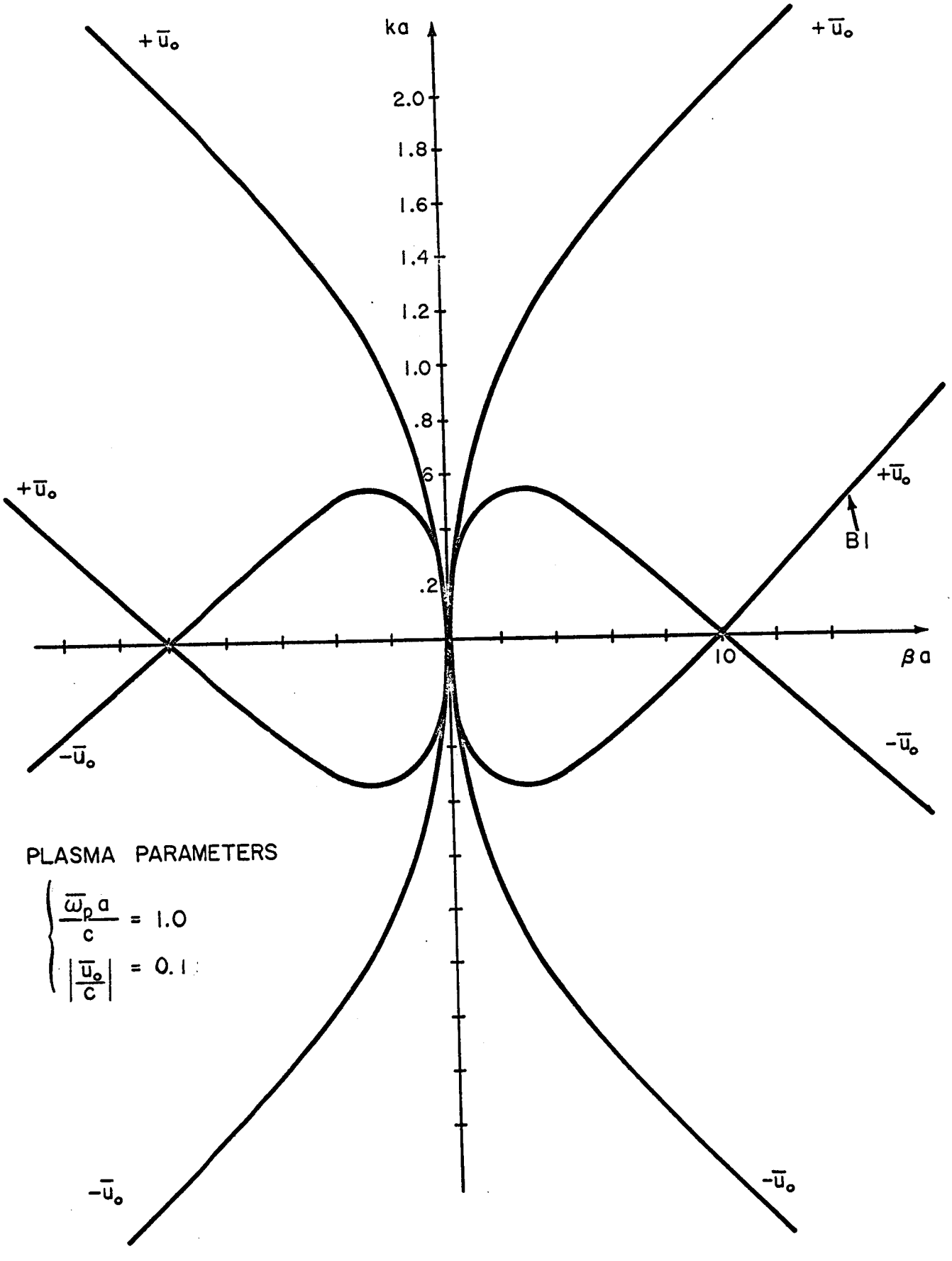

Figure 5. Complete Dispersion Curves.

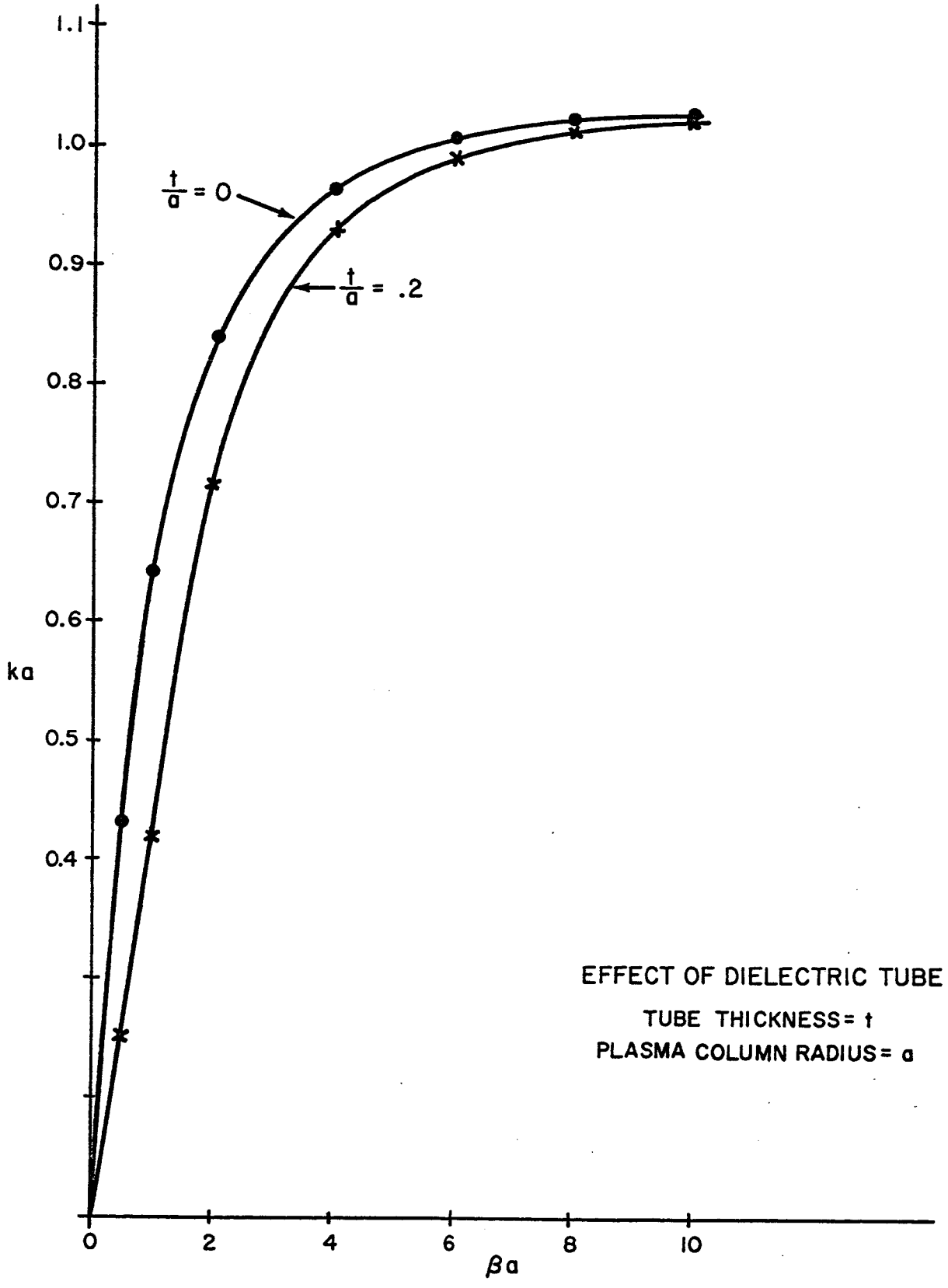

Figure 6. Dispersion Curves Showing the Effect of the Dielectric Tube.

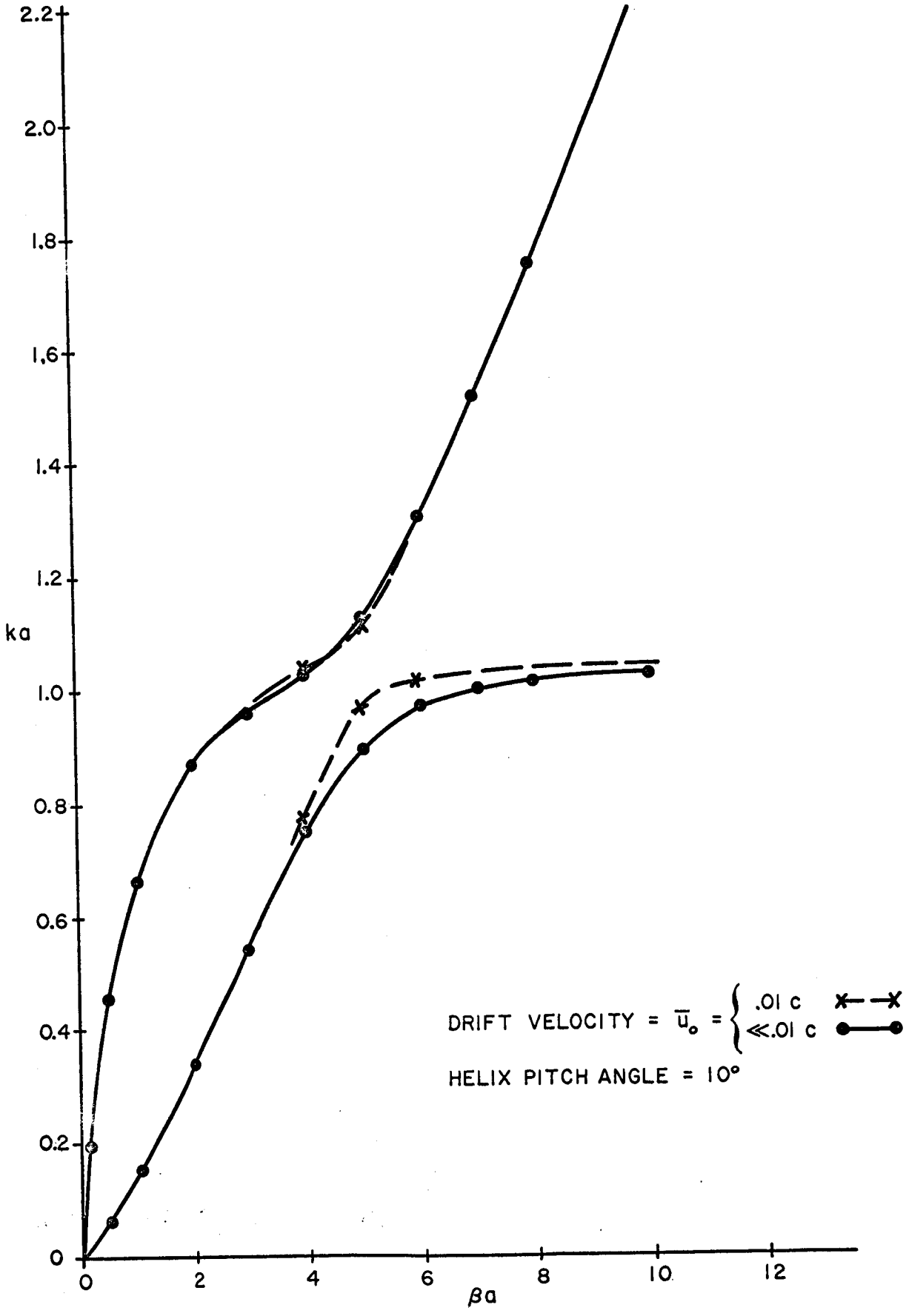

Figure 7. Plasma - Helix System Dispersion Curves.

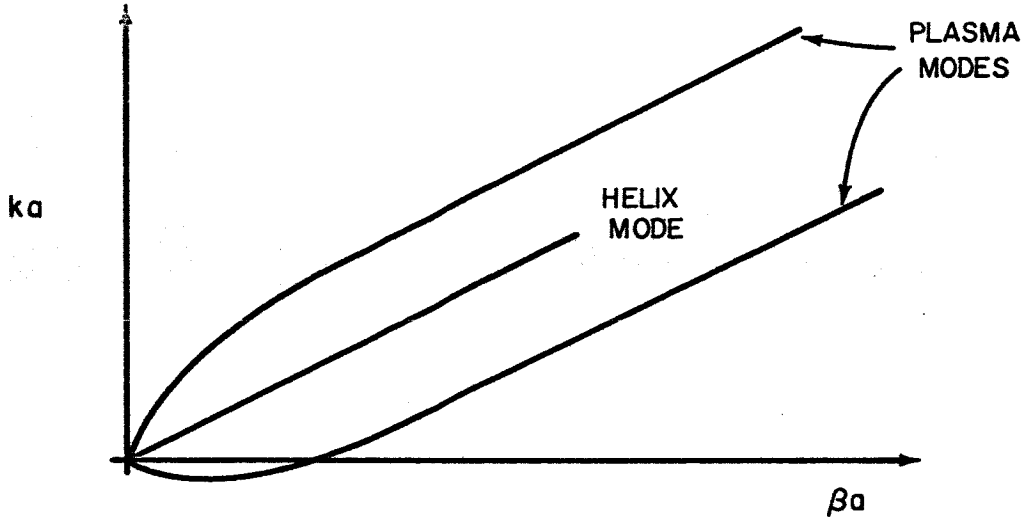

Figure 8. Plasma - Helix Dispersion Curves - Uncoupled Systems.

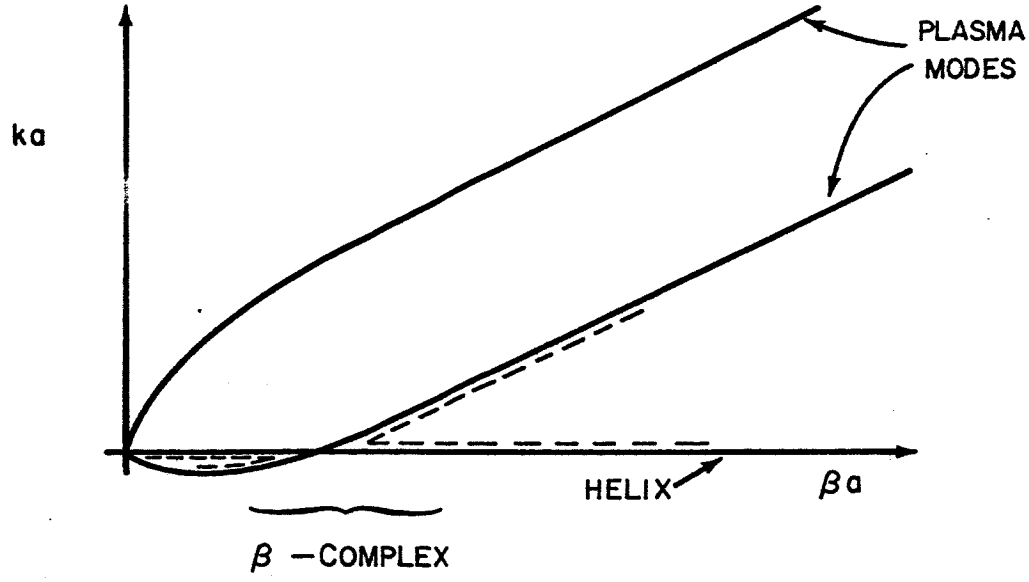

Figure 9. Plasma - Helix Dispersion Curves - Coupled System.

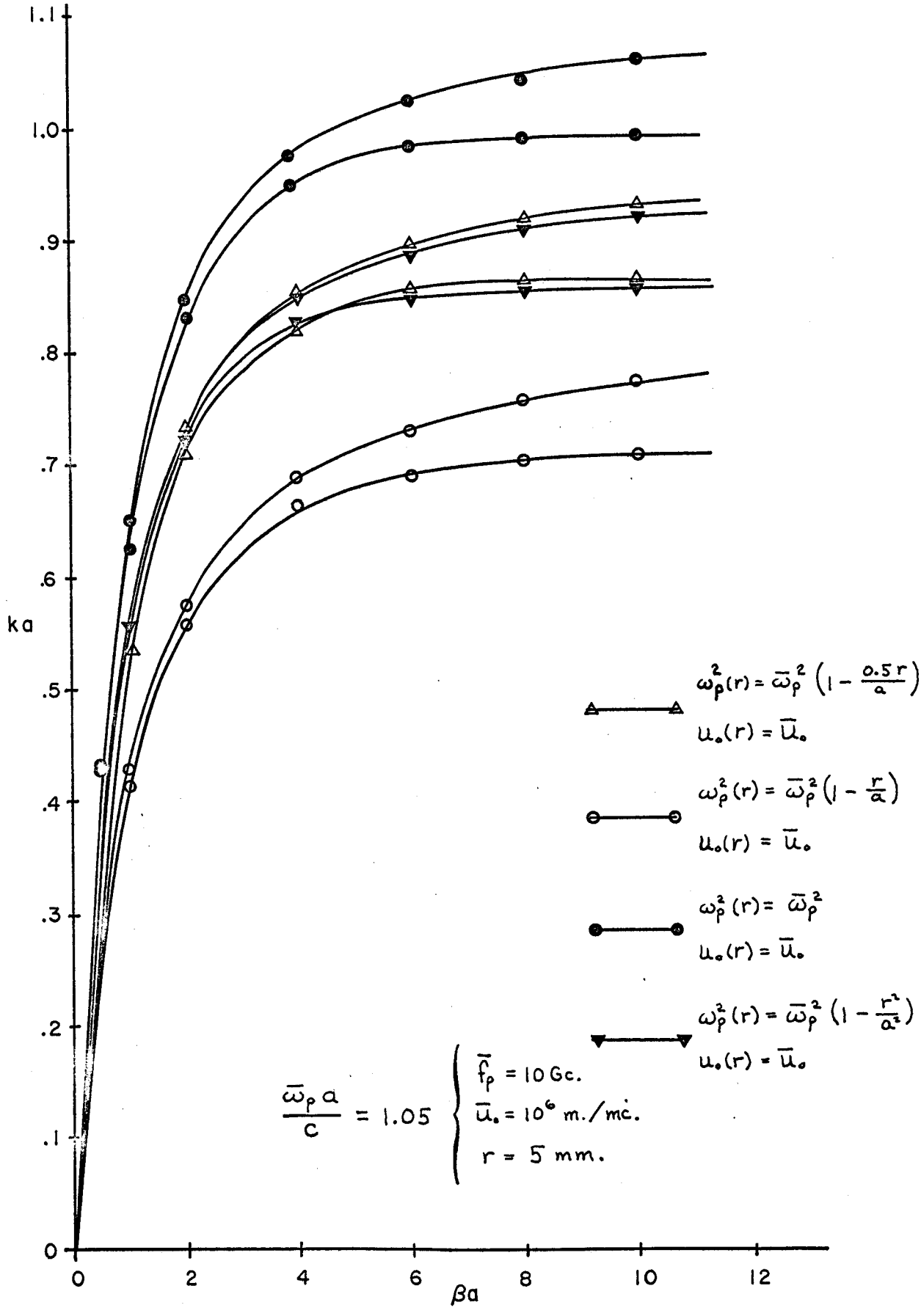

Figure 10. Inhomogeneous Drifting Plasma Dispersion Curves.

3.3 Measurement of Plasma Transport Properties in a Na-K Seeded Argon Plasma

Dr. Chad F. Gottschlich, Mr. T. K. Chu

The objective of this work is to measure the non-equilibrium ionization produced by an externally applied electric field in a Na-K seeded argon plasma.

Non-equilibrium ionization occurs because the electric field supplies energy preferentially to electrons. Although the atoms and ions are raised in temperature by collisions with the electrons, because of the large mass difference between electrons and atoms, only a small fraction of the electron's energy is transferred to the atom in an electric collision. The result is a large difference between electron and atom translational temperatures.

The existing theory of an elevated electron temperature is quite simple and has been discussed by Kerrebrock[1] and Hurwitz, et. al.[2] as well as by others. For a steady-state, spatially uniform plasma the electron temperature may be calculated from an energy balance in terms of the rate at which energy is delivered to the electrons and the rate at which the electrons transfer energy to the heavy particles by collisions. Under steady state conditions, the predicted temperature difference is

$$T_e - T_A = \frac{2}{3} \frac{M_A}{R\delta} \left(\frac{\sigma E}{e n e}\right)^2$$

where T_e is the electron temperature, T_A is the atom temperature, M_A is the molecular weight of the atoms, R is the universal gas

constant, σ is the electrical conductivity, E is the electric field intensity, e is the electronic charge, n_e is the electron number density, and δ is a constant characteristic of the heavy particles. For electron collisions with atoms δ is about 2. For collisions with molecules δ is of the order of 10 to 1000.

Experimental work (Ref. 1, 3, 4) has confirmed this equation at least qualitatively. The average temperature and conductivity of a presumably spatially-non-uniform plasma has been reported. In all of these experiments the temperature of the gas was assumed to be unchanged by the presence of an electric field.

The purpose of this research is to measure the following quantities:

1. The electron temperature and its spatial variation.
2. The gas temperature and its spatial variation.
3. The average conductivity of the plasma.

In this experiment from local measurements of electron and gas temperature, the local value of conductivity can be deduced; this value can then be compared with the measured average value.

The experimental setup is shown schematically in Fig.3.3-1. A liquid sodium-potassium alloy is metered and injected through the syringe (Ref. 5) and then mixed with preheated argon before it goes into the vaporizing boiler. The boiler is situated in a muffle furnace maintained at $800^{\circ}C$. The argon-Na-K vapor then goes into a mixing chamber where it is mixed with additional argon gas heated by an arc jet. The mixed and heated gas then enters the test section. The entire system can give a test section gas temperature as low as $1250^{\circ}K$.

The test section is shown in Fig. 3.3-2. The opening mid-way of the test section is for visual and spectroscopic observation. The probes inserted in the gas, allow measurement of voltage drops along the gas column from which average conductivity values can be deduced.

In this experiment the gas temperature is measured by using thermocouples with electrically insulated hot junctions (See Fig. 3.3-3). The radiation correction is made by using a series of shields of graded size. By plotting the observed temperature versus the shield diameter and extrapolating to zero diameter, the gas temperature is obtained. A block diagram of the system for electron temperature measurement is shown in Fig. 3.3-4.

The experimental program is nearly completed. Data is currently being analyzed, and preliminary results have been obtained.

Fig. 3.3-5 shows the gas temperature and its radial variation at a location midway in the test section, with a current density in the plasma of 8.18 amps/cm^2. For the most part, the temperature profile is uniform. Fig. 3.3-6 shows the centerline gas temperature as a function of applied current. The gas temperature increases as much as 300^{o}C when current is increased from zero to 15 amps/cm^2. This is particularly important as previous work has assumed no dependence of the gas temperature on the applied electric field.

The electron temperature and electron number densities are obtained from intensity measurements with a spectrophotometer. Fig. 3.3-7 shows an intensity measurement as it appears on the strip chart recorder. The symmetry of the profile is good. An approximate

inversion yields the radial distribution of electron number density and hence the electron temperature. These results are shown in Fig. 3.3-8. Again, all radial gradients are mild.

Fig. 3.3-9 shows resulting conductivity values as a function of current density. It should be mentioned that both the gas temperature and the electron temperature are different for each experimental point on this curve.

Since most of our data are being analyzed presently, final conclusions cannot yet be drawn. Qualitatively, however, we can conclude that:

1. Increased ionization above that found for equilibrium plasmas does exist in an argon-Na-K system when it is subjected to a sufficiently large externally applied electric field. In this non-equilibrium state, bound and free electrons are in thermodynamic equilibrium.

2. For a cylindrical test section the radial distribution of gas and electron temperature is approximately uniform except in a region near the wall. This indicates that conductivity values obtained by averaging over the cross-section agree closely with the local conductivity values.

3. The gas temperature increases as current density in the plasma increases. This observed rise of gas temperature casts doubts on the validity of experimental conductivity values previously reported in the literature (Ref. 1, 3, 4). This is particularly so at high current density when the rise of gas temperature is large.

The results and tentative conclusions presented above are all preliminary.

References

1. J. L. Kerrebrock, AIAA 2, 1072, and M. A. Hoffman, 1080.

2. H. Hurwitz, Jr., G. W. Sutton, S. Tamor, ARS Journal 32.

3. E. E. Zukoski, E. G. Cool, and G. Gibson, AIAA 2, 1410.

4. T. A. Cool and E. E. Zukoski, Sixth Symposium on Engineering Aspects of MHD.

5. S. Greehalgh, To be published in Review of Scientific Instruments.

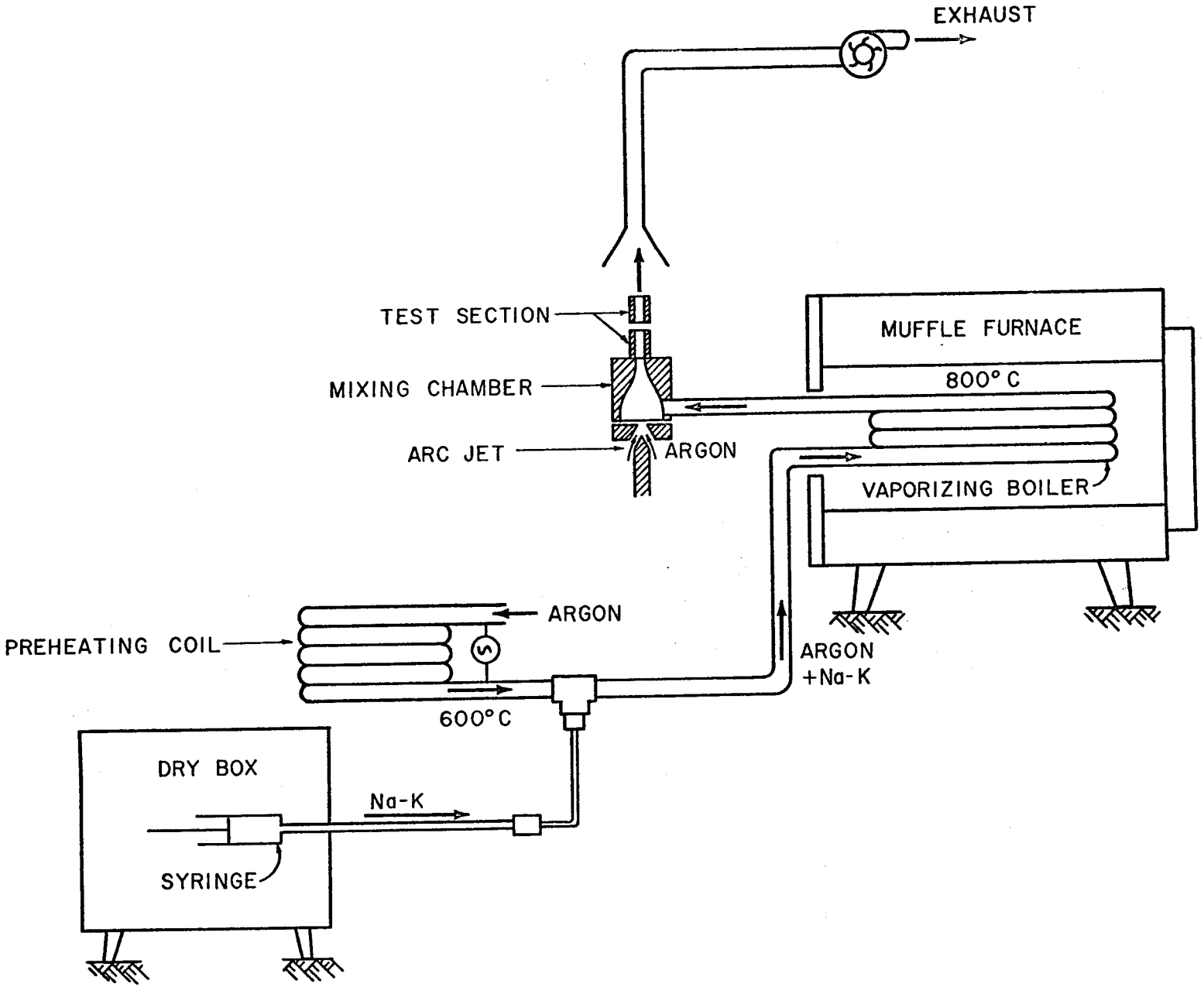

Fig. 3.3-1 SCHEMATIC DIAGRAM OF EXPERIMENTAL SETUP

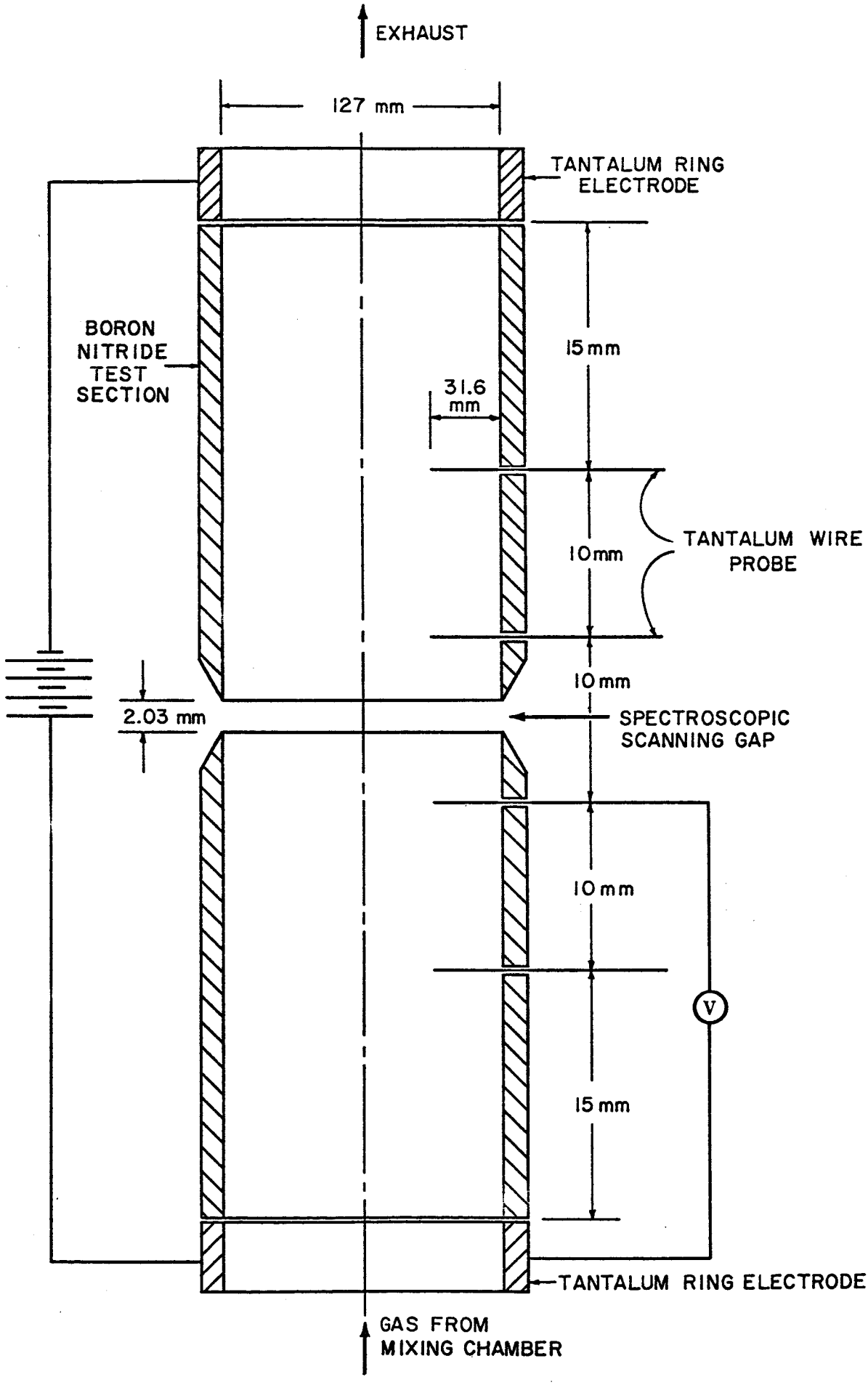

Fig. 3.3-2 TEST SECTION

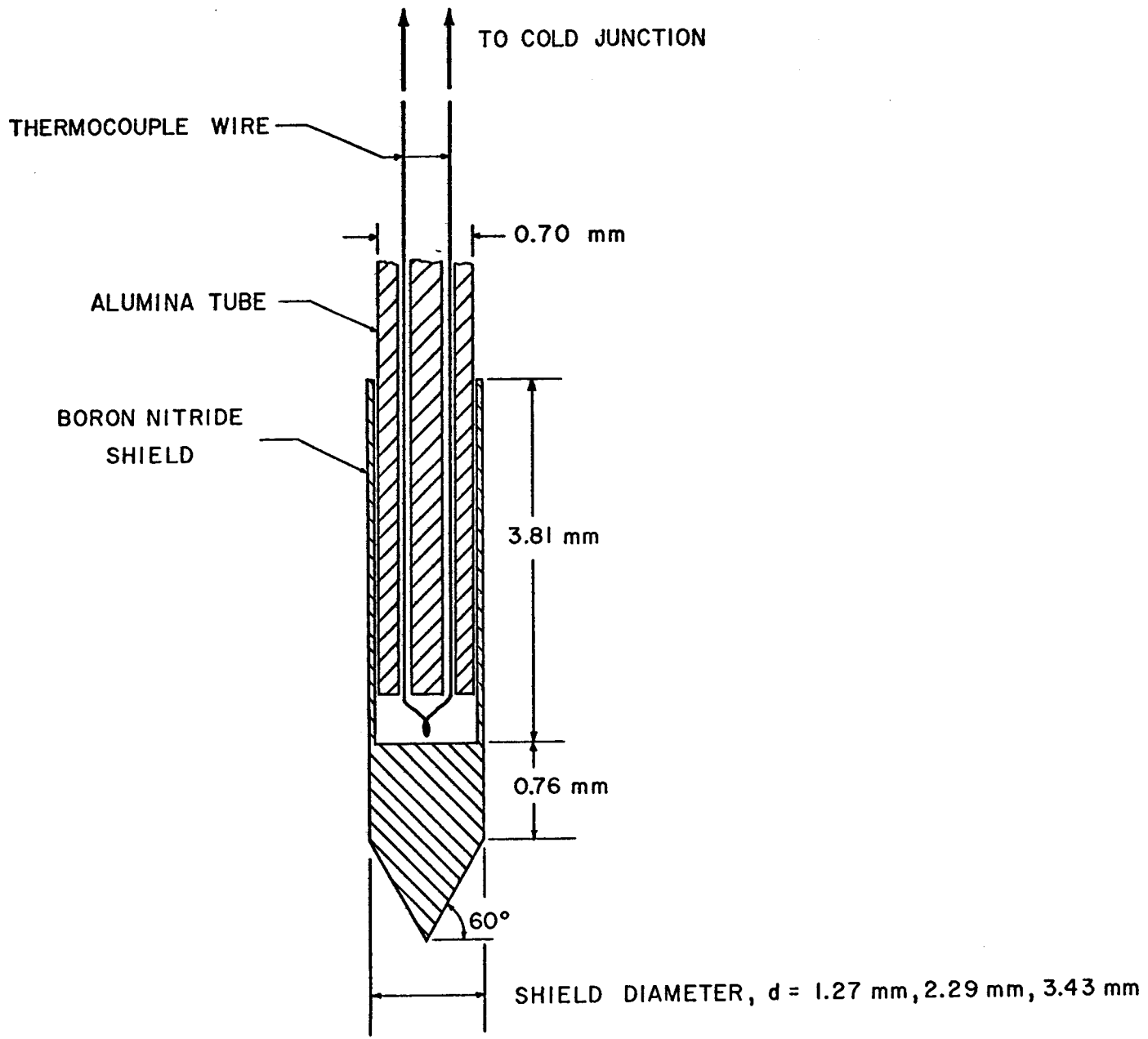

Fig. 3.3-3 HOT-JUNCTION INSULATING SHIELD FOR THERMOCOUPLES

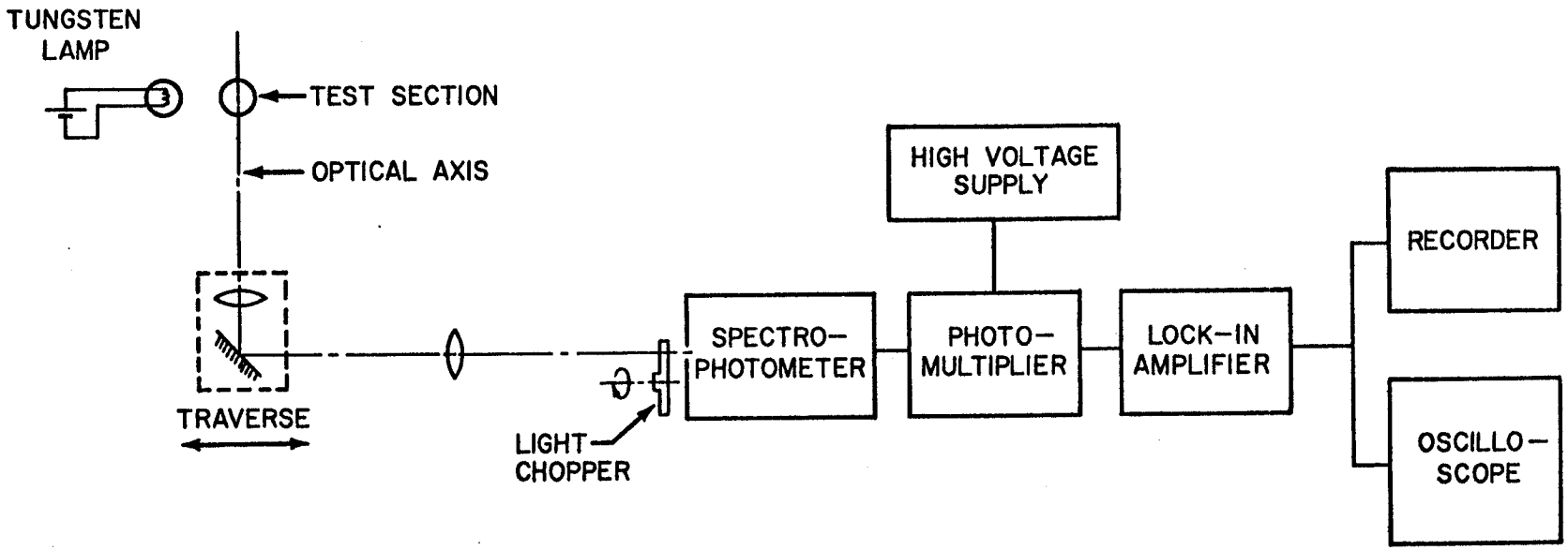

Fig. 3.3-4 INSTRUMENT BLOCK DIAGRAM FOR MEASUREMENT OF ELECTRON TEMPERATURE

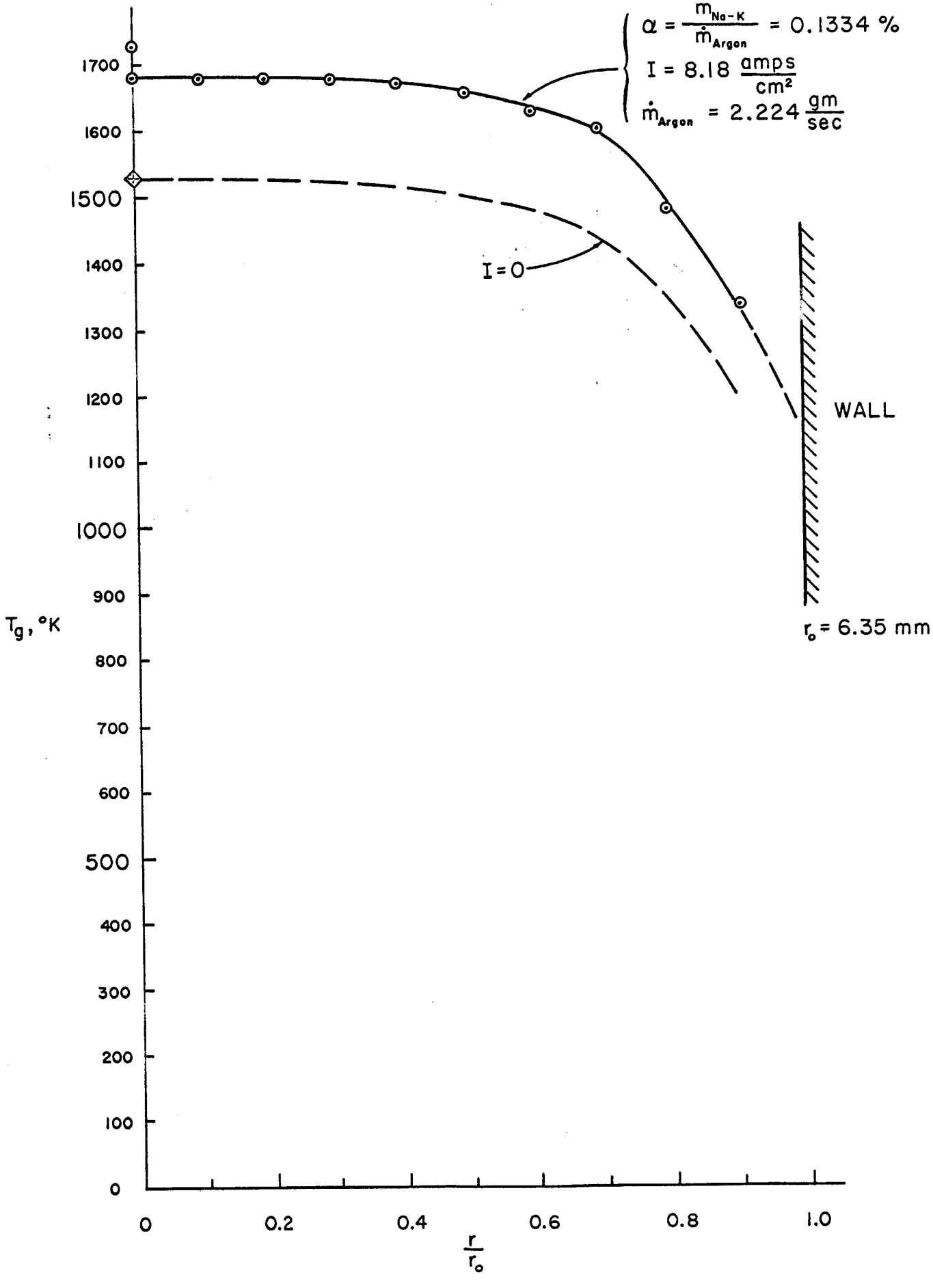

Fig. 3.3-5 RADIAL DISTRIBUTION OF GAS TEMPERATURE

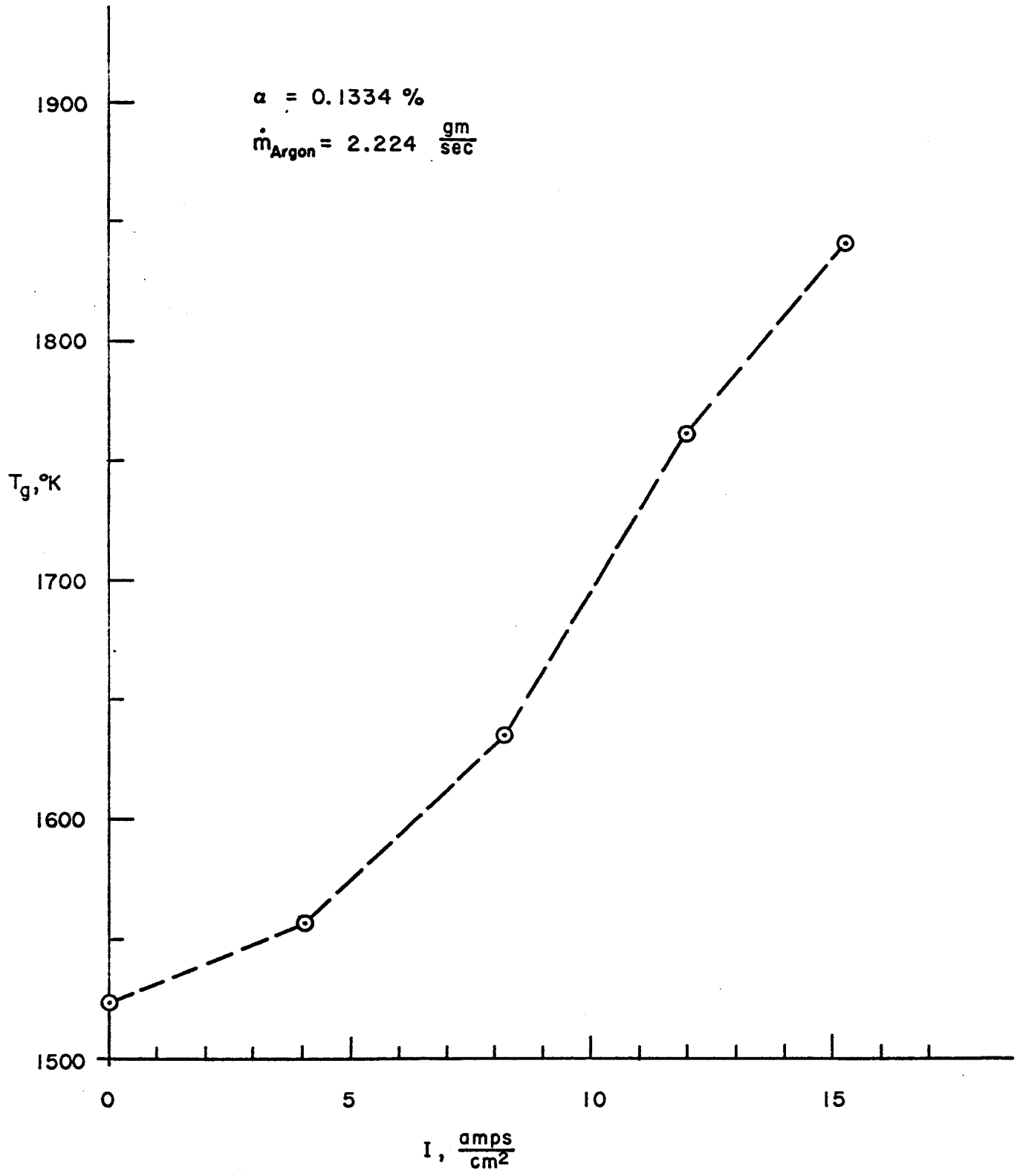

Fig. 3.3-6 CENTERLINE GAS TEMPERATURE VS. CURRENT DENSITY

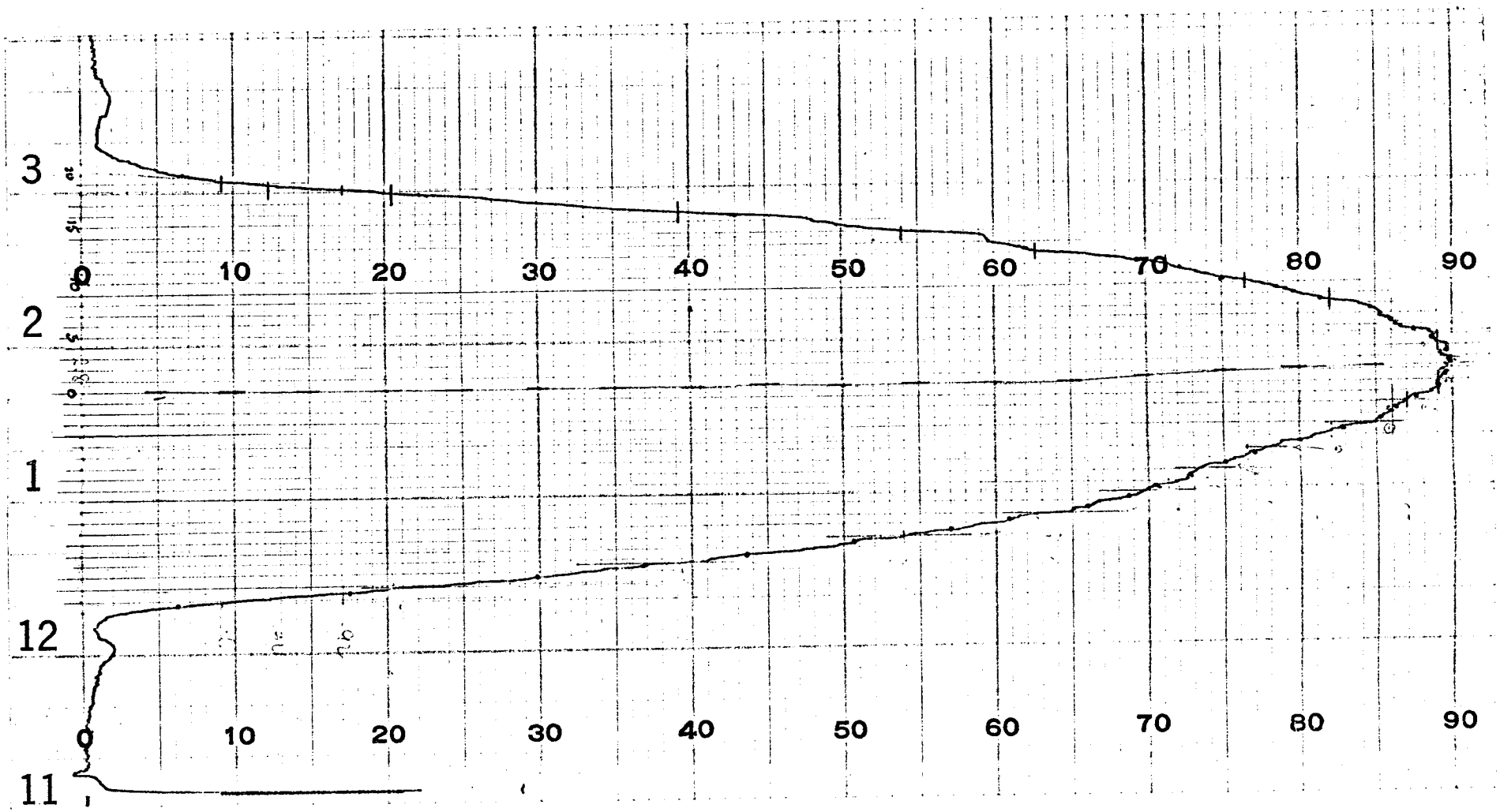

Fig. 3.3-7 SPECTROSCOPIC SCANNING

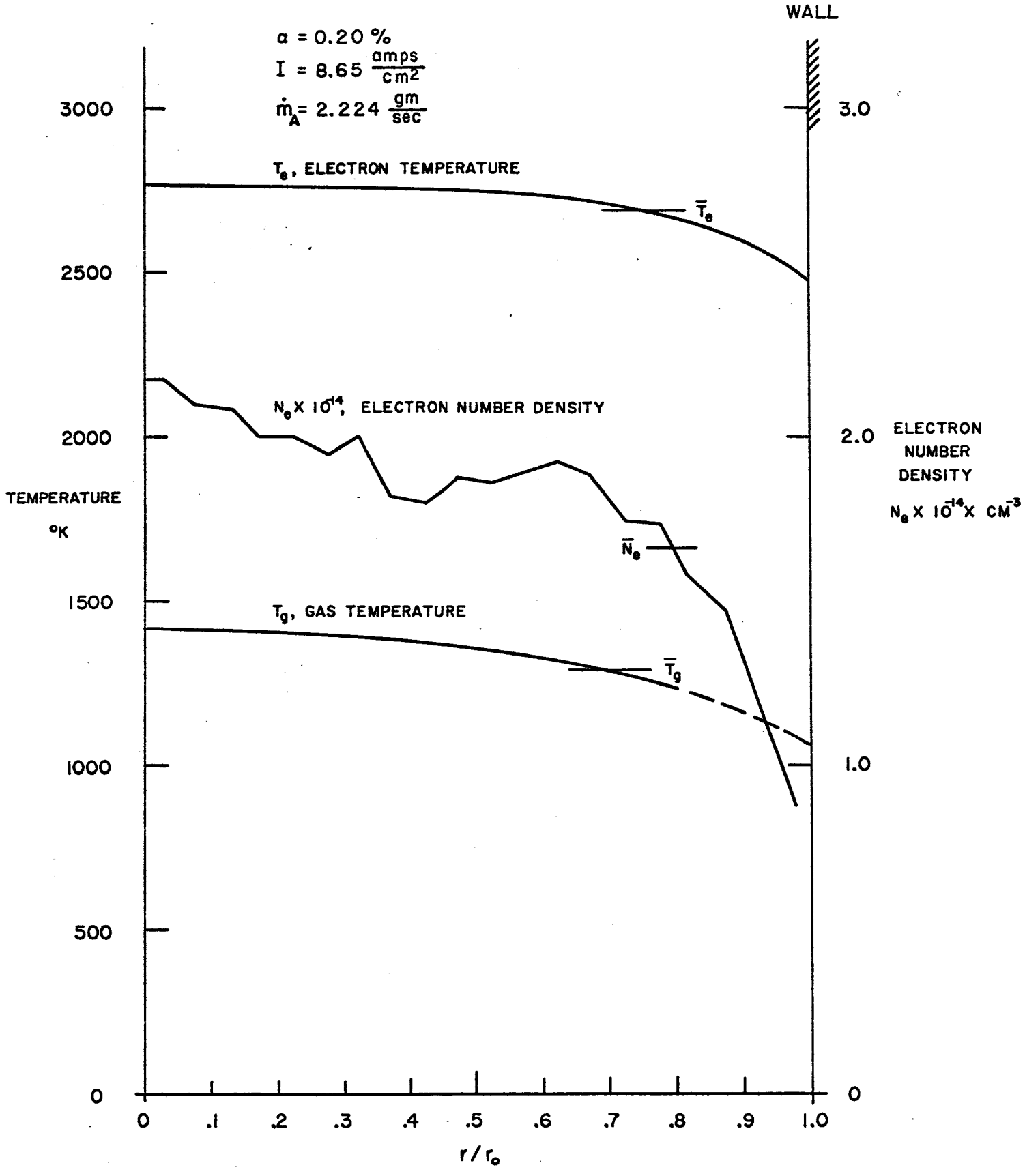

Fig. 3.3-8 RADIAL DISTRIBUTIONS OF ELECTRON TEMPERATURE AND NUMBER DENSITY

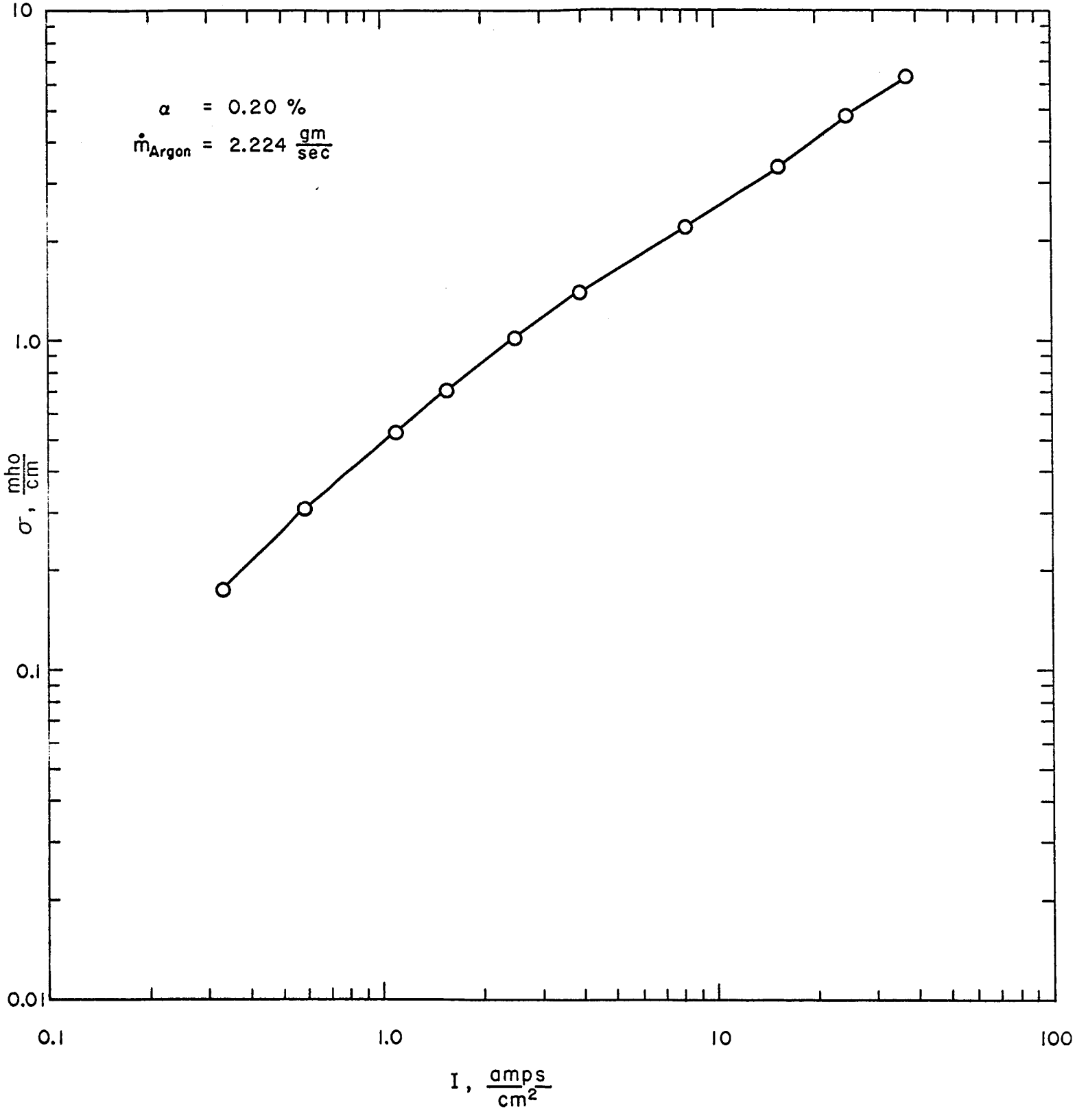

Fig. 3.3-9 CONDUCTIVITY VS. CURRENT DENSITY

3.4 Surface Physics

Dr. Michael Kaplit, Dr. George L. Schrenk

Research is being carried out to expand our knowledge of electron and ion emission from metals in a gaseous environment. One aspect of this work has been an investigation of the models used to correlate emitter performance in thermionic converters. Presently, both quantum-chemical and semi-classical models appear able to correlate the emitter performance of a close-spaced thermionic converter; these models, however, sometime predict different results for untried systems. For example, one quantum-chemical model predicts that for a given adsorbate the greater the work function of the substrate the larger the maximum decrease in work function due to adsorption by highly electropositive elements such as cesium or barium; a semi-classical model predicts no such general rule.

Using the Thomas-Fermi-Dirac theory, both the microscopic charge distribution and the total energy of the interface have been evaluated in such a way that one can distinguish between the classical and the quantum mechanical contributions. The systems investigated (an adsorbed cesium monolayer on the (100) face of tungsten, a 1/2 monolayer of adsorbed barium on the same tungsten face, and a 1/2 monolayer of adsorbed barium on a (110) face of tungsten) were chosen because of their importance to thermionic energy conversion. The results show that the quantum mechanical corrections are indeed a significant part of the total energy and may not be neglected.

Details of this research are presented in the paper that follows.

Research has also been carried out to develop a quantum-chemical microscopic model of electron emission for tertiary systems, such as cesium-fluorine-molybdenum. Results from this work were presented in a paper at the Thermionic Specialist Conference held in San Diego, California on October 25-27, 1965.

MODELS FOR ELECTRON EMISSION FROM METALS WITH ADSORBED MONOLAYERS

M. Kaplit and G. L. Schrenk

Institute for Direct Energy Conversion
University of Pennsylvania
Philadelphia, Pennsylvania

Abstract—The ability of a semi-classical model to describe a metal-gas interface has been investigated theoretically, and the differences between various macroscopic models is discussed. Using the Thomas-Fermi-Dirac theory, both the microscopic charge distribution and the total electronic energy of the interface have been evaluated in such a way that one can distinguish between the classical and quantum mechanical contributions. It has been shown that the quantum mechanical corrections are a significant part of the total energy and may not be neglected. It is concluded that a semi-classical model, using only the concepts of classical atomic physics, is not an adequate representation of the electronic properties of alkali-refractory metal or alkali earth-refractory metal interfaces. Detailed results for both cesium and barium adsorption on (100) and (110) faces of tungsten are presented.

INTRODUCTION

The operation of closely spaced thermionic converters depends primarily on the interaction of the emitter with the surrounding gas. Presently both semi-classical and quantum chemical models appear to be able to correlate emitter performance; these models, however,

sometimes predict different results for untried systems. For example, one quantum chemical model predicts that for a given adsorbate a substrate with a higher work function should exhibit a larger maximum change in the work function as a result of adsorption [1]. A semi-classical model predicts no such general rule [2].

The object of this study is to investigate theoretically the validity of the semi-classical model, using only the concepts of classical physics, to describe a metal-gas interface. Both the microscopic electronic charge distribution and the total energy of a metal-gas interface are calculated quantum mechanically. The total energy is evaluated in such a way that one can distinguish between the classical and the quantum mechanical contributions. It is shown that the quantum mechanical corrections are a significant part of the total energy and may not be neglected. These results imply that the quantum-chemical model rather than the semi-classical model is a better representation of the electronic properties of alkali metal-refractory metal or alkaline earth-refractory metal interfaces. The systems investigated in this work (cesium and barium adsorbed on the (100) and (110) faces of tungsten) were chosen because of their importance to thermionic energy conversion.

A primary difference between the quantum chemical phenomenological model for correlating the macroscopic characteristics of a metal vapor interface and the semi-classical model is the degree or strength of interaction between the adsorbate and the substrate. Gurney [3], Slater [4], Gomer and Swanson [5], Culver and Tompkins [6], and many others describe a weak interaction between the substrate and adsorbate as one for which the energy distribution in the valence

band of the adsorbate does not change appreciably upon adsorption. A strong interaction implies a significant alteration of the energy distribution in the valence bond upon adsorption. As the strength of the interaction increases, it becomes increasingly important to include quantum chemical effects in the surface model.

Rasor and Warner [2], Becker [7], Trapnell [8], Hughes [9], Hughes and Levinstein [10], Luke and Smith [11], MacDonald and Barlow [12], Dobretsov [13], etc., have used semi-classical concepts to describe electron and ion emission from metals immersed in gaseous environment. Rasor and Warner have also tried to justify the weak interaction concept by demonstrating that the shift due to adsorption of the valence of the adsorbed particle is much less than the thermal energy of the adsorbed particle. Their models regard each adsorbed particle as a hard sphere resting either on a perfectly conducting plane or on a site of other hard spheres representing the substrate. Adsorption occurs as either atoms or ions; extensive use is made of image force concepts to derive theoretical correlations. Since the adsorbed particles act as a perturbation to the surface of the substrate, any change in work function due to adsorption is attributed to a change in the surface double layer.

Levine and Gyftopoulos [1], Moore and Allison [14], Taylor and Langmuir [15], Eley [16], Stevenson [17], deBoer [18], Danforth [19], Zandburg [20], Higuchi, Ree and Eyring [21], etc., have presented various quantum chemical models for metals in gaseous environments. They propose a surface model in which adsorbed particles exist only as a single species bound to the surface by polarized or partially ionic and partially covalent bonds. Their justification for

this model is that the particle desorption energies are great enough (1 ev. or more) to demand a chemisorbed species. These models also assume that the change in work function can be attributed solely to changes in the surface double layer.

Although the quantum chemical models assume a greater valence band broadening than the semi-classical models, the degree of this broadening cannot be determined directly. Instead, measurements of electron and ion currents, atom and ion desorption rates, etc., are made on imperfect surfaces. The Levine-Gyftopoulos quantum chemical model predicts that for a given adsorbate a clean substrate with a higher work function should show a larger maximum change in the work function as a result of adsorption [1]. The Rasor-Warner semi-classical theory yields no such general rule [2]. Lack of theoretical consistency among predictions such as the above presently remains unresolved.

Much of our present theoretical knowledge of the electronic structure of surfaces has been gleaned from numerous theoretical studies of clean surfaces. In 1932 Tamm and Blochinzev were the first to use wave mechanics to calculate the electron distribution near a metal surface [22]. Their one dimensional model, which has since been used extensively for surface calculations, assumes that the non-interacting electrons are in a potential well having a constant inner potential and planer bounding potential walls of finite height. The potential is a function only of the distance along the surface normal as is shown in Figure 1. In this model the ionic charge is smeared out uniformly within each cell; thus, its properties — specifically its cohesive energy — differ from those of a simple metal of the same

electron density. Several decades later, this theoretical model of a metal was named "jellium" by Herring [23].

In 1936 Bardeen [24], using the "jellium" model for the potential of the positive ions, made the first physically meaningful calculation of the surface charge distribution by obtaining a self-consistent solution of the Hartree-Fock equations. Since then, Freenberg [25], Brager and Schuchowitzky [26], Huang and Wyllie [27], Huntington [28], Swiatecki [29], Juretschke [30], Stratton [31],and Scott [32] have refined Bardeen's calculations. Recently, in 1961 Loucks and Cutler [33] used a Bohm-Pines formalism with the "jellium" model to obtain a rather accurate picture of the surface electron distribution.

In 1941 Smoluchowski [34] used the Thomas-Fermi Theory with the Weizsäcker kinetic energy correction to study the influence of crystallographic structure on the work function and the electronic surface structure. His computed work function differences are probably unreliable because he neglected correlation and exchange energies [35] and used a value of the Weizsäcker kinetic energy correction presently known to be nine times too large [36]. In spite of these defects, however, Smoluchowski's calculations represent the only detailed estimates of both differences in work function and of surface electronic structure due to differences in atomic arrangements. His introduction of the concepts of spreading and smoothing were major advances in the study of the electronic structure of surfaces.

The surface structure of clean metals has not been so thoroughly investigated; thus, there are only a few basic calculations of the electronic structure of metals in gaseous environments. Shockley [37],

Grimley [38], Kontecky [39], and Huang and Wyllie [40] have tried to solve this problem by means of quantum mechanical wave functions of the periodic lattice structure of the surface. Their results, however, are only grossly qualitative. Bardeen [41], Margenau and Pollard [42], Pollard [44], Prosen and Sachs [45], and Neustadter and Luke [46] have calculated the heat of adsorption for an atom on a surface and have obtained reasonable agreement with experiment. In addition, Bardeen [41], and Sachs and Dexter [43] have shown that the concept of an image force is valid except for distances between the charged body and metal surface such that surface structure effects are important.

SURFACE MODEL

The model for this analysis assumes that the energy distribution in the valence band of the adsorbate does not change appreciably upon adsorption and that all changes in the work function due to adsorption can be attributed to changes in the surface double layer. The metal-gas interface is regarded as a superposition of the surface double layer upon the bulk substrate. Since we are interested primarily in predicting changes in the work function due to adsorbed partial monolayers, only the surface double layer will be studied.

At a given instant of time, the metal-gas interface is approximated by a lattice consisting of the outermost layer of atoms of the homogeneous substrate and a homogeneous array of adsorbed particles. Depending upon the relative values of the substrate work function, adsorbate ionization potential, and adsorbate valence, there will be a transfer of charge from adsorbate to substrate or vice-versa. The

remaining electronic valence charge will distribute itself in this potential well, forming the surface double layer with its moment perpendicular to the surface. A positive surface double layer, by definition, has its positive charge on the outside of the surface and its negative charge on the inside; hence, it tends to lower the work function of a clean substrate.

Those electrons not a part of the adsorbate valence charge are assumed to be symmetrically distributed around their respective nuclei forming what shall be called a core. The substrate atoms are regarded as spheres having zero valence but still capable of receiving and holding a spherically symmetric charge distribution; thus, both the substrate atoms and the adsorbate cores present point charge potentials to the fraction of valence electrons now in the interface. This procedure is a necessity since the exact charge distribution near the nuclei of these atoms in a lattice-like configuration is unknown. The finite size of a core is included in the mathematical formulation by assuming that the particle density is that of equation (5) for each period except in the cores where it is assumed to be zero. For analytical convenience the cores are represented as cubes with a volume equal to that of a sphere of radius r_m for the substrate or r_i for the adsorbate; these cubes are assumed to be centered at the center of the spheres with their sides parallel to the coordinate axes.

An average of the periodic variation of the valence charge in the directions parallel to the surface must be incorporated into the relationship between the macroscopic work function, which we measure, and the calculated microscopic charge density. This is accomplished in most macroscopic studies by regarding the electron cloud as being

concentrated along a line through each adsorbed particle. Since each adsorbed particle occupies an identical cell, the surface double layer due only to the valence electron cloud is the product of the moment of a single line of concentrated charge and the number of adsorbed particles per unit area. The total surface double layer consists of two parts—that due to the fixed charges and that due to the valence electron cloud. The change in work function, $\Delta \phi$, is proportional to the potential difference across the surface double layer, and is given by

$$\Delta \phi = - \frac{\vec{\tau} \cdot \hat{n}}{\epsilon_0} \qquad (1)$$

where $\vec{\tau}$ is the total dipole moment per unit area, $\hat{n}$ the outward unit normal to the surface, and ϵ_0 the permittivity of free space, all in MKS units. Other averages can be used; however, they do not change the fundamental physics of this analysis.

The effects of mutual and self-depolarization of the adsorbed atoms are included by varying the effective fraction of valence charge comprising the electron cloud in order to obtain the observed change in work function.

TFDC Theory

Because of the simplicity of its fundamental physical principles, the Thomas-Fermi-Dirac theory with the addition of a correlation correction is used in this analysis. As is well known, the TFD theory is obtained from an expansion in powers of $\hbar$ of the Hartree-

Fock density in the classical limit $\hbar \to 0$ [36]. The inhomogeneity corrections proportional to higher powers of $\hbar$ are not easily interpreted; in fact, the convergence of these expansions has not been demonstrated [47]. These inhomogeneity corrections are neglected, but the correlation energy is introduced in the same way as did Gombas [48]. This composite theory will hereafter be called the TFDC theory.

The TFDC theory can be applied to many-body problems in several ways. Because of the intricate surface geometry, a trial particle density with at most five independent variational parameters was chosen, and the total energy minimized with respect to these parameters. The total energy E in MKS units of the electronic charge distribution, according to the TFDC theory [48, 49], is

$$E = \frac{3h^2}{10m}\left(\frac{3}{\pi}\right)^{2/3}\int\left[n(\vec{r})\right]^{5/3}d\vec{r} - e\int n(\vec{r})\,V_n(\vec{r})\,d\vec{r}$$

$$- \frac{e}{8\pi\epsilon_0}\iint\frac{n(\vec{r})\,n(\vec{r}')}{|\vec{r}-\vec{r}'|}\,d\vec{r}\,d\vec{r} - \frac{3e^2}{16\pi\epsilon_0}\left(\frac{3}{\pi}\right)^{1/3}\int\left[n(\vec{r})\right]^{4/3}d\vec{r}$$

$$- \int\frac{0.88\times 13.6\times 1.6\times 10^{-19}}{\left(\frac{3}{4\pi}\right)^{1/3}\Big/\,0.5227 + 7.8\left[n(\vec{r})\right]^{1/3}}\,n(\vec{r})\,d\vec{r} \qquad (2)$$

where $n(\vec{r})$ is the particle density, $\vec{r}$ and $\vec{r}'$ the position vectors, $d\vec{r}$ and $d\vec{r}$ the volume elements of the integrals at $\vec{r}$ and $\vec{r}'$, respectively. The integrals are to be taken over all regions appropriate to the problem. The first term is the kinetic energy; the next two terms are the potential energies due to the electron-nuclear and electron-

electron interactions, V_{ie} and V_{ee} respectively; the next the exchange energy V_{ex}; and the last the correlation energy, V_{cor}. According to Juretschke [30], this form of the exchange energy is not correct at a surface, since, by comparison with his calculations, it is too small. However, his results are obtained under somewhat restrictive conditions—namely, the "jellium" model.

The Surface Charge Distribution

Since the adsorbed particles are assumed to influence only the surface double layer, only the outermost layer of substrate particles, along with the adsorbed particles, is treated in this analysis. The outermost layer of the substrate is represented by a homogeneous planar rectangular array of spheres, each of radius r_m, with their centers in the x, y plane of a rectangular coordinate system, and the adsorbed particles, represented by spheres of radius r_f, are arranged periodically on sites consisting of four substrate particles. The positive z axis is to pass through the center of an adsorbed particle at $z = z_o$, and the x and y axes are oriented as shown in Figs. 2 a and 2b. The substrate is assumed to have a periodicity of length p_x, p_y in the x, y directions respectively in its interior and on its surface. By geometry

$$z_o^2 = \left[r_m + r_f \right]^2 - \left[\frac{p_x}{2} \right]^2 - \left[\frac{p_y}{2} \right]^2 \qquad (3)$$

Define $2x_o, 2y_o$ to be the lengths of a unit cell (i.e., a region containing only one adsorbed particle) in the x, y directions, respectively and L_1, L_2 be the lengths of the sides of the equivalent cubes for the substrate, adsorbate, respectively. Since the adsorbate

core is the size of its positive ion of radius r_i, then

$$L_1 = \left(\frac{4}{3}\pi\right)^{1/3} r_m \quad ; \quad L_2 = \left(\frac{4}{3}\pi\right)^{1/3} r_f \tag{4}$$

Figs. 2a and 2b show two views of these systems for adsorbate-substrate geometries to be used later.

The exact surface charge distribution depends on the particular adsorbate-substrate system. This analysis is intended primarily for the adsorption of alkali metals, such as cesium, and alkaline-earth metals, such as barium, on refractory metals, such as tungsten. For these systems, Gurney [3] has shown that some of the adsorbate valence electrons will be transferred to the substrate; let F_R be that fraction of adsorbate valence electrons not transferred. To visualize the exact nature of this transfer, consider each particle to be a symmetric sphere of charge, uninfluenced by its neighbors both before and after the transfer has occurred. The fraction $(1 - F_R)$ of the valence charge leaves an adsorbed particle to distribute itself equally and symmetrically around each of the four neighboring substrate atoms. The fraction of valence charge not transferred to a substrate particle, F_R, remains in the potential wells of the substrate and adsorbate cores. Since the degree of interaction between substrate and adsorbate has been assumed to be small, F_R can be expected to be near unity.

Assume the following function to be an approximate representation of the valence particle distribution for a periodic region in the x, y direction, centered at the origin and containing only one

adsorbed particle

$$n(\vec{r}) = N \exp\left[-\alpha|x| - \beta|y| + \gamma_1(z-\delta)\right] \qquad z \leq \delta$$

$$n(\vec{r}) = N \exp\left[-\alpha|x| - \beta|y| - \gamma_2(z-\delta)\right] \qquad z \geq \delta$$

$$n(\vec{r}) = 0 \qquad \text{in a core} \qquad (5)$$

where N is a normalization constant and α, β, γ_1, γ_2, δ are positive parameters, chosen so as to minimize the total energy. The charge is assumed to decrease away from each adsorbate core, to be symmetric about the origin with respect to each of two axes parallel to the interface, and to be asymmetric with respect to the surface normal. The parameter δ serves only to shift the peak along the direction of the surface normal. Because some of the negative valence charge of the adsorbate is transferred to the substrate, it is expected that more of the remaining valence charge will be located in the region $z > z_o$ than in the region $z < z_o$. For this configuration the rate of decay of the charge distribution in the z direction for $z < \delta$ should be greater than the rate of decay in the z direction for $z > \delta$ i.e., $\gamma_1 > \gamma_2$. Also, since for these systems the adsorbate charge distribution is only perturbed by the substrate, symmetry leads us to expect that δ should be greater than z_o. The constant N is determined by the constraint that the total number of particles per period, excluding the cores, must be F_R times the valence of the adsorbate $\mathcal{J}$.

$$N = \mathcal{J} F_R \Big/ \int \frac{n(\vec{r})}{N} \, d\vec{r} \qquad (6)$$

An integration over one adsorbate-substrate period in the coordinates x, y and from minus infinity to plus infinity in the z direction but excluding the cores is represented by

$$d\hat{r} = 4\int_{-\infty}^{\infty} dz \int_{0}^{X}\int_{0}^{X_0} dx\,dy - \iiint_{\text{SUBSTRATE CORES}} dx\,dy\,dz - 4\int_{z_0-L_z/2}^{z_0+L_z/2}\int_{0}^{L_x/2}\int_{0}^{L_y/2} dx\,dy\,dz \qquad (7)$$

This particular form of particle distribution was chosen because it is a physical representation of the true distribution and because it is easily introduced into the equation for the total energy of the TFD theory when the geometric effects of the cores are included. Of course, this charge distribution must be superimposed upon that of the bulk to obtain the total particle distribution for $z \leq z_o$; the effect of bulk charges is expected to be negligible for $z \geq 0$.

This completes the discussion prerequisite to finding the total energy of the metal-vapor interface.

Total Energy

In order to find the total energy, consistent with our assumptions about the cores, it is necessary to substitute the particle density of equation (5) into equation (2). This is a straightforward but rather tedious task. In the following sections each energy term is evaluated as a function of the five parameters. Since a unit cell in the x, y directions contains only one adsorbed particle, the effect of the adsorbate core is included explicitly in the general analysis; the effect of the substrate cores, however, must be deferred until specific substrates are studied.

Evaluation of N and F_R

N and F_R are two physically meaningful independent parameters that are evaluated in this section as functions of $\alpha, \beta, \gamma_1, \gamma_2, \delta, \Delta\phi$.

To obtain N as a function of F_R substitute equation (5) into equation (6), yielding

$$N = J F_R / I^{(1)} \tag{8}$$

where

$$I^{(q)} = \left[\frac{n(\hat{r})}{N}\right]^q d\hat{r}$$

$$= \frac{4}{q^3} \frac{\exp(\alpha q X_0)-1}{\alpha} \frac{\exp(\beta q \gamma_0)-1}{\beta} \left[\frac{1}{\gamma_1} + \frac{1}{\gamma_2}\right]$$

$$- \frac{4}{q^3} \frac{\exp(\alpha q L_2/2)-1}{\alpha} \frac{\exp(\beta q L_2/2)-1}{\beta} \left\{\frac{1}{\gamma_1}\left[1\right.\right.$$

$$\left. - \exp\left(q\gamma_1\left(z_0 - L_2/2 - \delta\right)\right)\right]$$

$$\left. + \frac{1}{\gamma_2}\left[1 - \exp\left(-q\gamma_2\left(z_0 + L_2/2 - \delta\right)\right)\right]\right\}$$

$$- 2\exp(-\gamma_1 q \delta) \frac{\sinh(\gamma_1 q L_2/2)}{q\gamma_1} \iint_{\text{substrate cores}} e^{-\alpha|x|} e^{-\beta|\gamma|} dx\, d\gamma \tag{9}$$

The dipole moment per unit area of the electron cloud in the z direction is, by definition

$$\tau_e = - e \sigma_f \int z\, n(\vec{r})\, d\vec{r} \tag{10}$$

where e is the electronic charge and σ_f the number of adsorbed particles per unit area. Here the valence charge is treated as being concentrated on a line through the center of the adsorbed particle. Upon evaluation, this becomes

$$\begin{aligned}\tau_e = &- 4 e N \sigma_f \frac{\exp(\alpha x_0) - 1}{\alpha} \frac{\exp(\beta y_0) - 1}{\beta} \left[\frac{\gamma_1 \delta - 1}{\gamma_1^2} + \frac{\gamma_2 \delta + 1}{\gamma_2^2} \right] \\ &+ 4 e N \sigma_f \frac{\exp(\alpha L_3/2) - 1}{\alpha} \frac{\exp(\beta L_3/2) - 1}{\beta} \left[\frac{\gamma_1 \delta - 1}{\gamma_1^2} + \frac{\gamma_2 \delta + 1}{\gamma_2^2} \right. \\ &- \frac{(\gamma_1 (z_0 - L_3/2) - 1) \exp(\gamma_1 (z_0 - L_3/2 - \delta))}{\gamma_1^2} \\ &\left. - \frac{(\gamma_2 (z_0 + L_3/2) + 1) \exp(-\gamma_2 (z_0 + L_3/2 - \delta))}{\gamma_2^2} \right] \\ &+ e \sigma_f \int_{\text{substrate cores}} z\, n(\vec{r})\, d\vec{r}\end{aligned} \tag{11}$$

For the cores, taken as point charges, the dipole moment per unit area in the z direction is

$$\tau_c = \nu e z_0 \tag{12}$$

The change in work function is then

$$\Delta \phi = - \frac{\tau_e + \tau_c}{\epsilon_o} \tag{13}$$

where τ_e and τ_c are given by equations (11) and (12).

By eliminating N from equations (11) to (13), F_R can be evaluated as a function of only $\alpha, \beta, \gamma_1, \gamma_2, \delta, \Delta\phi$:

$$F_R = \left[\frac{\epsilon_o \Delta \phi}{\nu \sigma_f} + z_o \right] \Big/ \left[(\tau_e + \tau_c) I^{(4/3)} \right] \tag{14}$$

N is then obtained as a function of $\alpha, \beta, \gamma_1, \gamma_2, \delta, \Delta\phi$ by substituting equation (14) into equation (8).

The Kinetic Energy and the Exchange Energy

The kinetic energy and the exchange energy are evaluated together since they are algebraically similar. The kinetic energy of the Thomas-Fermi-Dirac theory is [49]

$$T = \frac{3h^2}{10m} \left(\frac{3}{\pi} \right)^{2/3} N^{5/3} I^{5/3} \tag{15}$$

where $I^{(5/3)}$ is defined by equation (9).

Similarly, the exchange energy is [49]

$$V_{ex} = - \frac{3e^2}{16\pi\epsilon_o} \left(\frac{3}{\pi} \right)^{1/3} N^{4/3} I^{4/3} \tag{16}$$

The relatively simple form of T and V_{ex} is due to the exponential dependence of $n(\vec{r})$ on position, and also to the equivalent cube representation of the cores.

The Correlation Energy

As represented in equation (2) the correlation energy must be evaluated numerically for the particle density of equation (5). An estimate of the correlation energy can be obtained by representing both the correlation energy and the exchange energy as follows [48, 49, 50]:

$$V_{ex} = -\frac{3e^2}{16\pi\epsilon_0}\left(\frac{3}{\pi}\right)^{1/3} N_{eff}^{4/3} \tag{17}$$

$$V_{cor} = -\frac{0.88 \times 13.6 \times 1.6 \times 10^{-19}}{R_s/a_0 + 7.8}\,\nu F_R \tag{18}$$

where $R_s = \left(\frac{3}{4\pi}\right)^{1/3} N_{eff}^{-1/3}$ is the effective radius of the electronic "S" sphere [50] and a_0 is the first Bohr radius in meters. By solving equation (17) for N_{eff} and then calculating R_s, the correlation energy can be estimated.

The Electron-Electron Interaction Energy

We begin the evaluation of the electron-electron potential energy per unit cell by finding the potential due to all of the valence electronic charge. Let us represent the valence charge density

by a double Fourier series in the x, y coordinates and by a Fourier integral in the z direction. Thus

$$\rho(\vec{r}) = \frac{1}{2\pi} \int_{\text{real k axis}} \sum_{n=0}^{\infty} \sum_{m=0}^{\infty} \cos\frac{n\pi x}{2X_o} \cos\frac{m\pi y}{2Y_o} \frac{\exp(-ikz)\,dk}{1+2\delta_{no}\delta_{mo}+\delta_{no}+\delta_{mo}} \times \left[A_{onm} A_o(k) + A_{csnm} A_{cs}(k) + A_{wnm} A_w(k) \right] \tag{19}$$

where δ_{ij} is the Kronecker delta function.
The Fourier coefficients can be shown to be:

$$A_{onm} = -\frac{4eN}{X_o Y_o} \frac{1}{\alpha_n^2} \frac{1}{\beta_m^2} \times \begin{cases} \left(-\alpha(-1)^{n/2} \exp(-\alpha X_o) + \alpha\right) & n \text{ even} \\ \left(\frac{n\pi}{2X_o}(-1)^{(n+3)/2} \exp(-\alpha X_o) + \alpha\right) & n \text{ odd} \end{cases} \times \begin{cases} \left(-\beta(-1)^{m/2} \exp(-\beta Y_o) + \beta\right) & m \text{ even} \\ \left(\frac{m\pi}{2Y_o}(-1)^{(m+3)/2} \exp(-\beta Y_o) + \beta\right) & m \text{ odd} \end{cases} \tag{20}$$

with

$$\alpha_n^2 = \alpha^2 + \left(\frac{n\pi}{2X_o}\right)^2 \tag{21}$$

$$\beta_n^2 = \beta^2 + \left(\frac{m\pi}{2Y_o}\right)^2 \tag{22}$$

$$A_o(k) = \frac{(\gamma_1 + \gamma_2)\, exp(-ik\delta)}{(k + i\gamma_1)(k - i\gamma_2)} \tag{23}$$

$$A_{csnm} = \frac{4eN}{x_o y_o} \frac{1}{\alpha_n^2} \frac{1}{\beta_n^2} \times$$

$$\left[exp(-\alpha L_2/2)\left(-\alpha \cos \frac{n\pi L_2}{4x_o} + \frac{n\pi}{2x_o} \sin \frac{n\pi L_2}{4x_o}\right) + \alpha \right] \times$$

$$\left[exp(-\beta L_2/2)\left(-\beta \cos \frac{m\pi L_2}{2y_o} + \frac{m\pi}{2y_o} \sin \frac{m\pi L_2}{4x_o}\right) + \beta \right] \tag{24}$$

$$A_{cs}(k) = \frac{i\, exp(-ik\delta)}{k + i\gamma_1}\left[1 - exp\{(z - L_2/2 - \delta)(\gamma_1 - ik)\} \right]$$

$$- \frac{i\, exp(\gamma_2 \delta)}{k - i\gamma_2}\left[1 - exp\{(z + L_2/2 - \delta)(\gamma_2 + ik)\} \right] \tag{25}$$

$$A_{wnm} = \frac{4eN}{x_o y_o} \frac{1}{\alpha_n^2} \frac{1}{\beta_n^2}\, exp(-\alpha x_o - \beta x_o) \times$$

$$\left\{ exp(-\alpha L_1/2)\left[-\alpha \cos \frac{n\pi}{2x_o}(x_o/2 + L_1/2) + \frac{n\pi}{2x_o} \sin \frac{n\pi}{2x_o}(x_o/2 + L_1/2) \right] \right.$$

$$\left. - exp(\alpha L_1/2)\left[-\alpha \cos \frac{n\pi}{2x_o}(x_o/2 - L_1/2) + \frac{n\pi}{2x_o} \sin \frac{n\pi}{2x_o}(x_o/2 - L_1/2) \right] \right\} \times$$

$$\left\{ exp(-\beta L_1/2)\left[-\beta \cos \frac{m\pi}{2y_o}(y_o/2 + L_1/2) + \frac{m\pi}{2y_o} \sin \frac{m\pi}{2y_o}(y_o/2 + L_1/2) \right] \right.$$

$$\left. - exp(\beta L_1/2)\left[-\beta \cos \frac{m\pi}{2y_o}(y_o/2 - L_1/2) + \frac{m\pi}{2y_o} \sin \frac{m\pi}{2y_o}(y_o/2 - L_1/2) \right] \right\} \tag{26}$$

$$A_w(k) = \frac{2i \exp(-\gamma_1 \delta) \sinh(\gamma_1 - ik) L/2}{k + i\gamma_1} \tag{27}$$

The A's with the subscripts n, m are associated with the x, y directions and the A's that are functions of k with the z direction. Also, the subscript o designates the Fourier coefficients without the inclusion of core effects, and the subscripts cs and w denote the adsorbate and substrate cores (mnemonically chosen to denote cesium and tungsten since cesium adsorbed on tungsten is a system of considerable interest.) The second and third terms of equation (19) represent the influence of the adsorbate and substrate cores, respectively.

The valence charge and its potential, V_e are related by Poisson's equation

$$\nabla^2 V_e = -\rho/\epsilon_o \tag{28}$$

so that

$$V_e(\vec{r}) = \frac{1}{2\pi\epsilon_o} \int_{\text{real k axis}} \sum_{n=0}^{\infty} \sum_{m=0}^{\infty} \left[A_{onm} A_o(k) + A_{csnm} A_{cs}(k) + A_{wnm} A_w(k) \right] X$$

$$\cos \frac{n\pi x}{2x_o} \cos \frac{m\pi y}{2y_o} \frac{\exp(-ikz)}{k^2 + k_{nm}^2} \frac{1}{(1 + 2\delta_{no}\delta_{mo} + \delta_{no} + \delta_{mo})} dk \tag{29}$$

where

$$k_{nm}^2 = \left(\frac{n\pi}{2x_o}\right)^2 + \left(\frac{m\pi}{2y_o}\right)^2 \tag{30}$$

The electron-electron interaction potential V_{ee} is given by

$$V_{ee} = \frac{1}{2} \int \rho(\vec{r})\, V_e(\vec{r})\, d\vec{r} \tag{31}$$

Evaluating equation (31) for V_{ee} gives

$$\begin{aligned} V_{ee} = {} & \frac{x_o y_o}{4\epsilon_o} \sum_{n=0}^{\infty}\sum_{m=0}^{\infty} \frac{F_{nm}(\gamma_1)}{\gamma_1(\gamma_2^2-\gamma_1^2)(k_{nm}^2-\gamma_1^2)(1+2\delta_{no}\delta_{mo}+\delta_{no}+\delta_{mo})} \\ & + \frac{x_o y_o}{4\epsilon_o} \sum_{n=0}^{\infty}\sum_{m=0}^{\infty} \frac{F_{nm}(\gamma_2)}{\gamma_2(\gamma_1^2-\gamma_2^2)(k_{nm}^2-\gamma_2^2)(1+2\delta_{no}\delta_{mo}+\delta_{no}+\delta_{mo})} \\ & + \frac{x_o y_o}{4\epsilon_o} \sum_{n=0}^{\infty}{}'\sum_{m=0}^{\infty}{}' \frac{F_{nm}(k_{nm})}{k_{nm}(\gamma_1^2-k_{nm}^2)(\gamma_2^2-k_{nm}^2)(1+2\delta_{no}\delta_{mo}+\delta_{no}+\delta_{mo})} \end{aligned} \tag{32}$$

where the primes on the summation signs of the last term indicate that the term in that series with $n = m = 0$ is not to be included. The first term is due to the poles at $\pm i\gamma_1$, the second to that at $\pm i\gamma_2$, and the third to those at $\pm iK_{nm}$. Finally $F_{nm}(p)$ is given by

$$\begin{aligned} F_{nm}(p) = {} & (\gamma_1+\gamma_2)^2 A_{onm}^2 \\ & + 2A_{wnm}^2(\gamma_2^2+p^2)\exp(-2\gamma_1\delta)\left[\cosh(\gamma_1 L_1) - \cosh(pL_1)\right] \\ & + A_{csnm}^2\left[(\gamma_1^2+\gamma_2^2)+(\gamma_2^2+p^2)\exp\left(2\gamma_1(z_o - L_1/2 - \delta)\right)\right. \\ & \qquad \left. + (\gamma_1^2+p^2)\exp\left(-2\gamma_2(z_o+L_1/2-\delta)\right)\right] \\ & - 2A_{csnm}^2(\gamma_1+\gamma_2)(\gamma_2-p)\exp\left[(\gamma_1+p)(z_o - L_1/2 - \delta)\right] \\ & - 2A_{csnm}^2(\gamma_1+\gamma_2)(\gamma_1-p)\exp\left[-(\gamma_2+p)(z_o+L_1/2-\delta)\right] \end{aligned} \tag{33}$$

$$+2A^{e}_{csnm}(\gamma_1-p)(\gamma_2-p)\exp\left[(\gamma_1-\gamma_2)(z_o-\delta)+(\gamma_1-\gamma_2-2p)L_2/2\right]$$

$$+2A_{onm}A_{wnm}(\gamma_1+\gamma_2)(\gamma_2-p)\exp(-\gamma_1\delta)\left[\exp(\gamma_1 L_1/2-p(\delta-L_1/2))\right.$$

$$\left.-\exp(-\gamma_1 L_1/2-p(\delta+L_1/2))\right]$$

$$+2A_{onm}A_{csnm}(\gamma_1+\gamma_2)\left[(\gamma_1+\gamma_2)+(\gamma_2-p)\exp\{(\gamma_1+p)(z_o-L_2/2-\delta)\}\right.$$

$$\left.-(\gamma_1-p)\exp\{-(\gamma_2+p)(z_o+L_2/2-\delta)\}\right]$$

$$+2A_{wnm}A_{csnm}\exp(-\gamma_1\delta)(\gamma_2-p)\left\{(\gamma_1+\gamma_2)\exp(\gamma_1 L_1/2)\exp\left[p(L_1/2-\delta)\right]\right.$$

$$-(\gamma_1+\gamma_2)\exp(-\gamma_1 L_1/2)\exp\left[-p(L_1/2+\delta)\right]-(\gamma_2-p)\exp(\gamma_1(z_o-\delta-L_2/2))\times$$

$$\left[\exp(\gamma_1 L_1/2)\exp(p(L_1/2+L_2/2-z_o))-\exp(-\gamma_1 L_1/2)\exp(p(-L_1/2+L_2/2-z_o))\right]$$

$$-(\gamma_1-p)\exp(-\gamma_2(z_o-\delta+L_2/2))\left[\exp(\gamma_1 L_1/2)\exp(p(L_1/2-L_2/2-z_o))\right.$$

$$\left.\left.-\exp(-\gamma_2 L_2/2)\exp(-p(L_1/2+L_2/2+z_o))\right]\right\} \qquad (33)$$

The Electron-Core Interaction Energy

It is convenient here to represent the electron-core energy as an interaction between the charged cores with charge density ρ_c and the potential of the valence electrons V_e i.e.,

$$V_{ie}=\int\rho_c(\vec{r})\,V_e(\vec{r})\,d\vec{r} \qquad (34)$$

The cores are assumed to have a spherically symmetric charge distribution and can therefore be regarded as point charges in the

potential of the valence electrons. For evaluating V_{ie} the core charge density can be represented as

$$\rho_c(\bar{r}) = e\nu\,\delta(x)\,\delta(y)\,\delta(z-z_0) - \frac{e\nu(1-F_R)}{4}\sum_{i=1}^{4}\delta(\bar{r}-\bar{r}_{ci}) \tag{35}$$

where $\delta(x)$ is the Dirac delta function and $\bar{r}_{ci}$ the position vector of the ith substrate core with charge $-\frac{e\nu(1-F_R)}{4}$. As in the previous section, let us employ a Fourier representation for the core charge. Thus

$$\rho_c(\bar{r}) = \frac{1}{2\pi}\int_{\text{real k axis}}\sum_{n=0}^{\infty}\sum_{m=0}^{\infty}\cos\frac{n\pi x}{2x_0}\cos\frac{m\pi y}{2y_0}\;\frac{\exp(ikz)\,dk}{1+2\delta_{n0}\delta_{m0}+\delta_{n0}+\delta_{m0}}\;\times$$

$$\left[B_{csnm}\,B_{cs}(k) + B_{wnm}\,B_w(k)\right] \tag{36}$$

where

$$B_{csnm}\,B_{cs}(k) = \frac{e\nu}{x_0 y_0}\exp(-ikz_0) \tag{37}$$

$$B_{wnm}\,B_w(k) = -\frac{e\nu(1-F_R)}{x_0 y_0}\cos\frac{n\pi}{4}\cos\frac{m\pi}{4} \tag{38}$$

Substituting equations (29) and (36) into equation (34) gives

$$V_{ie} = \frac{x_0 y_0}{\epsilon_0}\sum_{n=0}^{\infty}\sum_{m=0}^{\infty}\frac{H_{nm}}{(1+2\delta_{n0}\delta_{m0}+\delta_{n0}+\delta_{m0})}$$

$$+\frac{x_0 y_0}{\epsilon_0}\sum_{n=0}^{\infty}{}'\sum_{m=0}^{\infty}{}'\frac{I_{nm}}{K_{nm}(1+2\delta_{n0}\delta_{m0}+\delta_{n0}+\delta_{m0})} \tag{39}$$

with

$$H_{nm} = A_{onm}\, B_{wnm}\, \exp(-\gamma_1 \delta) \Big/ (k_{nm}^2 - \gamma_1^2)$$

$$+ A_{onm}\, B_{csnm}\, \exp(-U|z_o - \delta|) \Big/ (k_{nm}^2 - U^2)$$

$$+ A_{wnm}\, B_{wnm}\, \exp(-\gamma_1 \delta) \Big/ (k_{nm}^2 - \gamma_1^2)$$

$$+ A_{csnm}\, B_{csnm}\, \exp(-U|z_o - \delta|) \Big/ (k_{nm}^2 - U^2)$$

(40)

$$I_{nm} = \frac{A_{wnm}\, B_{wnm}\, (\gamma_1 + \gamma_2)\, \exp[-k_{nm}(\delta - R_1)]}{(\gamma_1 - k_{nm})(\gamma_2 + k_{nm})}$$

$$+ \frac{A_{onm}\, B_{csnm}\, (\gamma_1 + \gamma_2)\, \exp[-k_{nm}|z_o - \delta|]}{(\gamma_1 - V)(\gamma_2 + V)}$$

$$+ A_{csnm}\, B_{wnm} \left\{ \frac{(\gamma_1 + \gamma_2)\, \exp(-k_{nm}\delta)}{(\gamma_1 - k_{nm})(\gamma_2 + k_{nm})} \right.$$

$$- \frac{\exp[\gamma_1(z_o - L_2/2 - \delta) + k_{nm}(z_o - L_2/2)]}{\gamma_1 - k_{nm}}$$

$$\left. - \frac{\exp[-\gamma_2(z_o + L_2/2 - \delta) - k_{nm}(z_o + L_2/2)]}{\gamma_2 + k_{nm}} \right\}$$

$$+ A_{csnm}\, B_{csnm} \left\{ \frac{\exp(-k_{nm}|z_o - \delta|)}{(\gamma_1 - V)(\gamma_2 + V)} \right.$$

$$\left. - \frac{\exp[\gamma_1(z_o - L_2/2 - \delta) - k_{nm} L_2/2}{\gamma_1 + k_{nm}} \right.$$

$$- \frac{\exp\left[-\gamma_2\left(z_o + L_2/2 - \delta\right) - k_{nm}\, L_2/2\right]}{\gamma_2 + k_{nm}} \Bigg\}$$

$$+ A_{wnm}\, B_{wnm}\, \exp(-\gamma_1 \delta) \left\{ \frac{\exp\left[L_1(\gamma_1 - k_{nm})/2\right]}{\gamma_1 - k_{nm}} \right.$$

$$\left. - \frac{\exp\left[-L_1(\gamma_1 + k_{nm})/2\right]}{\gamma_1 + k_{nm}} \right\}$$

$$+ \frac{A_{wnm}\, B_{csnm}\, \exp\left[-\gamma_1(\delta - R_1)\right]}{\gamma_1 + k_{nm}} \left\{ \exp\left[L_1(\gamma_1 - k_{nm})/2\right] \right.$$

$$\left. - \exp\left[-L_1(\gamma_1 + k_{nm})/2\right] \right\} \qquad (41)$$

where for $\delta \geq z_o'$

$U = \gamma_1$

$V = K_{nm}$

and for $\delta \leq z_o'$

$U = \gamma_2$

$V = -K_{nm}$

Since

$$E = T + V_{ee} + V_{ie} + V_{ex} + V_{cor}, \qquad (42)$$

the evaluation of the total energy of the surface charge distribution is now complete.

Once the crystalographic structure of the substrate is known, A_{wnm} and B_{wnm} can be evaluated and the total energy minimized to find $\alpha, \beta, \gamma_1, \gamma_2, \delta$. This analysis has been applied to both cesium-tungsten and barium-tungsten systems.

RESULTS

Minimization Procedure

In order to obtain numerical values for the parameters describing the surface charge density it is necessary to minimize the total energy. Due to the algebraic complexity of the total energy, a direct search minimization technique was employed so that numerical or algebraic evaluation of the gradient of the function was not necessary. Nelder and Mead's [51] simplex method for function minimization was found to be the best procedure for this problem.

A FORTRAN IV program was developed to do the minimization on the IBM 7040 at the University of Pennsylvania Computer Center. This program evaluates the parameters $\alpha, \beta, \gamma_1, \gamma_2, \delta$ as functions of substrate-adsorbate geometry and either the experimentally observed change in work function $\Delta \phi$ or the fraction of adsorbate valence charge not transferred to the substrate F_R. To eliminate many small difference errors in the minimization, the indices n, m found in equation (32) for V_{ee} and equation (39) for V_{ie} went from $n = m = 0$ to $n = m = 11$ except for the first term of equation (39) for V_{ie} where n, m went from $n = m = 0$ to $n = m = 19$.

Numerical Results

This analysis has been applied to four distinct systems. The first two are the adsorption of either cesium or barium on the (100) surface of tungsten. Although cesium and barium are both highly electropositive elements, the ionization potential of cesium 3.87 ev. [52] is less than the effective work function of polycrystalline tungsten $\approx$ 4.62 ev. [53] and the ionization potential of barium $\approx$ 5.19 ev. [52] is higher than the effective work function of polycrystalline tungsten. In addition, the valence of cesium is + 1 and that of barium is + 2 . Since both changes in work function and ion emission due to adsorption are strongly dependent on the valence of the adsorbate and the difference between the substrate work function and adsorbate ionization potential, cesium-tungsten and barium-tungsten systems sometimes exhibit different electronic behavior.

The other two systems studied are the adsorption of cesium and barium on a surface similar to the (110) plane of tungsten. These systems were chosen to illustrate the influence of the lattice constant of the substrate on the surface charge distribution.

For all four systems the substrate-adsorbate geometry is that shown in Figs. 2a and 2b with $p_x = p_y$ so that $\alpha = \beta$. Table I shows the values of the constants used for each analysis. Notice that for the first two systems, Cs-W (100) and Ba-W (100), the observed change in work function $\Delta \Phi$ is a given constant while for the Cs-W and Ba-W (110) systems F_R is the given constant. Table II shows the calculated values of the energies T, V_{ee}, V_{ie}, V_{ex}, V_{cor}, the parameters α, β, γ_1, γ_2, δ describing the surface charge distribution, and the value of F_c , the fraction of charge in the region $z \geq z_o$.

The values of p_x, p_y are those given by Seitz [54], and the different radii are those given by von Hippel [55]. The changes in substrate work function for the Cs-W (100) and the Ba-W (100) systems are those measured by Swanson, Strayer, and Charbonier [56], and Moore and Allison [14], respectively. For the Cs-W and Ba-W (110) systems the values of F_R were those found previously for the Cs-W and Ba-W (100) system. For convenience all lengths are expressed in angstroms and all energies in rydbergs (1 Ry = 13.6 ev.).

The computed parameters in Table II are consistent with the assumptions and expectations for this model. It is evident that the kinetic energy is 10% to 35% of the magnitude of the total energy and that the exchange energy is 15% to 30% of the total energy. The total coulomb interaction energy $V_{ie} + V_{ee}$ is between 70% and 95% of the total energy. Thus, in this analysis of the surface charge distribution of a metal in a gaseous environment, the quantum mechanical kinetic, and exchange energies must be included. For all these systems, $\gamma_1 > \gamma_2$ because of the transfer of about 20% of the negative adsorbate valence charge to the substrate. In addition for each system, $\delta > z_o$, $F_R > .70$ and $N \approx 1$. More of the valence electronic charge not transferred to the substrate is in the region $z \geq z_o$ than in the region $z < z_o$. Also, since $\gamma_1, \gamma_2 > 1$ and $\gamma_1 > \gamma_2$, the surface charge does not penetrate a distance as much as one lattice constant (3.16 Å and 2.65 Å for the (100) and (110) system respectively) into the substrate from the center of the adsorbate core and only slightly further outwards.

The (100) and (110) systems differ only in that the substrate atoms are nearer in the (110) system. Since each unit cell of these systems contains the same amount of electronic charge, it is appropriate

to compare these systems in order to study the influence of substrate geometry on the surface charge distribution.

In describing the electron distribution near the surface of a clean metal, Smoluchowski [34] distinguished between two effects, which he called "smoothing" and "spreading." The smoothness of the surface charge is a measure of its variation in the directions parallel to the surface. The spreading is measured by the distance normal to the contours of constant charge density from which the electron density decreases from its interior value to a negligible external value. Smoluchowski concluded, as did Kelly [57], that for a given amount of charge the closer packed the surface atoms the less the maximum variation of the surface charge density parallel to the surface.

From equation (5) it is evident that the variation of surface charge in the x direction is proportional to $\exp(-\alpha x_o)$, a quantity which is larger for both (100) systems than for both (110) systems. Since the (110) systems have a higher density of surface atoms than the (100) systems, it can be concluded that the closer packed the surface atoms of the substrate, the closer packed the adsorbed particles for the geometry shown in Figs. 2a and 2b and the less the maximum variation of the surface charge density parallel to the surface.

The fraction of charge located in the region $z \geq 0$, F_c for both (110) systems is greater than that for their respective (100) systems while the opposite change was found for the values of $\Delta\phi$. These results are due to the fact that a greater density of negatively charged substrate particles pushes the electronic charge farther out from the surface.

CONCLUSION

It is evident that neither of the magnitudes of the quantum mechanical kinetic and exchange energy, nor the magnitude of the classical coulomb energy were negligible compared to the magnitude of the total energy. Because the quantum mechanical kinetic and exchange energies exerted such a strong influence on the microscopic electronic properties of the metal-gas interfaces studied, the quantum chemical macroscopic phenomenological models appear to be a better representation of the electronic properties of a metal in a gaseous environment than the semi-classical models.

ACKNOWLEDGEMENTS

The authors would like to thank Professor L. W. Zelby for his interest and encouragement.

REFERENCES

[1] E. P. Gyftopoulos and J. D. Levine, J. Appl. Phys. 43, 67 (1962). J. D. Levine and E. P. Gyftopoulos, J. Surface Sci. 1, 171, 225, 349 (1964).

[2] N. S. Rasor and C. Warner, J. Appl. Phys. 35, 2589 (1960).

[3] R. W. Gurney, Phy. Rev. 47, 479 (1935).

[4] J. C. Slater, Quantum Theory of Matter (McGraw-Hill Book Co., Inc., New York, 1951), p. 283.

[5] R. Gomer and L. W. Swanson, J. Chem. Phys. 38, 1613 (1963).

[6] R. V. Culver and F. C. Thompkins, Adv. in Catalysis (Academic Press, Inc., New York, 1959) Vol. II.

[7] J. A. Becker, Advances in Colloidal Science (Interscience Publishers, Inc., New York, 1935) Vol. 8.

[8] B. M. W. Trapnell, Chemisorption (Butterworth Publishers, London, 1957) p. 1957.

[9] F. L. Hughes, Phys. Rev. 113, 1036 (1958).

[10] F. L. Hughes and H. Levinstein, Phys. Rev. 113, 1029 (1958).

[11] K. P. Luke and J. K. Smith, "Theoretical Study of Zero-Field Electron Work Function of Metal Immersed in Gas - Direct Application to Cesium Thermionic Diode," NASA TN D-2357; July, 1964.

[12] J. K. MacDonald and C. A. Barlow, J. Chem. Phys. 39, 412 (1963).

[13] L. N. Dobretsov, Elektronnaya i Ionnaya Emissiya (State Publishing House for Technical and Theoretical Literature, Moscow-Lenningrad, 1952).

[14] G. E. Moore and H. W. Allison, J. Chem. Phys. 23, 1609 (1955).

[15] J. B. Taylor and I. Langmuir, Phys. Rev. 44, 423 (1933).

[16] D. D. Eley and A. Cooper, Disc. Faraday Soc. 8, 172 (1950).

[17] D. P. Stevenson, J. Chem. Phys. 23, 203 (1954).

[18] J. D. deBoer, Advances in Colloidal Science (Interscience Publishers, Inc. New York 1950).

[19] W. E. Danforth, J. Appl. Phys. 33, 1972 (1962).

[20] E. Ya. Zandberg, Soviet Phys-Tech. Phys. 5, 1152 (1961).

[21] I. Higuchi, T. Ree, and H. Eyring, J. Chem. Phys. 77, 4969 (1955) J. Chem. Phys. 79, 1330 (1956).

[22] I. Tamm and D. Blochinzev, Z. Physik 77, 774 (1932), Physik Seeds. Sowjetunion 3, 170 (1933).

[23] C. Herring, Metal Interfaces (American Soc. for Metals, 1952).

[24] J. Bardeen, Phys. Rev. 49, 653 (1936).

[25] E. Freenberg, Phys. Rev. 60, 204 (1941).

[26] A. Brager and A. Schuchowitzky, Acta Physiochim. URSS, 21, 13 (1946)

[27] K. Huang and G. Wylie, Proc. Phys. Soc. (London) A62, 180 (1949).

[28] H. B. Huntington, Phys. Rev. 81, 1035 (1951).

[29] W. J. Swiatecki, Proc. Phys. Soc. (London) A64, 226 (1950).

[30] H. J. Juretschke, Phys. Rev. 92, 1140 (1953).

[31] R. Stratton, Phil. Mag. 44, 1236, 1247 (1953) Phil. Mag. 2, 702 (1957).

[32] A. B. Scott, Phil. Mag. 45, 1173 (1954).

[33] T. L. Loucks and P. H. Cutler, J. Phys. Chem. Solids 25, 105 (1964).

[34] R. Smoluchowski, Phys. Rev. 60, 661 (1941).

[35] C. Herring and M. H. Nichols, Rev. Mod. Phys. 21, 185 (1949).

[36] S. Golden, Phys. Rev. 105, 604 (1956).

[37] W. Shockley, Phys. Rev. 56, 317 (1939).

[38] T. R. Grimley, Advances in Catalysis (Adademic Press, Inc., New York, 1960) Vol. 12.

[39] J. Koutecky, J. Phys. Chem. Solids 14, 223 (1960).

[40] K. Huang and G. Wyllie, Disc. Faraday 90c. 8, 18 (1950).

[41] J. Bardeen, Phys. Rev. 58, 727 (1940).

[42] H. Margenau and W. G. Pollard, Phys. Rev. 60, 128 (1941).

[43] R. G. Sachs and D. L. Dexter, J. Appl. Phys. 21, 1304 (1950).

[44] W. G. Pollard, Phys. Rev. 60, 578 (1941).

[45] E. J. R. Prosen and R. G. Sachs, Phys. Rev. 61, 65 (1942).

[46] H. E. Neustadter and K. P. Luke, "Low-Coverage Heat of Adsorption I: Alkali Metal Atoms on Tungsten: Metal Interaction Theories," NASA TN D-2430; August 1964.

H. E. Neustadter, K. P. Luke, and T. Sheahan, "Low-Coverage Heat of Adsorption II: Alkali Metal Atoms on Tungsten; Leonard-Jones Atom-Atom Interaction Theory," NASA TN D-2431; August 1964.

H. E. Neustadter and K. P. Luke, "Low-Coverage Heat of Adsorption III: Alkali Metal Atoms on Tungsten; Atom-Metal Interaction Theory," NASA TN D-2460.

[47] H. M. Schey and J. L. Schwartz, Phys. Rev. 137, A709 (1965).

[48] P. Gombas, Z. Physik. 121, 523 (1943).

[49] N. H. March, Adv. Phys. 6, 1 (1957).

[50] S. Raimes, The Wave Mechanics of Electrons in Metals (North Holland Publishing Co., Amsterdam, 1961).

[51] J. A. Nelder and R. Mead, Computer J. 7, 308 (1965).

[52] Handbook of Chemistry and Physics (Chemical Rubber Publishing Co., Cleveland, Ohio 1958) 39th ed.

[53] H. J. Caufield, J. Appl. Phys. 35, 2862 (1961).

[54] F. Seitz, The Modern Theory of Solids (McGraw-Hill Book Co., Inc., New York, 1940).

[55] A. R. von Hippel, Molecular Science and Engineering (John Wiley and Sons, New York, 1959) p. 148.

[56] L. W. Swanson, R. W. Strayer, and F. M. Charbonnier, Proc. Twenty-Fourth Annual Conf. on Physical Electronics (M.I.T., Cambridge, Mass. 1964) p. 120.

[57] C. H. Kelly, The Kinetic Energy of Electrons Associated With the Line Boundary of a Two-Dimensional Crystal (thesis, Polytechnic Institute of Brooklyn, 1954).

TABLE I

PHYSICAL CONSTANTS FOR METAL-GAS SYSTEMS *

	Cs-W (100)	Cs-W (110)	Ba-W (100)	Ba-W (110)
p_x, p_y	3.16	2.65	3.16	2.65
r_m	1.3	1.3	1.3	1.3
r_f	2.62	2.62	2.17	2.17
r_i	1.7	1.7	1.38	1.38
Z_o	4.52	4.74	3.95	4.22
$\Delta \phi$	-3.0	--	-2.34	--
F_R	--	0.745	--	0.815

* Work function changes in electron volts and lengths in angstroms.

TABLE II

RESULTS FOR FOUR SYSTEMS*

	Cs-W (100)	Cs-W (110)	Bu-W (100)	Bu-W (110)
F_R	0.745	--	.815	--
F_c	0.562	0.744	.604	.707
α, β	1.35	1.36	1.56	1.84
γ_1	1.61	1.57	1.46	1.86
γ_2	1.43	1.04	1.36	1.45
δ	4.94	4.89	4.06	4.36
T	0.092	0.095	.368	.487
V_{ee}	.145	.071	.967	.732
V_{ie}	-.597	-.355	-3.50	-2.50
V_{ex}	-0.133	-0.135	-.404	-.470
V_{cor}	-0.023	-.023	-.035	-.036
E	-0.516	-0.347	-2.60	-1.787
$\Delta \phi$	--	-1.178	--	-.867

*Energies in Rydbergs and lengths in angstroms

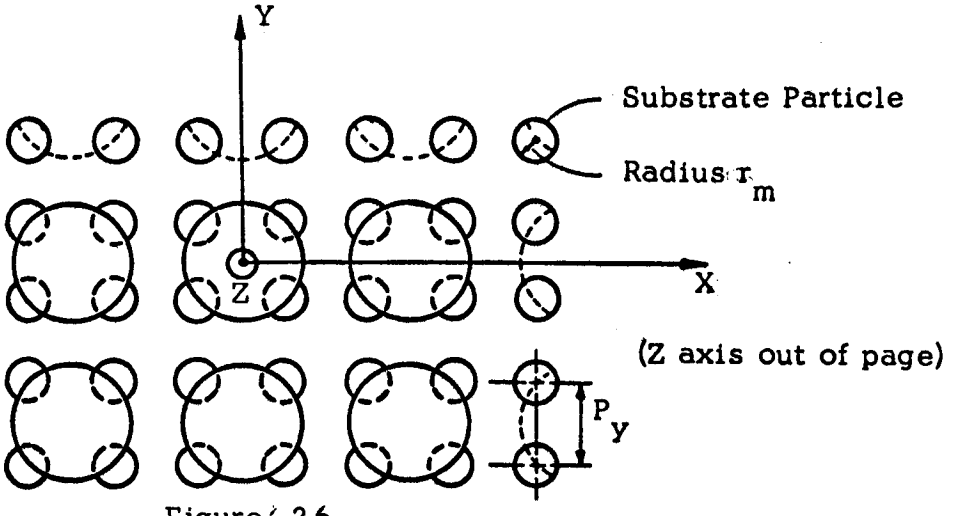

Figure 2a

Adsorbate-Substrate Geometry and Coordinate System:
Outside View

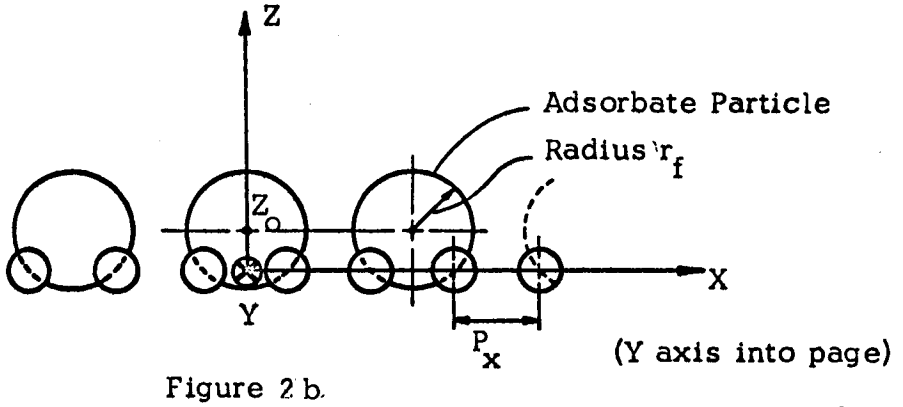

Figure 2b

Adsorbate-Substrate Geometry and Coordinate System:
Side View

3.5 Plasma Centrifuge

Dr. M. Altman, Dr. M. Brull, P. Hsueh

In recent years the effects of crossed electromagnetic fields on fluid flow have been investigated with increasing interest because of the practical needs of astronautics, plasma physics, and aerospace engineering. Problems concerning the motion of a plasma in the presence of mutually perpendicular electric and magnetic fields have attracted a large amount of interest. A collection of theoretical and experimental problems have been isolated which require further work to exploit their possibilities in practical devices such as plasma accelerators, MHD power generators, and ion centrifuges.

This research is concerned with a plasma which is contained in a vessel bounded by coaxial cylindrical electrodes and insulated bases, as illustrated in the following diagram:

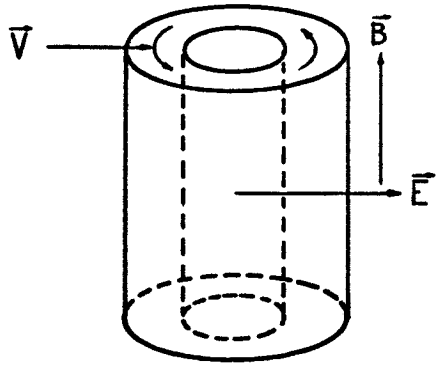

$\vec{B}$ - Magnetic field intensity

$\vec{E}$ - Applied electric field intensity

$\vec{V}$ - velocity

$\vec{j}$ - current density

A crossed field is applied to the plasma with an electric field in a radial direction and a magnetic field in the axial direction.

It is well known that the plasma will rotate around the axis of the cylinder as a result of the body force $\vec{j} \times \vec{B}$. It will start from rest and reach an equilibrium state when the body force is compensated for by dissipation. Thus, this device should be useful to accelerate conducting fluids to very high velocities with no moving parts.

A complete analysis of the flow phenomena taking into account end effects has not yet been reported. Thus, the first part of this research consists of a theoretical analysis of several models of increasing complexity.

A breakdown of the topics currently under investigation is shown in the following table:

Plasma Centrifuge—Theoretical Analysis

I. Infinitely Long Cylinder
   a. Inviscid Solution
   b. Viscous Solution
II. Finite Cylinder
   a. Zero Order Solution
   b. First Order Solution
III. Stability Investigation
   a. Dynamic Instabilities in r and z Directions
   b. Instabilities in θ Direction Due to Temperature Gradients and Centrifugal Force Field

Analytical solutions have been obtained for the inviscid and the viscous infinite cylinder cases. Figure 3.5-1a shows a typical result using mercury as a working fluid. From this figure it is apparent

4. Electrochemical Engineering

Branch Chief: Dr. Leonard Nanis

Senior Member: Dr. John O'M. Bockris

that for the assumed conditions the velocity profiles of an inviscid and a viscous fluid differ significantly. From physical reasoning it is clear that as the ratio of electromagnetic to viscous forces increases, the velocity profile should begin to approximate that of the inviscid fluid. Figure 3.7-1b shows that this is indeed the case. With a $\vec{B}$ field of 10^{-1} or greater, only the velocity in the immediate vicinity of the wall varies appreciably from the inviscid solution. This clearly places a lower limit on B and thus a limit in the velocity ultimately attainable for a given $\vec{E}$ field [V = E/B].

Finite cylinder results are almost complete and the stability investigations are currently being initiated.

VELOCITY vs. RADIAL POSITION
FLUID ROTATION IN AN INFINITELY LONG CYLINDER

FIG. 3.5-1a

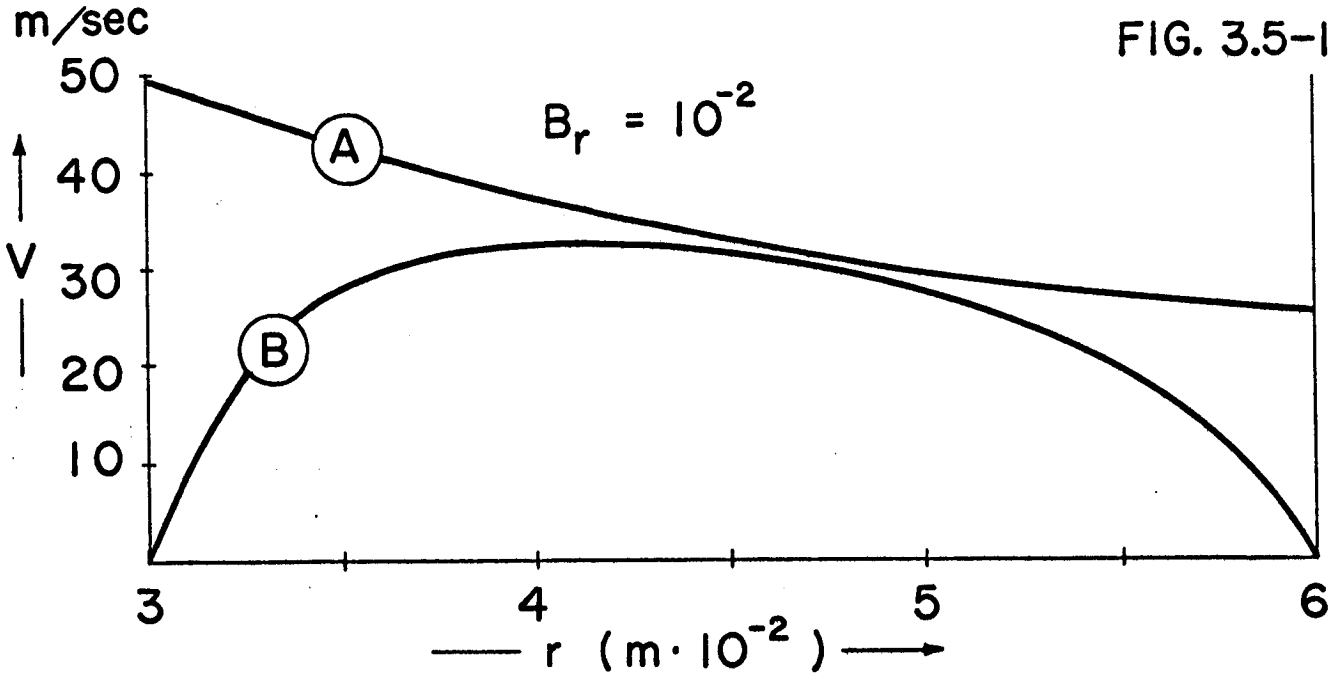

(A) INVISCID FLUID

(B) VISCOUS FLUID $\nu = 1.15 \times 10^{-7}$

$r_1 = 3 \times 10^{-2}$, $r_2 = 6 \times 10^{-2}$, $u_0 = 10^{-2}$

$\sigma = 10.8 \times 10^5$, $\rho = 13.5 \times 10^3$

FIG. 3.5-1b

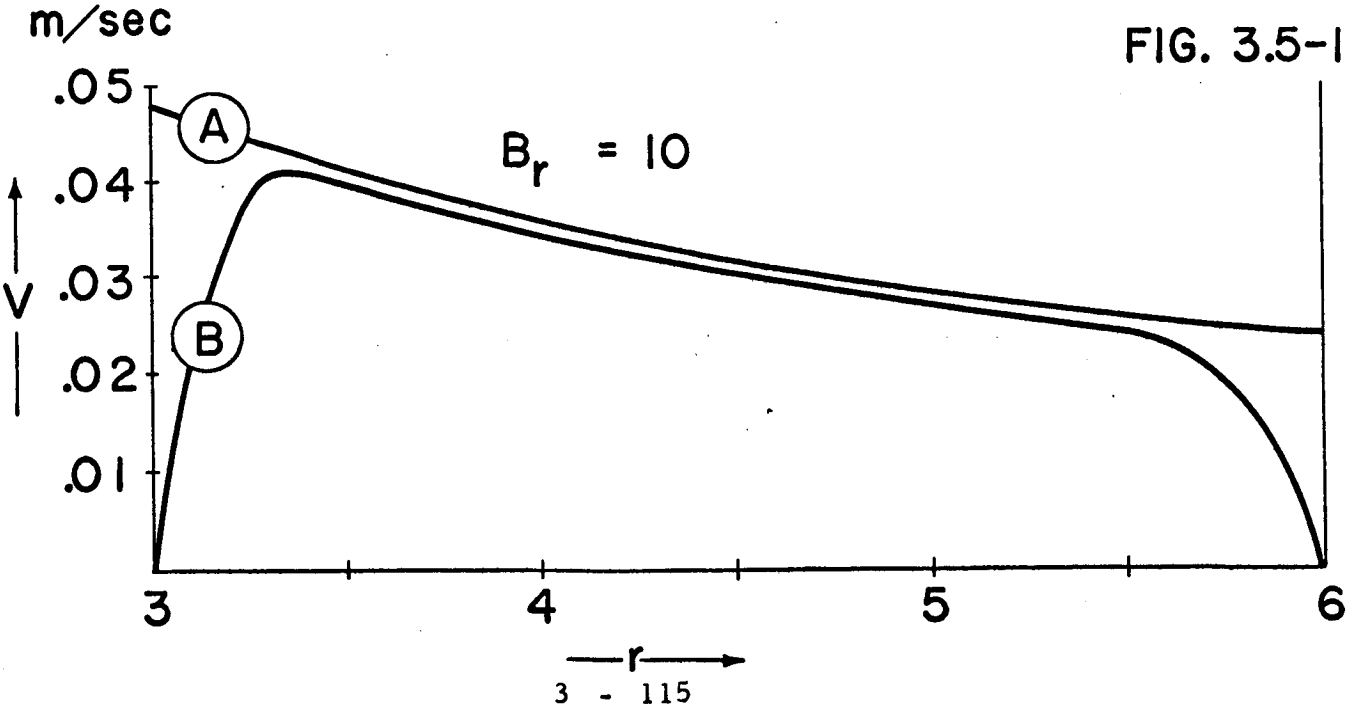

4.1 Atomic Scale Electrode Processes

Gabriel Di Masi, Ph.D. Candidate

Dr. Leonard Nanis, Thesis Advisor

4.1.1 Abstract

The field ion emission microscope has been put into operational order. For combination with electrochemical studies, many features involving redesign of the basic apparatus have become evident. Work is continuing with tungsten tips.

4.1.2 Theory

The field ion emission microscope is a relatively new research tool which has, as yet, not received full attention by electrochemists. The device is unique in that it offers the possibility for observing individual atom positions. The mode of operation is fundamentally based upon the ionization of helium atoms in a very high electrical field produced as the potential gradient at the surface of a very fine metal tip. The application of a few thousand volts between the tip and ground potential results in a field on the order of 10^8 volts per centimeter since the radius of curvature of the tip itself is a few hundred Angstrom units. The ionized helium ions (total pressure ca. 0.5 mm Hg of helium) are accelerated in the field and strike a fluorescent screen at ground potential. Since the field at the tip surface is somewhat increased at the atoms themselves, as they protrude above the average surface, a greater ionization is produced and an image is perceived on the screen which is brighter due to the increased arrival of helium ions. The surface of the tip is thus virtually mapped out with a resolution of about 2 Å. A

photograph of the screen is generally made for study. With careful control of the applied potential, individual atom layers may be stripped from the tip. With this technique, it will be possible to remove electrodeposited layers in order to correlate the growth behavior of initial layers with the substrate orientation and also to reveal incorporated addition agents. It should be noted that the tip is screened from contamination by residual water vapor or oxygen in the vacuum system during the helium ionization process.

The many advantages for the study of electrode surfaces inherent in the use of the field ion microscope clearly outweigh the attendant difficulties of operation. Since electrochemical treatment must be performed external to the apparatus, a tip must first be cleaned and a surface map obtained, followed by removal from vacuum to an electrolytic system. After treatment, the tip must be washed and returned to vacuum for a post-treatment mapping. A control tip will also be required in which the same external treatment is performed with, however, the absence of the electrochemical step.

4.1.3 Experimental

The Central Scientific Field Ion Microscope was thoroughly checked for vacuum tightness and all connections were regreased where necessary. A connector between the vacuum pump manifold and a liquid nitrogen trap was modified and finally replaced by a short length of vacuum tubing. After rough pumping, to about 2 micron Hg, the glassware was baked to desorb moisture; the final vacuum was attained in a closed system by evaporation of a titanium filament onto the glass wall of the liquid nitrogen trap. Provision for filling with the correct pressure of helium is made by the breaking of a sealed helium ampule

within the closed system. This was accomplished after attainment of a pressure of 0.005 micron Hg.

During this period of experiment, several features of the device were recognized as meriting improvement. These will be deferred until a final test is made of the feasibility of the method for electrode studies. However, substantial improvement is needed in the reliability of vacuum connectors, helium supply and liquid nitrogen level control. Many ambiguities in the instruction manual were discovered and were worked out by trial and error. This was especially true concerning proper placement of the ground connector for the conductive coating on the inside of the actual ionization tube. It was also noted that full current could not be obtained for titanium evaporation and a separate higher rated power supply for heating would be desirable.

The obtaining of a tip picture offered no difficulties other than the necessity to adjust the Polaroid camera focus in total darkness. The obtaining of a successful picture of a tungsten tip is being followed by experiments to anneal the tip for the purpose of checking out this circuit. Platinum tips will be used thereafter in preparation for electrochemical treatment to anodically form adsorbed oxide at less than a monolayer, using a range of +200 to +500 mV with respect to the normal hydrogen electrode in 1N sulfuric acid.

4.1.4 Further Study

Experience gained in successfully mapping a tungsten tip has indicated that specific modifications are needed for electrochemical purposes. Most importantly, allowance must be made for more rapid tip removal and replacement. A design study has been initiated for construction of a horizontally facing tube into which tips may be placed

through a vacuum sealed antechamber. It is anticipated that this will be feasible with a combination of large bore vacuum stopcock and precision bore tubing which can fit through the bore of the stopcock. Tungsten seals through the closed end of precision bore tubing will permit attachment of tips and application of heater current for annealing and, of course, high voltage for operation in the field ion mode. The remaining design problem is in providing tip cooling which is necessary for successful operation in terms of image resolution. If, in fact, surface oxide is readily detectable, some sacrifice of resolution by operation at room temperature may be possible for mapping relative oxide coverage as a function of electrode potential.

With the expiration of the study year provided for Mr. DiMasi by the Army Electronics Command, the field ion electrochemical studies will be assumed by Mr. Philippe Javet, presently associated with the Laboratoire Suisse de Recherches Horlogeres, Neuchatel, Switzerland. Mr. Javet will join the Institute in April 1966.

5. INTERDISCIPLINARY RESEARCH

5.1 Optimization of Large Systems with Non-Linear Heat Transfer Phenomena*

Dr. George L. Schrenk
Frederick Costello

The purpose of the research was to develop a procedure by which the conduction, convection, or radiation heat-transfer paths to the environment can be selected to maintain, without controls, a given structure within a pre-selected temperature range.

The application of this procedure is of greatest economic significance to the temperature-control system design of spacecraft, where the coating pattern must be selected to accomodate all possible environmental and operating conditions.

A "worst-case" function W, is defined as the maximum deviation of any temperature in the system from its most desirable value, measured in units of the allowable temperature range.

$$W = \max_{i,\,k} \left| \frac{T_{i,\,k} - \bar{T}_i}{(\Delta T)_i} \right|$$

where $T_{i,k}$ is the temperature of the i^{th} element of the system for the k^{th} environmental and operating condition. The temperatures are governed by the heat-balance equations, which include the heat-transfer parameters defining the relationship between system and environment. The function W, which is shown to have only one

---

* This research was supported in part by NASW-960 contract to the General Electric Company, where Mr. Frederick Costello performed part of this research.

minimum point, is to be minimized with respect to these heat transfer parameters, which form the independent variables of the problem and which are restricted to those ranges attainable in practice.

The minimization procedure is a modification, called TREND, of the classical maximum-rate-of-descent (MRD) method. If two successive steps of MRD cross the same ridge, or discontinuity in the derivation of W, an extrapolation from the base point through the second point yields an improved value of W, following the downward trend of the ridge. Movement along the ridge is accelerated by factors as high as 10, compared to the usual MRD method.

An essential element in the optimization problem is the solution to the non-linear heat-balance equations. Seven different iterative schemes were investigated. Four were adaptations of methods frequently applied to linear equations: maximum-rate-of-descent, conjugate gradients, and two variations of the Gauss-Seidel method. A Newton-Raphson technique was included, as well as two new methods resembling an implicit time integration using a pseudo-time parameter. One of the pseudo-time techniques proved most efficient for the repeated solutions required in the optimization process.

The procedure finally developed uses the TREND procedure for following the "worst-case" criterion surface toward its minimum point. The temperatures required to evaluate the "worst-case" function are determined using a pseudo-time integration. The procedure has been applied to particular space-craft designs, using an IBM 7094 digital computer to perform the calculations. This procedure resulted in computer programs that require approximately one-eighth the running time required by pervious methods. Thus, it is now possible to

investigate physically complex systems that were previously impractical to solve.

The above research is the basis of a Ph.D. dissertation for Mr. Frederick Costello, as supervised by Dr. George L. Schrenk.

Publications in Preparation

1. F. A. Costello and G. L. Schrenk, "The Solution to Systems of Non-Linear Equations Involving Diagonally Dominant Stieljes Matrices."
2. F. A. Costello and G. L. Schrenk, "An Acceleration Procedure for the Maximum-Rate-Of-Descent Method."
3. F. A. Costello and G. L. Schrenk, "Temperature-Control Systems Optimization."

6. PH.D'S GRANTED

Ph.D's Granted

M. Kaplit: Ph.D. Dissertation, The Surface Double Layer of a Metal Work Function in a Gaseous Environment.

Y. K. Rao: Ph.D. Dissertation, Thermodynamic Properties of Binary Liquid Magnesium Solutions.

Frederic Costello: Ph.D. Dissertation, Optimization of Large Systems with Non-Linear Heat Transfer Phenomena.

Daniel P. Ross: Ph.D. Dissertation, Droplet Formation and Vaporization in the Wake of a Melting Body.

Han Chang: Ph.D. Dissertation, An Unsteady-State Technique to Measure Thermal Diffusivity of High Temperature Materials.

William Mehuron: Ph.D. Dissertation, Electromagnetic Wavee Interaction in an Inhomogeneous Drifting Plasma.

Alan Whitman: Ph.D. Dissertation, Theory of Electrostatic Probes in a Magnetohydrodynamic Fluid.

7. PUBLICATIONS LIST

Publications List

INDEC-1 H. Yeh and T. K. Chu, "The Optimization of MHD Generators with Arbitrary Conductivity," ASME Paper 63-WA-349.

INDEC-2 M. Altman, D. P. Ross, H. Chang, "The Prediction of Transient Heat Transfer Performance of Thermal Energy Storage Devices, Proceedings of 6th National Heat Transfer Conference, Boston, Mass., 1963.

INDEC-3 G. R. Belton and Y. K. Rao, "The Binary Eutectic as a Thermal Energy Storage System: Equilibrium Properties," paper presented at the 6th National Heat Transfer Conference, Boston, Mass. Aug. 11-14, 1963.

INDEC-4 J. Dunlop and G. Schrenk, "Theoretical Model of a Thermionic Converter," Proceedings of Thermionic Specialist Conference, Gatlinburg, Tenn., pp. 57-62, Oct. 7-9, 1963.

INDEC-5 R. Sharma and H. Chang, "Thermophysical and Transport Properties of High Temperature Energy Storage Materials," paper presented at the Third Annual Symposium, High Temperature Conversion Heat to Electricity, Tucson, Arizona, Feb. 19-21, 1964.

INDEC-6 G. L. Schrenk, "Solar Collection Limitations for Dynamic Converters-Simulation of Solar-Thermal Energy Conversion Systems," Proceedings of AGARD Conference, Cannes, France, March 16-20, 1964.

INDEC-7 M. Altman, "Prospects for Thermal Energy Storage," Proceedings of AGARD Conference, Cannes, France, March 16-20, 1964.

INDEC-8 L. Zelby, "The Hollow Thermionic Converter," IEEE Annual Meeting on Energy Conversion, Clearwater, Florida, May 1964.

INDEC-9 M. Altman, "The Institute for Direct Energy Conversion," paper presented at Am. Soc. Eng. Ed. Annual Meeting, University of Maine, Orono, Maine, June 22-26, 1964.

INDEC-10 G. Schrenk, "Emitter Sheath Polarity in Plasma Diodes, Proceedings of Thermionic Specialist Conference, Cleveland, Ohio, Oct. 26-28, 1964, pp. 249-257.

INDEC-11 M. Kaplit, G. Schrenk, L. Zelby, "Electron Emission from Metals in Gaseous Environment," Proceedings of Thermionic Specialist Conference, Cleveland, Ohio, Oct. 26-28, 1964, pp. 4-10.

INDEC-12 G. Schrenk, "Criteria for Emitter Sheath Polarity in Plasma Diodes," paper presented at ASME Winter Annual Meeting, New York, No. 29-Dec. 3, 1964.

INDEC-13 R. J. Blasco and E. Gileadi, "An Electrochemical and Microbiological Study of the Formic Acid-Formic Dehydrogenlyase System," Advanced Energy Conversion, Vol. 4, pp. 179-186, 1964.

INDEC-14 G. Schrenk and A. Lowi, "Mathematical Simulation of Solar Thermionic Energy Conversion Systems," Proceedings of the International Thermionic Electrical Power Generation Conference, IEEE, London, England, Sept. 20-24, 1965.

INDEC-15 R. McKinnon, A. Turrin, G. Schrenk, "Cavity Receiver Temperature Anslysis," AIAA paper No. 65-470, July 26-29, 1965.

INDEC-16 G. Schrenk and M. Kaplit, "Electron Emission from Metals in Vapors of Cesium and Fluorine," Proceedings of the Thermionic Specialist Conference, San Diego, California, Oct. 25-27, 1965.

INDEC-17 C. A. Renton and L. W. Zelby, "Longitudinal Interaction of Microwaves with an Argon Discharge," Appl. Phys. Ltrs., Vol. 6, No. 8, pp. 167-169, Sept. 15, 1965.

INDEC-18 L. W. Zelby, "Microwave Interaction with a Non-Uniform Argon Discharge," Proceedings of the Symposium of Microwave Interaction with Ferrimagnetics and Plasmas, London, England, pp. 32-1 to 32-3, Sept. 13-17, 1965.

INDEC-19 M. Altman and J. H. Jones, "Two-Phase Flow and Heat Transfer for Boiling Liquid Nitrogen in Horizontal Tubes," Chemical Engineering Progress Symposium Series, Volume 61, No. 57, Oct. 1965.

INDEC-20 S. Schweitzer and M. Mitchner, "Electrical Conductivity of a Partially Ionized Gas in a Magnetic Field," Submitted to the AIAA Journal.

INDEC-21 M. Kaplit and G. L. Schrenk, "Models for Electron Emission from Metals with Adsorbed Monolayers," Submitted to Advanced Energy Conversion.

INDEC-22 M. Kaplit and G. L. Schrenk, "Models for Electron Emission from Metals with Adsorbed Monolayers," paper presented at Twenty-Sixth Annual Conference on Physical Electronics,

Massachusetts Institute of Technology, Cambridge, Mass., March 21-23, 1966.

INDEC-23 L. W Zelby, "Slow Wave Interaction with an Argon Discharge," (Abstract) Symposium on Properties and Applications of Low-Temperature Plasmas, XX-th International Congress of I.V.P.A.C., Moscow, USSR, July 15-18, 1965.

INDEC-24 L. W. Zelby, "Understanding Plasma Diodes and Amplifiers," Electronic Industries, Vol. 24, No. 11, p. 64, Nov. 1965.

INDEC-25 L. W. Zelby, "A Simplified Approach to the Analysis of Electromagnetic Wave Propagation Characteristics of Plasma Coated Surfaces," RCA Review, Vol. 26, No. 4, p. 497, Dec. 1965.

INDEC-26 L. W. Zelby, "Plasma Coated Surface as a Wave Guide," RCA Engineer, Vol. 11, No. 4, p. 50, Jan. 19, 1966.

INDEC-27 L. W. Zelby, W. O. Mehuron, R. Kalagher, "Measurements of Collision Frequency in an Argon Discharge," Submitted to Appl. Phys. Ltrs., March 1966.

INDEC-28 R. Kalagher, "Effects of Inhomogeneous Electron Density in a Cylindrical Plasma Column Surrounded by a Helix," Submitted to IEEE Transactions on Microwave Theory and Techniques, March 1966.

INDEC-29 Samuel Greenhalgh, "Syringe for Injecting Sodium Potassium Alloy," Submitted to The Review of Scientific Instruments, August 13, 1965.